PHYSICAL PROPERTIES OF HYDRATE-BEARING SEDIMENTS

W. F. Waite,[1] J. C. Santamarina,[2] D. D. Cortes,[2] B. Dugan,[3] D. N. Espinoza,[2] J. Germaine,[4] J. Jang,[2] J. W. Jung,[2] T. J. Kneafsey,[5] H. Shin,[2] K. Soga,[6] W. J. Winters,[1] and T.-S. Yun[7]

Received 1 December 2008; revised 18 June 2009; accepted 14 July 2009; published 31 December 2009.

[1] Methane gas hydrates, crystalline inclusion compounds formed from methane and water, are found in marine continental margin and permafrost sediments worldwide. This article reviews the current understanding of phenomena involved in gas hydrate formation and the physical properties of hydrate-bearing sediments. Formation phenomena include pore-scale habit, solubility, spatial variability, and host sediment aggregate properties. Physical properties include thermal properties, permeability, electrical conductivity and permittivity, small-strain elastic P and S wave velocities, shear strength, and volume changes resulting from hydrate dissociation. The magnitudes and interdependencies of these properties are critically important for predicting and quantifying macroscale responses of hydrate-bearing sediments to changes in mechanical, thermal, or chemical boundary conditions. These predictions are vital for mitigating borehole, local, and regional slope stability hazards; optimizing recovery techniques for extracting methane from hydrate-bearing sediments or sequestering carbon dioxide in gas hydrate; and evaluating the role of gas hydrate in the global carbon cycle.

Citation: Waite, W. F., et al. (2009), Physical properties of hydrate-bearing sediments, *Rev. Geophys.*, *47*, RG4003, doi:10.1029/2008RG000279.

Table of Contents

[1]U.S. Geological Survey, Woods Hole, Massachusetts, USA.
[2]School of Civil and Environmental Engineering, Georgia Institute of Technology, Atlanta, Georgia, USA.
[3]Department of Earth Science, Rice University, Houston, Texas, USA.
[4]Department of Civil and Environmental Engineering, Massachusetts Institute of Technology, Cambridge, Massachusetts, USA.
[5]Lawrence Berkeley National Laboratory, Berkeley, California, USA.
[6]Department of Engineering, University of Cambridge, Cambridge, UK.
[7]School of Civil and Environmental Engineering, Yonsei University, Seoul, South Korea.

8755-1209/09/2008RG000279
Paper number 2008RG000279

1. INTRODUCTION

[2] Gas hydrates are crystalline clathrates composed of low molecular weight gases, the most common of which is methane, encaged in a lattice of hydrogen-bonded water molecules. Methane gas hydrate, found beneath permafrost and in marine continental margin sediments worldwide [*Kvenvolden and Lorenson*, 2001], is the most common naturally occurring gas hydrate and has attracted interest as a possible energy resource [*Collett*, 2002; *Dallimore and Collett*, 2005; *Grauls*, 2001; *Holder et al.*, 1984; *Ruppel*, 2007] and as a potential agent in climate change [*Archer*, 2007; *Dickens et al.*, 1995; *Ruppel and Pohlman*, 2008] and seafloor instability [*Kayen and Lee*, 1991, 1993; *McIver*, 1982; *Mienert et al.*, 2005; *Nixon and Grozic*, 2007].

[3] Gas hydrate research, as measured by publication numbers, has grown exponentially through the 20th century [*Sloan*, 2004]. Much of the measurement work has focused on gas hydrate as a pure material, referred to here as "hydrate," and has been comprehensively reviewed by *Sloan and Koh* [2008]. As research shifts to hydrates in sediments, it is appropriate to review the current understanding of the evolution, behavior, and physical properties of hydrate-bearing sediments.

[4] Consider the process of methane recovery from hydrate-bearing sediments, discussed in sections 1.1–1.3 in terms of the critical roles physical properties play in the exploration, production, and reservoir management phases. Sections of this paper that address the corresponding governing parameters are given in parentheses.

1.1. Exploration

[5] Host sediment properties (section 6), particularly sediment grain size, play a prominent role in evaluating sites for their resource potential. Exploration for hydrate as an energy resource focuses on sands rather than fine-grained material to facilitate extraction while minimizing technical production challenges [*Boswell and Collett*, 2006; *JIP Leg II Science Team*, 2009]. A "petroleum systems" approach has been adopted to target sands with high hydrate saturations [*Hutchinson et al.*, 2008; *Jones et al.*, 2008]. One component of this approach is to identify sands that are linked to a methane source (section 2) via faults or other permeable pathways [*Frye*, 2008].

[6] Migration pathways and general reservoir properties (section 4) can be identified from seismic or other remote sensing data [*Hutchinson et al.*, 2008; *Jones et al.*, 2008]. These mapping techniques rely on the effects of hydrates on sediment properties relative to hydrate-free sediment. Electrical survey data are sensitive to the resistivity increase as hydrate replaces conductive pore water in the sediment (section 9) [*Weitemeyer et al.*, 2006], whereas seismic survey data are sensitive to the increase in wave velocity that hydrate imparts to the host sediment (section 10) [*Dai et al.*, 2008b].

[7] The extent to which a given volume of hydrate alters the host sediment properties depends on where hydrate forms within the pore space (section 3) [*Dvorkin et al.*, 2000]. Careful consideration must therefore be given in laboratory studies when mimicking hydrate-bearing sediments, when linking pore space hydrate saturations to measured physical properties (section 5), and when interpreting field data [*Dai et al.*, 2008b].

1.2. Production

[8] Hydrate dissociation during drilling or production reduces the volume of a solid phase in the formation and converts it into a mixed fluid phase that is several times larger in volume, with immediate implications for fluid pressure, effective stress [*Rutqvist et al.*, 2008], strength (section 11), and volumetric deformation (section 12) [*Kwon et al.*, 2008]. Potential implications include the collapse of the production borehole [*Birchwood et al.*, 2008]. Strength loss due to hydrate dissociation must also be considered while producing conventional hydrocarbons underlying hydrate-bearing strata as relatively warm hydrocarbons pumped through hydrate-bearing layers can destabilize hydrate surrounding the production well [*Briaud and Chaouch*, 1997; *Hadley et al.*, 2008].

1.3. Reservoir Management

[9] The economical viability of a reservoir depends on a combination of several factors such as thermal properties, formation permeability, and sediment spatial variability. The rate at which dissociation can occur, for instance, is limited by the reservoir temperature and ability to conduct the heat needed to drive the endothermic dissociation of gas hydrate (section 7) [*Anderson et al.*, 2008; *Kneafsey et al.*, 2007]. The formation permeability and the relative permeability in the presence of gas and water (section 8) determine the ease with which methane can be transported into the production well [*Sakamoto et al.*, 2008]. Sediment properties (section

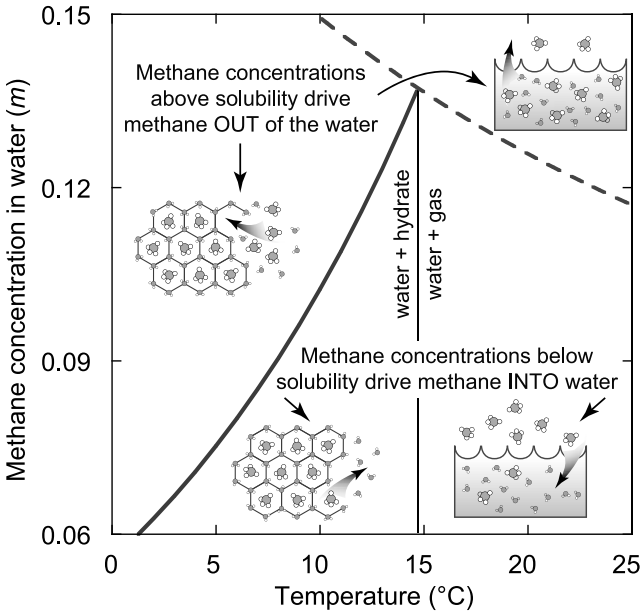

Figure 1. Solubility curves for methane in water with hydrate (solid curve) and without hydrate (dashed curve). Pressure is assumed constant at 12 MPa. Depending on the temperature, a solution with excess methane will either precipitate hydrate or push methane into the gas phase (top schematics) until the methane concentration falls to the solubility value. A solution with a methane deficit will dissolve hydrate or absorb free gas (bottom schematics) until the solution's methane concentration rises to the solubility value. When methane is entering and exiting the solution at equal rates, the system is in dynamic equilibrium at the solubility concentration.

6) determine other production-related processes, such as fines migration during the production and clogging of permeable pathways around the production well [*Valdes and Santamarina*, 2007; *Walsh et al.*, 2009]. Reservoir models used to optimize recovery strategies and forecast the economic potential of a given hydrate reservoir must properly account for interdependencies between physical properties in order to reliably capture the inherently coupled hydromechanical, thermomechanical, and chemomechanical processes that govern the behavior of hydrate-bearing sediment [*Anderson et al.*, 2008; *Walsh et al.*, 2009; *Wilder et al.*, 2008].

[10] The production example given in section 1.2 is not merely hypothetical. The Chevron–Department of Energy (DOE) Joint Industry Project (JIP) in the Gulf of Mexico completed a drilling program in May 2009 to test whether the "petroleum system" approach mentioned in section 1.1 is applicable to locating sand units with high hydrate saturations [*JIP Leg II Science Team*, 2009]. On Alaska's North Slope, a ConocoPhillips–DOE JIP is planning a long-term production test from a subpermafrost hydrate-bearing sand [*ConocoPhillips–University of Bergen Hydrates Team*, 2008]. Several countries are currently exploring for hydrate-bearing reservoirs [*Expert Panel on Gas Hydrates*, 2008], and Japan aims to produce methane from hydrate at a commercial scale by 2016 [*Sakamoto et al.*, 2008].

[11] In support of ongoing efforts in hydrate exploration, reservoir assessment, analyses of gas hydrate's role in climate change, and evaluation of seafloor instability conditions, this review collects the current understanding of physical properties of hydrate-bearing sediment. Where possible, connections are made between these properties to indicate the ways in which hydrate-bearing sediment evolves in response to changes in its surroundings.

2. SOLUBILITY OF HYDRATE-FORMING GAS IN AQUEOUS SYSTEMS

[12] Hydrate forms in the presence of water when there is enough hydrate-forming gas and both pressure and temperature are conducive to hydrate stability. Conversely, the hydrate crystal may break down and release methane by either dissolution, when there is not enough hydrate-forming gas in the surrounding water, or dissociation, when the pressure and temperature requirements for stability are not met. Whereas hydrate dissolution results in only a small net volume increase [*Lu et al.*, 2008; *Sultan et al.*, 2004a], dissociation generates a free methane gas phase and a much larger volume increase [*Kwon et al.*, 2008; *Xu and Germanovich*, 2006].

[13] The equilibrium concentration of hydrate-forming gas (the solute) in the surrounding water or aqueous system (the solvent) is given in units of molarity, M, defined as moles of solute per liter of solution. Solute concentration can also be given in terms of molality, m, defined as the moles of solute per kilogram of solvent. For simplicity, the solute considered herein is methane, CH_4.

[14] Dissolution and precipitation occur when hydrate is in contact with water. During dissolution, hydrate dissolves into the water phase, increasing the methane concentration in the water. During precipitation, hydrate formation extracts methane from the water phase, lowering the methane concentration in the water. In the presence of hydrate, dissolution and precipitation occur at the same rate when the concentration of methane in the water reaches the solubility limit. In the absence of hydrate, methane molecules move at equal rates between the free gas phase and the dissolved phase when the concentration of methane in water reaches the solubility limit (Figure 1).

2.1. Theoretical Determination of Solubility Concentrations

[15] The solubility of each chemical species in the gaseous, liquid, and hydrate phases can be calculated from thermodynamic properties by minimizing the system's Gibbs free energy or, equivalently, equating the potential energy changes in the system, as shown in Table 1 [*Sun and Duan*, 2007; *Zatsepina and Buffett*, 1998]. In step 3 in Table 1, the *Trebble and Bishnoi* [1987] equation of state has been shown to work well for the methane-water system [*Englezos and Bishnoi*, 1988; *Zatsepina and Buffett*, 1998]. Solubility can also be estimated directly from fugacity-based models,

TABLE 1. Obtaining the Equilibrium Solubility Concentration, x_i^j, of Species *i* in Phase *j* From Minimizing Gibbs Free Energy, *G*[a]

Step	Process	Equation
1	minimize Gibbs free energy, G, or equate chemical potentials, μ	$G = \sum_{i,j} n_i^j \mu_i^j$ or $\Delta\mu_w^H = \mu_w^\beta - \mu_w^H = \mu_w^\beta - \mu_w^L = \Delta\mu_w^L$
2	relate chemical potential to activity, a, or fugacity, f	$\mu_i^j - \mu_i^0 + RT \cdot \ln(a_i^j) = \mu_i^0 + RT \cdot \ln\left(\frac{f_i^j}{f_i^0}\right)$
3	relate activity or fugacity to concentration, x	$a_i^j = \frac{f_i^j}{f_i^0} = \nu_i^j x_i^j$

[a]Notation is as follows: n is number of moles; μ_i^j is chemical potential or free energy per mole of species i in phase j, with $j = 0$ representing a convenient reference state; activity, a, is a measure of how nonideal molecules such as methane and water interact; fugacity, f, is a measure of how stable a species is in a given phase; ideal gas constant $R = 8.314$ J (mol K)$^{-1}$; T is temperature in kelvins; and ν is the activity coefficient determined from an equation of state. Subscript w refers to water. Superscripts H, β, and L refer to water in the hydrate phase, in a hypothetical empty hydrate with no guest molecules, and in the liquid phase, respectively.

though expressions for activity and fugacity can be complex when the combined effects of temperature, pressure, salinity, and pore size are included. Solubility "calculators" that account for some of these effects can be found online (http://www.geochem-model.org/?page_id=48) [*Duan and Mao*, 2006; *Sun and Duan*, 2007].

2.2. Data

[16] Experimental measurements and theoretical estimates for methane solubility in water with and without hydrate are compiled in Tables 2a–2c. Here we summarize the dependence of methane solubility in water on temperature, pressure, salinity, capillary pressure, and pore size.

2.2.1. Temperature

[17] The solubility of methane in water is primarily controlled by temperature and the presence of hydrate. In the absence of hydrate (dashed curve in Figure 1), methane becomes less soluble as the temperature increases because the increasing kinetic energy allows molecules to break intermolecular bonds in the liquid water and move into the gas phase. The same general concept applies in the presence of hydrate, where increasing temperature means more energetic methane molecules can break out of the solid hydrate and enter the liquid water, increasing the water's methane concentration (solid curve in Figure 1) [*Subramanian and Sloan*, 2002].

2.2.2. Pressure

[18] In the absence of hydrate, the solubility rises with increasing pressure, indicating an increased preference for methane to exist in the dissolved phase rather than the gas phase [*Servio and Englezos*, 2002]. In the presence of hydrate, solubility falls slightly with increasing pressure, indicating a preference for methane to exist in the hydrate rather than the water phase [*Lu et al.*, 2008].

2.2.3. Salinity

[19] The addition of salt drives methane out of solution, shifting the curves in Figure 1 to lower values. Methane is forced into hydrate if it is present or into the gas phase in the absence of hydrate [*Davie et al.*, 2004; *Sun and Duan*, 2007; *Tishchenko et al.*, 2005; *Zatsepina and Buffett*, 1998]. Solubility changes due to salt are secondary to those of temperature in natural settings but are important in flow assurance applications, such as preventing hydrate formation in pipelines, where electrolytes and other chemical inhibitors are used extensively [*Sloan and Koh*, 2008].

2.2.4. Capillary Pressure and Pore Size

[20] Capillary pressure is the pressure difference across an interface between two immiscible phases, such as water and hydrate or water and gas. The capillary pressure, ΔP, across a spherical interface of radius r and interfacial tension $\gamma_{i,w}$ between species i (hydrate or free methane gas in this case) and water is

$$\Delta P = P_i - P_w = \gamma_{i,w}\left(\frac{2}{r}\right). \quad (1)$$

The pressure, P_i, in the hydrate or free gas bubble is therefore higher than the pressure in the water, P_w, by an amount equal to the capillary pressure, ΔP. Equation (1) indicates that the capillary pressure increases with decreasing radius of interfacial curvature.

[21] Like the capillary pressure, the chemical potential in a hydrate crystal or free gas bubble scales inversely with the radius of curvature [*Clennell et al.*, 1999]. Smaller hydrate crystals or free gas bubbles therefore have higher chemical potentials than their larger counterparts and require higher methane concentrations in the surrounding water to balance that chemical potential [*Henry et al.*, 1999; *Kwon et al.*, 2008]. This process is only significant in small pores, which would need to have radii <18 nm for this solubility increase

TABLE 2A. Solubility References for Hydrate-Forming Gas in Water in the Presence of Hydrate: Methane and Pure Water

P (MPa)	T (K)	Reference[a]
0.1–50	273–278	*Handa* [1990], M
0.1–200	273–573	*Duan and Mao* [2006], M
0.6–8.9	274–282	*Englezos et al.* [1987], E and M
1–18	275–313	*Mohammadi et al.* [2006], E and M
1–35	283–318	*Chapoy et al.* [2003], E and M
2.7–78	274–302	*Hashemi et al.* [2006], M
3–50	273–293	*Tishchenko et al.* [2005], M
3.5–6.5	274–285	*Servio and Englezos* [2002], E
3.5–6.5	274–285	*Bergeron et al.* [2007], M
3.5–30	273–291	*Sun and Duan* [2007], M
5–20	276–282	*Kim et al.* [2003], E and M
6–20	274–286	*Seo et al.* [2002], E
10–30	273–300	*Davie et al.* [2004], M
10–40	277–295	*Lu et al.* [2008], E and M
10–60	324.65	*Masoudi et al.* [2004], M
20	273–300	*Zatsepina and Buffett* [1997, 1998], M

[a]E, experiment; M, model.

TABLE 2B. Solubility References for Hydrate-Forming Gas in Water in the Presence of Hydrate: Methane, Pure Water, and Salt[a]

P (MPa)	*T* (K)	Salt Content[b]	Reference[c]
0.1–50	273–278	3.5%	*Handa* [1990], M
0.1–200	273–573	0–6 *m* (0%–26%)	*Duan and Mao* [2006], M
5–50	273–293	2%, 3.5%, 5%, and 7%	*Tishchenko et al.* [2005], M
10–30	273–283	3% and 3.5%	*Sun and Duan* [2007], M
10–60	324.65	1 and 4 *M* (6% and 23%)	*Masoudi et al.* [2004], M

[a]Salt is NaCl.
[b]Original units are given. Results given in molarity (*M*) or molality (*m*) are also converted to percent (grams of salt per 100 grams of solution).
[c]M, model.

to balance the solubility decrease caused by the salinity in a standard seawater solution of 3.5 wt % salt [*Sun and Duan*, 2007]. By comparison, the pore space distribution in fine-grained hydrate-bearing sediment at Blake Ridge Ocean Drilling Program Hole 995A peaked near a radius of 100 nm [*Clennell et al.*, 1999]. The capillary pressure effect is even smaller in clean sands, where sediment grains are larger than 75 μm and pore sizes generally exceed $\sim$50 μm.

2.3. Geologic Implications

[22] In natural systems, the solubility of methane increases with depth, as shown in Figure 2 [*Nimblett and Ruppel*, 2003; *Xu and Ruppel*, 1999]. The solubility is nearly constant below the depth at which hydrate is no longer stable because the solubility increase with increasing pressure and decrease with increasing temperature nearly balance in the absence of hydrate.

[23] Fluid migrating up through the sediment column may not be fully saturated with methane at depth and hence cannot begin precipitating hydrate until it passes through the depth at which the solubility limit is low enough to equal the methane concentration in the rising fluid (bottom of hydrate occurrence zone in Figure 2). The actual base of hydrate occurrence is therefore often shallower than would be predicted from pressure and temperature considerations alone [*Xu and Ruppel*, 1999]. These concepts have been captured in numerical models predicting the hydrate distribution formed by methane dissolved in upwelling fluid over geologic time [*Garg et al.*, 2008; *Nimblett and Ruppel*, 2003] and when the rising fluid contains free methane gas [*Liu and Flemings*, 2007].

[24] While seafloor conditions may be within the stability field, hydrate does not tend to form at or close to the seafloor (top of hydrate occurrence zone in Figure 2) for three reasons [*Egorov et al.*, 1999; *Haeckel et al.*, 2004; *MacDonald et al.*, 1994]: (1) methane in upwelling water is consumed by hydrate formation at depth [*Xu and Ruppel*, 1999]; (2) sulfate reduction, anaerobic methane oxidation, and other chemical processes active in the shallow sediment consume available methane [*Egorov et al.*, 1999; *Malinverno et al.*, 2008; *Nimblett and Ruppel*, 2003; *Rehder et al.*, 2004]; and (3) low methane concentrations in seawater cause rapid hydrate dissolution [*Rehder et al.*, 2004]. Thus, hydrate outcrops at the seafloor tend to occur in conjunction with active methane gas vents that can sustain the hydrate outcrop.

TABLE 2C. Solubility References for Hydrate-Forming Gas in Water in the Presence of Hydrate: Methane, Pure Water, Salt, and Pore Size[a]

P (MPa)	*T* (K)	Salt Content (%)	Pore Size (nm)	Reference[b]
5–50	273–294	3.5	5–50	*Sun and Duan* [2007], M
3–14	271–287	0	9–30	*Anderson et al.* [2003], E
3–8	259–283	0	4–100	*Uchida et al.* [2002], E

[a]Salt is NaCl.
[b]E, experiment; M, model.

3. HYDRATE FORMATION IN SEDIMENT

[25] The pore-scale location of hydrate exerts a strong control on the macroscale physical properties of hydrate-

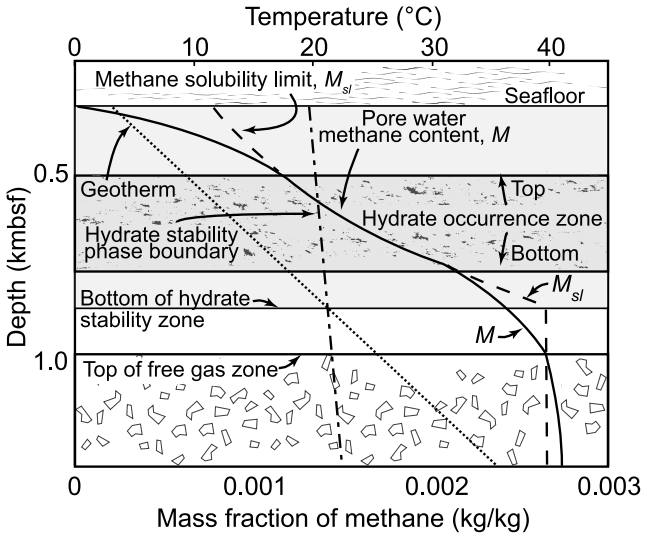

Figure 2. The zone in which methane gas hydrate occurs can be thinner than the stability zone. Fluid with a methane concentration M must rise to the depth at which the local solubility limit, M_{sl}, is less than M in order for hydrate to precipitate and form the base of hydrate occurrence. The top of hydrate occurrence is often below the seafloor even when hydrate is thermodynamically stable because methane consumption drives the methane concentration below the local solubility limit. Modified from *Xu and Ruppel* [1999], who assumed a water depth of 2500 m.

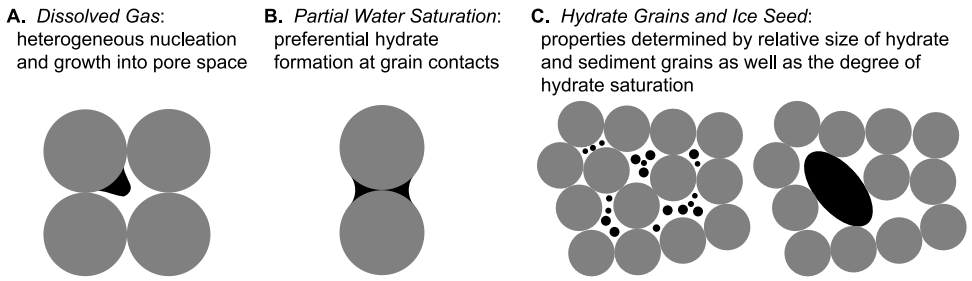

Figure 3. Dependence of hydrate habit on hydrate formation technique. Physical properties of hydrate-bearing sediments depend on the size and distribution of hydrate (black) relative to the sediment grains (gray).

bearing sediments. Pore-scale habits of hydrates, hydrate formation techniques used in the laboratory, and observations based on natural hydrate-bearing sediments are reviewed in sections 3.1–3.4 in the context of their impact on measured physical properties (based on J. Jang (personal communication, 2008) and *Lee et al.* [2007]).

3.1. Hydrate in Pores

[26] The effects of hydrate on host sediment properties depend on where hydrate forms in the pore space. The three most commonly discussed hydrate habits are as follows:

[27] The first habit is pore filling. Hydrates nucleate on sediment grain boundaries and grow freely into pore spaces without bridging two or more particles together. In this case, hydrate primarily affects the pore fluid bulk stiffness and fluid conduction properties [*Helgerud et al.*, 1999].

[28] The second habit is load bearing. Hydrate bridges neighboring grains and contributes mechanical stability to the granular skeleton by becoming part of the load-bearing framework. Pore-filling hydrate naturally turns into load-bearing hydrate when the pore space hydrate saturation exceeds S_h = 25%–40% [*Berge et al.*, 1999; *Yun et al.*, 2005, 2007].

[29] The third habit is cementation. Hydrate cements intergranular contacts. Even a small amount of hydrate can dramatically increase the sediment shear and bulk stiffnesses by bonding adjacent grains together [*Dvorkin et al.*, 1999].

[30] Hydrate nucleation and growth processes govern which hydrate habit occurs. As a result, different laboratory methodologies for forming hydrate can result in different hydrate habits and hence different physical properties for identical sediments with equal hydrate saturations, as discussed in sections 8, 10, and 11.

3.2. Hydrate Formation in the Laboratory

[31] The controlled synthesis of methane hydrate in sediments is challenging owing to methane's low solubility in water. Even for water in contact with hydrate at 4°C, there are ~750 water molecules per methane molecule [*Lu et al.*, 2008], as compared to ~6 water molecules per methane molecule required in the methane hydrate structure. Hydrate formation from methane gas dissolved in water is thus a slow process for laboratory studies, and more expedient techniques have been developed. These laboratory methods produce different pore-scale growth habits [*Ebinuma et al.*, 2005; *Spangenberg et al.*, 2005; *Zhong and Rogers*, 2000].

3.2.1. Dissolved Gas Method

[32] Water saturated with a hydrate-forming gas is circulated through sediment that is held within the hydrate pressure and temperature stability field. The hydrate growth rate is limited by the concentration of hydrate former in the water, so many of these experiments use carbon dioxide, CO_2 [*Katsuki et al.*, 2006; *Tohidi et al.*, 2001; *Zatsepina and Buffett*, 2001] due to its higher solubility in water relative to methane [e.g., *Spangenberg et al.*, 2005].

[33] Regardless of the hydrate former, bringing the system into the hydrate stability field does not immediately result in a measurable quantity of hydrate. Hydrate crystals must first nucleate, and then these nuclei must grow before the hydrate formation can be detected. The induction time, the delay between imposing hydrate stability conditions and observing hydrate formation [*Sloan and Koh*, 2008], can be quite long when forming hydrate from dissolved phase gases. Surfactants have been used to promote hydrate nucleation [*Zhong and Rogers*, 2000], and induction times have also been reduced by flowing fluid through hydrate granules stored in a separate chamber, thereby entraining hydrate nuclei that can facilitate hydrate growth once they reach the test sediment [*Waite et al.*, 2008].

[34] Heterogeneous nucleation in the dissolved gas method may occur anywhere on the mineral surface, with subsequent growth into the pore space (Figure 3a). Conceptually, the dissolved gas method is limited to forming hydrate saturations S_h below ~60%–70% for which water remains a percolating phase and can continue to circulate, though saturations have been reported as high as 95% after ~50 days of circulation [*Spangenberg et al.*, 2005].

3.2.2. Partial Water Saturation Method

[35] Soil grains are mixed with a limited amount of water and packed to form a partially water-saturated sediment. The system is pressurized with methane gas and cooled into the stability field to promote hydrate formation. Depending on the initial water saturation, this method can take just a few days to form hydrate-bearing sediments [*Kneafsey et al.*, 2007; *Waite et al.*, 2004]. Alternatively, the sample can be fully water saturated initially and have methane introduced as a bubble phase prior to cooling [*Winters et al.*, 2002]. Unlike the dissolved gas method, however, both partial water saturation approaches lead to preferential

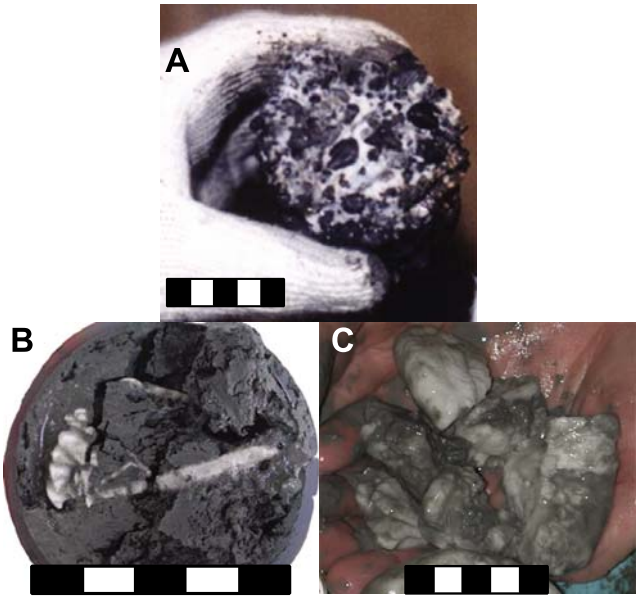

Figure 4. Modes of hydrate occurrence: (a) Hydrate (white) saturating pore space of a coarse-grained sample from the 1998 Mallik 2L-38 permafrost hydrate research well. (b) Veined hydrate (white) in fine-grained sediment from the Krishna Godavari Basin, offshore India. (c) Sediment-coated hydrate chunks from fine-grained sediment in the Gulf of Mexico. Photos in Figures 4a and 4c by W. Winters, U.S. Geological Survey. Photo in Figure 4b courtesy of the National Gas Hydrate Program (NGHP) Expedition 01 Scientific Party. Scale bars indicate 5 cm.

hydrate formation at contacts and stiffening of the sediment framework (Figure 3b) [*Chuvilin et al.*, 2003; *Ebinuma et al.*, 2005; *Klapproth et al.*, 2007; *Kneafsey et al.*, 2005, 2007; *Kono and Budhijanto*, 2002; *Masui et al.*, 2005; *Priest et al.*, 2005].

3.2.3. Ice-Seeding Method

[36] Cooled soil grains are mixed with small ice grains. The mixture is pressurized into the hydrate stability field with methane. The temperature is slowly increased. Hydrate nucleation is facilitated by the existing ice lattice, and hydrate can grow rapidly from the water liberated as the ice melts [*Stern et al.*, 1996, 1998]. Depending on the gas pressure, this method can be run to completion within a few days. As shown in Figure 3c, the relative size and volume fraction of mineral and hydrate grains will determine their relative load-bearing contribution to the mineral framework. Additionally, as with the partial saturation method, meltwater may accumulate at sediment grain contacts prior to hydrate formation (Figure 3b) [*Circone et al.*, 2004; *Ebinuma et al.*, 2005; *Holder and Kamath*, 1984; *Kamath et al.*, 1991; *Klapproth et al.*, 2007; *Masui et al.*, 2005; *Stern et al.*, 1998; *Ullerich et al.*, 1987; *Waite et al.*, 2002; *Yoon et al.*, 2004].

3.2.4. Hydrate Premixing Method

[37] Granular methane hydrate is prepared by spraying misted water in a pure methane gas atmosphere under phase equilibrium conditions [*Hyodo et al.*, 2005] or by melting small ice particles in the presence of methane at 25–30 MPa pressure [*Stern et al.*, 1998]. The methane hydrate granules are mixed with sediment at very low temperature and consolidated at the target effective stress for a few hours. The temperature of the prepared specimen is maintained within the stability field but briefly raised near the hydrate phase boundary to eliminate excess moisture and allow for hydrate annealing [*Hyodo et al.*, 2005]. As with the ice-seeding method, the load distribution within the hydrate-bearing sediment depends on the relative size of the hydrate granules and sediment grains (Figure 3c).

3.3. Hydrate Formation in Nature

[38] The formation patterns of naturally occurring hydrate are varied, with an observable distinction between disseminated, pore-filling hydrate in coarse sands compared to veined or nodule-type hydrate occurrences in fine-grained sediments (Figure 4). While the formation of hydrate near faults and at the base of the hydrate stability zone may take place in the presence of free gas, hydrate formation in sediments within the gas hydrate stability zone most likely utilizes dissolved, aqueous phase methane [e.g., *Buffett and Zatsepina*, 2000]. This requires a methane source within the sediment such as biogenic, microbial activity and/or the transport of either biogenic or thermogenic methane via diffusion or advection from deeper strata.

[39] Hydrate occurrences in the Nankai Trough offshore Japan have been characterized as pore filling [*Murray et al.*, 2006]. In the Blake Ridge, off the southeast coast of the United States, hydrate has been characterized as cementing by *Guerin et al.* [1999] but as load bearing by *Helgerud et al.* [1999]. As a rule of thumb, however, acoustic, electrical, or nuclear magnetic resonance (NMR) estimates of hydrate saturation suggest hydrate in sands can be characterized with load-bearing models when the hydrate saturation exceeds 25%–30% [*Kleinberg and Dai*, 2005; *Lee and Waite*, 2008] except in high gas flux areas [*Bohrmann et al.*, 1998] or where gas is recycled into the hydrate stability zone, allowing hydrate to form as a cement [*Guerin et al.*, 1999; *Yuan et al.*, 1999].

3.4. Laboratory Formation of Analog Hydrate

[40] Tetrahydrofuran (C_4H_8O, hereinafter referred to as THF) hydrate has been used in place of methane hydrate in laboratory studies [*Handa et al.*, 1984; *Leaist et al.*, 1982; *Lee et al.*, 2007; *Rueff and Sloan*, 1985; *Yun et al.*, 2005, 2007; *Cortes et al.*, 2009]. Concerns related to the polar nature of the THF molecule compared to the nonpolar nature of the methane molecule have been raised, but this polarity difference between THF and methane loses relevance in the context of hydration processes because the large size and structure of the THF molecule significantly weaken polarity-based ionic interactions between water and THF. Implications of THF's polar nature regarding hydrate research are discussed by *Lee et al.* [2007].

[41] The main advantage of THF relative to methane is its complete miscibility in water, which enables relatively rapid, homogeneous synthesis of THF hydrate and control of the hydrate volume fraction in sediments [*Yun et al.*, 2007; *Lee et al.*, 2007]. No gas phase is present during

hydrate formation, meaning hydrate is not forced to form at or near grain contacts. Instead, it is thought that THF hydrate nucleates on mineral surfaces and grows into the pore space. THF hydrate does not dissociate to a gaseous phase, however, meaning many production-related processes are difficult to study with this analog, though production issues based on THF data are discussed by *Lee et al.* [2009]. Within these limitations, hydrate-bearing sediments prepared with THF hydrate have allowed the study of a wide range of material parameters that provide valuable insight to natural hydrate-bearing sediments [*Lee et al.*, 2007; *Santamarina and Ruppel*, 2008; *Yun et al.*, 2005, 2007; *Lee et al.*, 2008; *Cortes et al.*, 2009].

4. SPATIAL VARIABILITY

[42] Spatial variability affects all Earth processes, including all forms of diffusion, flow, and conduction. In turn, these processes impose spatial variability on the pressures, temperatures, and availability of water and methane that define the local gas hydrate stability field [*Chen and Osadetz*, 2008; *Ginsburg and Soloviev*, 1998; *Judd and Hovland*, 2007; *Wood et al.*, 2002]. Spatially varying hydrate distributions affect the interpretation of measurements used to characterize gas hydrate, the procedures for extracting methane from hydrate as an energy resource, and the analysis of hydrate-related geohazards.

[43] Spatial variability in hydrate-bearing sediments is found from the scale of gas hydrate–bearing reservoirs to the submicron scale (Figure 5). Figure 5a presents a seismic line from the Indian National Gas Hydrate Program (NGHP) drill site NGHP-01-21. The vertical scale in Figure 5a is several hundred meters; thus the smallest observed spatial variability is on the order of tens of meters. The location of the ocean floor, a domed structure and stratolithologic variability of the medium below the ocean floor, locations of subocean floor gas, a significant fault, and a possible debris flow can all be inferred from the profile. The presence of methane hydrate, sustained by the confluence of gas accumulation in the dome-like structure with appropriate pressure and temperature conditions, further alters the system's permeability, stiffness, and thermal and electrical properties.

[44] Figure 5b contains well log and core sample data from hole NGHP-01-10D from the Indian NGHP. Logging provides a degree of ''ground truth'' quantification of physical property differences between stratigraphic layers inferred from seismic data. The finer resolution of logging relative to shipboard seismic data reveals vertical heterogeneities on the order of meters to centimeters in which properties such as water content and bulk density can vary significantly even within a single stratum.

[45] Figure 5c shows spatial variability of elastic wave velocities on the centimeter scale. Shear and compressional wave velocities (V_s and V_p) of a pressure core, continuously maintained at its in situ pore pressure, were measured approximately every 7 cm using the instrumented pressure testing chamber. The higher seismic velocities 35 cm from the top suggest increased sediment stiffness, possibly due to the presence of gas hydrate.

[46] Figure 5d demonstrates millimeter-scale variability in density images provided by 3-D X-ray computed tomography (CT) of preserved NGHP core. Additional NGHP CT tomographic images are given by *Clayton et al.* [2008] and *Holland et al.* [2008]. Dark, hydrate-bearing veins are apparent in this fine-grained sediment, demonstrating how hydrate can be inhomogeneously distributed even within a single hydrate-bearing layer. The veins themselves are often a collection of still finer-scale veins [*Priest et al.*, 2008].

[47] X-ray microtomography can reveal submillimeter-scale features, such as in the structure of a frozen sandstone from the Nankai Trough containing hydrate and ice, shown in Figure 5e with a pixel resolution of 5.5 μm. Though at this scale the sample appears somewhat homogeneous, the analysis of possible flow paths through a small portion of the sample shows considerable variability. As Figure 5f demonstrates for a laboratory-made specimen, flow variability can result from the heterogeneous, micron-scale pore space distribution of gas, hydrate, and water.

[48] Each of these measurement scales provides a different perspective on the system. Kilometer-scale measurements are needed to understand large-scale system behavior such as the geologic plumbing and structural traps needed for transporting and concentrating methane. Meter-scale logging and core-based measurements provide system characterizations relevant to methane production applications. Pore-scale observations underlie the conceptual models required for understanding electrical, mechanical, and hydraulic properties of hydrate-bearing sediments.

5. SAMPLING AND HANDLING EFFECTS

[49] Geologic sampling inevitably disturbs natural sediments. The presence of hydrate adds further difficulties during sampling and may aggravate sampling disturbance. Sampling effects in hydrate-free and hydrate-bearing sediments are reviewed here.

5.1. Hydrate-Free Sediments

[50] Sampling-induced changes in the mechanical properties of hydrate-free sediments have been recognized and extensively studied in the geotechnical community. Relevant observations include (1) pore pressure decreases from the in situ hydrostatic pressure when samples are extruded from core recovery systems, potentially subjecting the sample to an effective stress comparable to the in situ vertical effective stress [*Kimura and Saitoh*, 1984]; (2) reduced undrained strength due to the stress release [*Hight et al.*, 1992; *Ladd and Lambe*, 1963; *Santagata and Germaine*, 2002; *Skempton and Sowa*, 1963]; (3) more pronounced effects on the loss of effective stress and undrained strength for soils with plasticity index, PI, below 10%–15% [*Kimura and Saitoh*, 1984; *Matsuo and Shogaki*, 1988; *Siddique et al.*, 2000]; (4) decrease in small-strain shear stiffness (G_{max}) in stiff and/or cemented soils, yet an increase in G_{max} for very soft sediments (database and

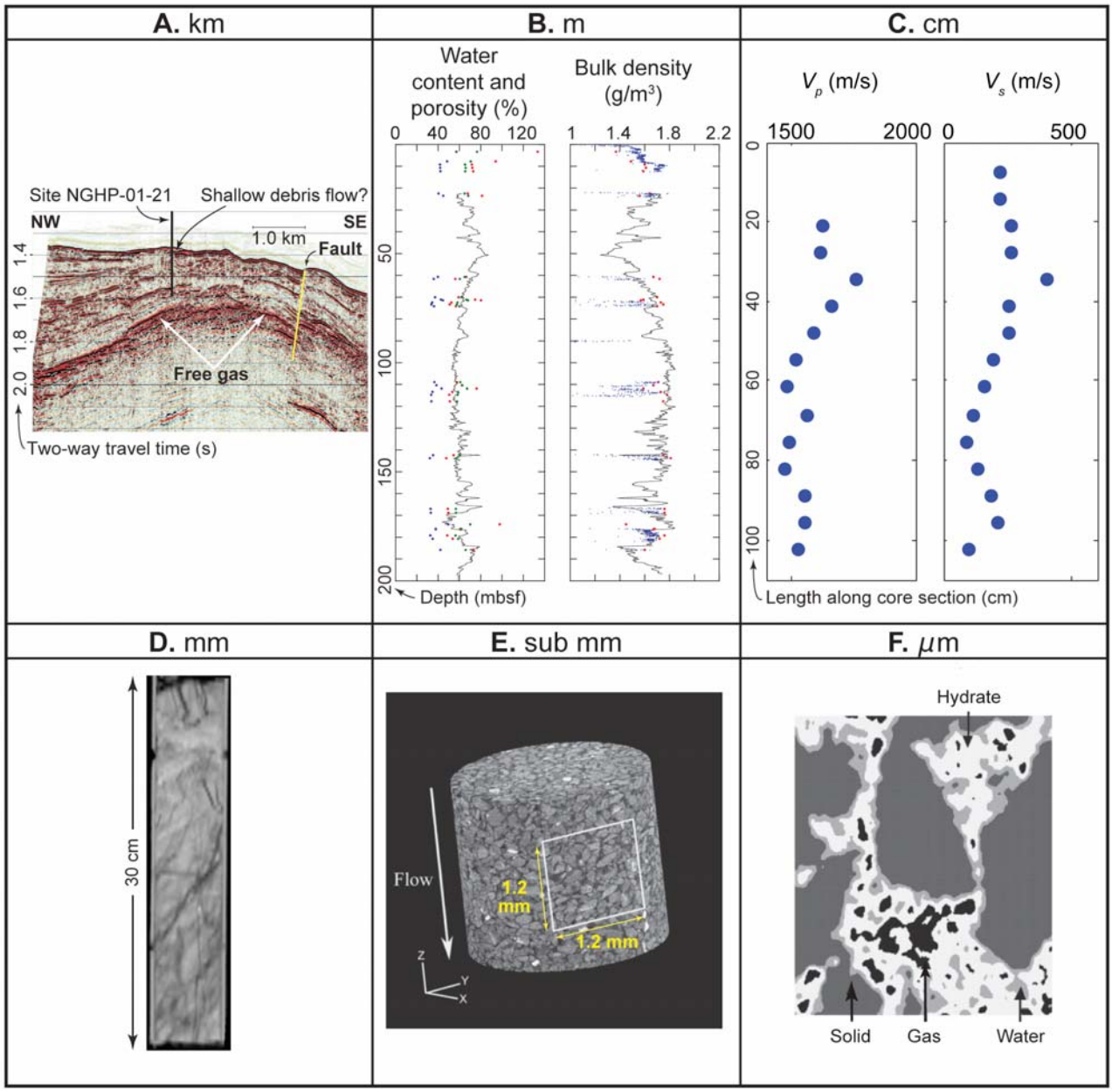

Figure 5. Spatial variability over a range of scales. (a) Seismic line crossing drill site NGHP-01-21 (modified from *Collett et al.* [2008]). Deep-seated high-amplitude reflectors indicate the occurrence of free gas as well as a potential shallow debris flow (vertical scale ~ 750 m). (b) Well log (curves) and core data (points) for site NGHP-01-10 showing profiles of water content and bulk density (modified from *Collett et al.* [2008]). (c) Compressional and shear wave velocity measured by the instrumented pressure testing chamber (NGHP specimen 21A-03E) (Yun et al., submitted manuscript, 2009) (modified from *Collett et al.* [2008]). (d) X-ray computed tomography (CT) scan of a core segment from NGHP 21H (T. Kneafsey, unpublished data, 2007). (e) Three-dimensional X-ray CT image of a sand sample retrieved from the Nankai Trough. The white box is 1.2 mm on a side (reproduced from *Jin et al.* [2007]). Flow is inhomogeneous through this seemingly uniform sample because of pore-scale variability, as observed in Figure 5f. (f) X-ray MicroCT imagery showing the distribution of mineral grains (dark gray), gas (black), water (light gray), and hydrate (white) in a laboratory-made sample (reproduced from *Jin et al.* [2006]).

interpretation by *Rinaldi and Santamarina* [2008]); (5) increased axial strain at peak deviatoric stress with increased disturbance [*Siddique et al.*, 2000]; and (6) friction between the sampler and sediments during sampling, which may produce shear failure and plastic deformation [*Arman and McManis*, 1977; *Hvorslev*, 1949; *Young et al.*, 1983].

5.2. Hydrate-Bearing Sediments

[51] Additional sample disturbance should be expected if pore fluid depressurization leads to gas coming out of solution [*Young et al.*, 1983] and hydrate dissociation. These changes are often not uniform and can impart additional spatial variability to the sample.

TABLE 3. Index Property Definitions[a]

Sediment Type	Property	Definition
General	soil classification	
	porosity, ϕ[b]	$\phi = V_v/V_T$
	specific gravity of solids, G_s	$G_s = \rho_s/\rho_w$
	bulk density, ρ_b (kg m^{-3})	$\rho_b = M_T/V_T$
	water content, w	$w = M_w/M_s$
	pore space hydrate saturation, S_h[b]	$S_h = V_h/V_v$
	mineralogy	
	organic content	
	carbonate content	
	preconsolidation stress (kPa)	
Coarse grained	particle size distribution	D_{10}, D_{60}, D_{30}
	particle size distribution	$C_{\text{unif}} = D_{60}/D_{10}$
	particle size distribution	$C_{\text{curv}} = (D_{30})^2/(D_{10}D_{60})$
	particle shape	
	pore size distribution	
	extreme void ratio, $e_{\min}$, $e_{\max}$	$e = V_v/V_s$
Fine grained	Atterberg limit: liquid limit	LL
	Atterberg limit: plastic limit	PL
	Atterberg limit: plasticity index	PI = LL − PL
	Atterberg limit: liquidity index	LI = (w − PL)/PI
	activity, mineralogy	
	specific surface, S_s (m^2 g^{-1})	
Pore fluid	salinity	
	pH	

[a]Notation is as follows: C_{curv}, coefficient of curvature; C_{unif}, coefficient of uniformity; D_{10}, diameter at which 10% of sample is finer; D_{30}, diameter at which 30% of sample is finer; D_{60}, diameter at which 60% of sample is finer; e, void ratio; $e_{\max}$, maximum void ratio (minimum grain packing); $e_{\min}$, minimum void ratio (maximum grain packing); LI, liquidity index; LL, liquid limit; PI, plasticity index; PL, plastic limit; M_s, mass of solids; M_T, total mass; M_w, mass of water; V_h, volume of hydrate; V_s, volume of solids; V_T, total volume; V_v, volume of voids; w, gravimetric water content based on mass of minerals; ρ_s, density of solids; ρ_w, density of water. These properties and the means by which they are measured are discussed further by *Lambe and Whitman* [1969] and *Mitchell and Soga* [2005].

[b]Though porosity, ϕ, and pore space hydrate saturation, S_h, are often reported as percentages, formulae in which they appear typically require the unitless values defined here in Table 3.

[52] Sampling disturbance in hydrate-bearing sediments can be reduced with pressure coring, in which pore fluid pressure and temperature conditions are maintained within the stability field. Pressure coring was first successfully applied to hydrate-bearing sediment during Ocean Drilling Program Leg 164 [*Dickens et al.*, 1997]. Two pressure coring systems currently in use, the HYACE Rotary Corer and the Fugro Pressure Corer, use a motor driven by mud circulation to rotate the cutting shoe and a water hammer driven percussion to drive the core barrel up to 1 m ahead of the drill bit. The sample is retrieved inside a pressure vessel after closing a valve to preserve the in situ pore fluid pressure.

[53] Pressure coring reduces, but does not eliminate, sample disturbance when recovering hydrate-bearing sediment [*Yun et al.*, 2006]. Current measurement techniques are ineffective at discerning whether observed features reflect in situ conditions or handling and measurement artifacts due to the following:

[54] 1. The loss of effective stress, which eventually decreases nearly to zero in the sediment, results in the sampling effects listed in section 5.1 for sediments without hydrates. The state of effective stress can be restored after sampling, but the in situ soil fabric and internal structure are not fully recoverable.

[55] 2. Shear along the soil–core liner interface affects the periphery of cores even when conditions are kept within the hydrate stability field for their entire recovery and measurement history, as observed in electrical conductivity profiles obtained with millimeter-scale resolution from the periphery of pressure cores (T. S. Yun et al., Hydrate bearing sediments from Krishna-Godavari Basin: Physical characterization, pressure core testing and scaled production monitoring, submitted to *Marine and Petroleum Geology*, 2009).

[56] 3. Creep and diffusion processes are anticipated to affect hydrate distribution and the physical properties measured after pressure cores have been stored for prolonged periods of time.

6. SEDIMENT INDEX PROPERTIES

[57] The properties and behavior of sediments result from complex mechanical, hydraulic, electrical, thermal, and chemical interactions between mineral grains and pore fluids. These interactions are expressed in terms of sediment index properties, which capture grain and pore fluid characteristics that have profound effects on the morphology, extent, and growth characteristics of natural gas hydrate [*Winters et al.*, 1999]. Index properties can be used to anticipate hydrate occurrence, foresee phenomena during production, and estimate engineering properties for design. Salient index properties are listed in Table 3. Note that Tables 3–5 draw a distinction between coarse sediments, with a fines content below 7%, and fine-grained sediment having a fines content exceeding 15% of the sediment by mass. This distinction is drawn because the fines content, meaning the fraction of sediment grains smaller than 0.075 mm, exerts considerable control over the sediment behavior.

6.1. Hydrate Saturation and Distribution

[58] Gas hydrates are found in coarse-grained, fine-grained, and fracture-dominated reservoirs [*Collett et al.*, 2008; *Trehu et al.*, 2006]. As shown in Table 4, field studies suggest that correlations can be made between grain size, other sediment characteristics, and the modes of hydrate occurrence [*Booth et al.*, 1996, 1998]. Coarse-grained reservoirs, such as those found in the Mallik permafrost site in Canada and the Nankai Trough offshore Japan, tend to develop gas hydrate as a pore-filling material, occasionally reaching pore saturations of 80% (Table 4) [*Dallimore et al.*, 1999; *Winters et al.*, 1999]. Low volume fractions of hydrate are reported in fine-grained layers at these sites.

[59] Hydrate has been found extensively in fine-grained sediments elsewhere, however. For some cores taken at sites including the Blake Ridge offshore the U.S. east coast, Gulf of Mexico, offshore Taiwan, Hydrate Ridge offshore western Canada, and Indian Ocean, hydrates were found in fine-grained clayey sediments where the mass of fines content is typically over 60% and as high as 90%. Because of their

TABLE 4. Dominant Characteristics of Gas Hydrate–Bearing Reservoirs

Reservoir Type	Sediment Type	Dominant Gas Hydrate Type	Maximum S_h (%)	LL (PI)	Locations	References
Coarse grained	sand, gravel	pore filling	80	–	Mackenzie Delta	*Dallimore et al.* [1999], *Uchida and Takashi* [2004], and *Winters et al.* [1999]
				–	Nankai Trough	*Uchida and Takashi* [2004]
Fine grained	clay, silt	finely disseminated, nodules, layers	typically 10 except in discrete layers of segregated hydrate	0.68–0.99 (0.44–0.64)	Blake Ridge	*Paull and Matsumoto* [2000], *Trehu et al.* [2004], *Winters* [2000], and *Winters et al.* [2007]
				0.51–1.02 (0.28–0.57)	Gulf of Mexico	*Francisca et al.* [2005] and *Yun et al.* [2006]
				0.64–0.87 (0.25–0.45)	Hydrate Ridge	*Tan et al.* [2006]
				0.73–0.75 (0.34–0.36)	offshore India	Yun et al. (submitted manuscript, 2009)
Fractured	clay, silt	complex vertical veins	100 in discrete fractures	unknown	offshore India	*Collett et al.* [2008] and *Winters et al.* [2008]

abundance, fine-grained marine sediments collectively contain more gas hydrate than all coarse-grained reservoirs, even though disseminated gas hydrate saturations in the pore space of fine-grained sediments are typically <10%. As indicated in Figures 4 and 5, however, hydrate in fine-grained sediments often forms in localized areas of elevated permeability associated with slightly increased sediment grain size [*Ginsburg et al.*, 2000] or faults [*Nimblett and Ruppel*, 2003; *Wood and Ruppel*, 2000]. In these cases, hydrate can form inhomogeneously as discrete nodules, sheets, or lenses [*Clennell et al.*, 1999; *Cook et al.*, 2008; *Stern and Kirby*, 2008; *Trehu et al.*, 2004].

6.2. Phenomena During Production

[60] Index properties can be used to predict sediment behavior during methane production. For example, sand production [*Walsh et al.*, 2009] or flow clogging due to migrating fine-grained material [*Goldsztein and Santamarina*, 2004; *Valdes and Santamarina*, 2007] may accompany methane production from coarse-grained hydrate-bearing sediments, while hydraulic fracturing and leaky reservoirs should be expected when producing methane from fine-grained sediments.

6.3. Estimation of Design Parameters

[61] The use of index properties to obtain qualitative or semiquantitative estimates of baseline (hydrate-free) sediment behavior is based on correlations developed for sediments around the world [*Lambe and Whitman*, 1969; *Mayne et al.*, 1992; *Mitchell and Soga*, 2005; *Santamarina et al.*, 2001; *Terzaghi et al.*, 1996]. Examples are presented in Table 5.

7. THERMAL PROPERTIES

[62] A material's response to the addition or loss of heat is described using the thermal conductivity, λ (W m^{-1} K^{-1}); specific heat, c_p (J kg^{-1} K^{-1}); and thermal diffusivity, κ (m^2 s^{-1}). Heat flow in materials undergoing a phase change such as hydrates undergoing formation or dissociation is described by the enthalpy of reaction, ΔH (J mol^{-1}). The thermal properties of hydrate-bearing sediment components are summarized in Tables 6 and 7.

TABLE 5. Correlations Between Baseline Hydrate-Free Sediment Index Properties[a]

Parameter	Correlation	Reference
Compressibility	$C_c \approx 0.009(\mathrm{LL} - 10)$	*Terzaghi et al.* [1996]
	$C_c \approx [(\mathrm{PI})G_s]/200$	*Wroth and Wood* [1978]
Shear strength	$S_u = \sigma_v'[0.11 + 0.0037(\mathrm{PI})]$	*Skempton* [1957]
Friction angle (fine)	$\Phi_{cv} = 0.8 - 0.094 \ln(\mathrm{PI})$	*Mitchell and Soga* [2005]
Friction angle (coarse)	$\Phi_{cv} = 42 - 17R$	*Santamarina and Cho* [2004]
Hydraulic conductivity (fine)	$K = \frac{1}{S_s^2}\frac{\theta\gamma_w}{\mu\rho_m^2}\frac{e^3}{1+e}$	*Perloff and Baron* [1976]
Hydraulic conductivity (coarse)	$K = C_H(D_{10})^2$	Hazen's equation [*Holtz and Kovacs*, 1981]
e_{max}	$e_{max} = 0.359 + 0.082R^{-1}$	*Santamarina and Cho* [2004]
e_{min}	$e_{min} = 0.554 + 0.154R^{-1}$	*Santamarina and Cho* [2004]

[a]Notation is as follows: C_c, compression index; C_H, Hazen's empirical coefficient, ~100 (cm s)$^{-1}$ or 1×10^4 (m s)$^{-1}$ [*Carrier*, 2003]. D_{10}, diameter at which 10% of sample is finer; e, void ratio; e_{max}, maximum void ratio; e_{min}, minimum void ratio; K, hydraulic conductivity; LL, liquid limit; PI, plasticity index; R, roundness (particle shape); S_s, specific surface; S_u, undrained shear strength; γ_w, unit weight of water = $\rho_w g$, where ρ_w is mass density of water and g is 9.8 m s^{-2}; μ, dynamic fluid viscosity; θ, shape and tortuosity factor; ρ_m, mass density of mineral grains; σ_v', effective overburden stress at failure; Φ_{cv}, friction angle during constant volume shear, also known as the critical state friction angle.

TABLE 6. Thermal Properties of Hydrate-Bearing Sediment Components[a]

Material	λ (W m^{-1} K^{-1})	κ (m^2 s^{-1})	c_p (J kg^{-1} K^{-1})	ρ (kg m^{-3})
Air	0.024[b] (273 K)	183×10^{-7}[c]	1010[b] (273 K)	1.298[d] (272 K)
Water	0.56[e] (273 K)	1.33×10^{-7}[c]	4218[e] (273 K)	999.9[e] (273 K)
Water	0.58[e] (283 K)	1.38×10^{-7}[c]	4192[e] (283 K)	999.7[e] (283 K)
Ice Ih	2.21[f] (270 K)	11.7×10^{-7}[c]	2052[g] (270 K)	917[h] (273 K)
Methane gas	0.0297[i] (260 K, 1 MPa)	18.0×10^{-7}[c]	2170[d] (260 K)	7.61[j] (260 K, 1 MPa)
Methane gas	0.099[i] (260 K, 40 MPa)	1.6×10^{-7}[c]	2170[d] (260 K)	286[j] (260 K, 40 MPa)
Methane hydrate, $CH_4 \cdot 6H_2O$	0.57[k] (263 K)	3.35×10^{-7}[l]	2031[m] (263 K)	929[n] (263 K)
THF + water, THF $\cdot$ 17H_2O	0.47[f,o] (283 K)	3.12×10^{-7}[c]	4080[p] (282 K)	982[q] (283 K)
THF hydrate, THF $\cdot$ 17H_2O	0.5[f] (261 K)	2.55×10^{-7}[f]	2020[f] (261 K)	971[r] (273 K)
THF hydrate, THF $\cdot$ 17H_2O	0.5[f] (261 K)	2.60×10^{-7}[c]	1980[s] (260 K)	971[r] (273 K)
Quartz	7.7 to 8.4[t]	41×10^{-7}[c]	730[b] (273 K)	2650[h]

[a]Temperature is in kelvins, and pressure is in megapascals. THF, tetrahydrofuran.
[b]Kaye and Laby (Tables of Physical and Chemical Constants, National Physical Laboratory, 2008, http://www.kayelaby.npl.co.uk/).
[c]Calculated from equation (4).
[d]Engineering ToolBox (Material Properties, available at http://www.engineeringtoolbox.com/).
[e]*Weast* [1987].
[f]*Waite et al.* [2005].
[g]*Leaist et al.* [1982].
[h]*Dvorkin et al.* [2000].
[i]*Vargaftik et al.* [1993].
[j]*Sychev et al.* [1987].
[k]*Huang and Fan* [2004].
[l]*Turner et al.* [2005].
[m]*Handa* [1986].
[n]*Waite et al.* [2007].
[o]*BASF Corporation* [1998].
[p]*Tombari et al.* [2006].
[q]*Smallwood* [2002].
[r]*Mork et al.* [2000].
[s]*Handa et al.* [1984].
[t]*Revil* [2000].

7.1. Thermal Conductivity, λ

[63] Thermal conductivity quantifies the efficiency of heat transport. In sediments, this involves transport (1) from grain to grain, (2) from grain to liquid to grain, and (3) through pore-filling liquid [*deMartin*, 2001; *Waite et al.*, 2002; *Yun and Santamarina*, 2008]. Rather than calculate the contribution of each heat transport path explicitly, thermal conductivity is often estimated using a two-phase mixing model to combine the thermal conductivities of the sediment grains with the pore fluid. As shown in Tables 6 and 7, the thermal conductivities of methane hydrate and water differ by <10% at the temperatures found in hydrate-bearing sediments [*Huang and Fan*, 2004; *Waite et al.*, 2007; *Weast*, 1987]. For this reason, first-order thermal conductivity estimates can neglect the presence of methane hydrate and assume the sediment pore space contains only water [*Ruppel*, 2000].

[64] The presence of gas complicates the analysis by adding a phase with strongly contrasting thermal properties (Table 6). The pore fluid can no longer be treated simply by averaging the thermal conductivities of water and gas because as the wetting phase, water migrates to contacts and enhances grain-to-grain conduction. Hence, even low degrees of water saturation have a strong effect on thermal conductivity [*Andersland and Ladanyi*, 2004; *Farouki*, 1985; *Lu et al.*, 2007; *Singh and Devid*, 2000].

[65] As described by *Cortes et al.* [2009], even in gas-free systems, precise thermal conductivity calculations must account for sediment-altering processes caused by hydrate formation, including porosity changes [*Tarnawski et al.*, 2002] and the associated effective stress changes [*Sridhar and Yovanovich*, 1996], as well as the improved thermal transport across the sediment grain–hydrate interface compared to the sediment grain–water interface [*Swartz and Pohl*, 1989].

[66] Despite these shortcomings, simple mixing models provide reasonable bounds for thermal conductivity values. As shown in Table 8 and Figure 6, the parallel model, in which heat travels simultaneously through the pore fill and the sediment grains, and the series model, in which heat

TABLE 7. Temperature Dependence of Methane Hydrate Thermal Properties[a]

Temperature Dependence Fit Equations	Temperature Range
λ (W m^{-1} K^{-1}) = $-(2.78 \pm 0.05) \times 10^{-4} T$ (°C) + (0.624 ± 0.001)	−20°C to 17°C[b]
λ (W m^{-1} K^{-1}) = $-1.99 \times 10^{-4} T$ (°C) + 0.682	−12°C to 4°C[c]
κ[d] (m^2 s^{-1}) = $(4.70 \pm 0.02) \times 10^{-5}/T$ (K) + $(1.35 \pm 0.03) \times 10^{-7}$	−128°C to 17°C[b] (145 to 290 K)
c_p (J kg^{-1} K^{-1}) = $(6.1 \pm 0.3)T$ (°C) + (2160 ± 20)	1°C to 17°C[b]
c_p (J kg^{-1} K^{-1}) = $13T$ (°C) + 2215	−9°C to 3°C[e]

[a]Temperatures in Celsius unless otherwise noted.
[b]*Waite et al.* [2007], measured at 31.5 MPa.
[c]*Rosenbaum et al.* [2007], measured between 2.5 and 43.7 MPa.
[d]The T^{-1} dependence of the κ fit requires input temperatures in kelvins.
[e]*Nakagawa et al.* [2008], measured at 5 MPa.

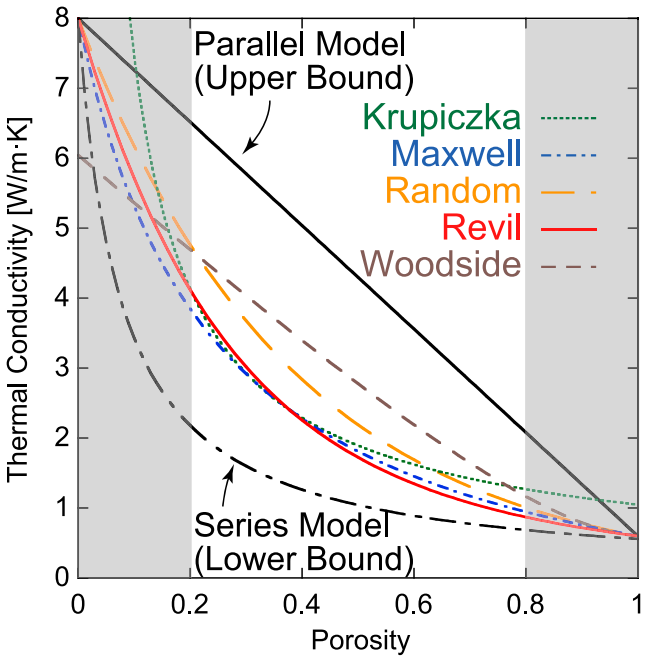

Figure 6. Model predictions for mixtures of quartz (8.0 W m^{-1} K^{-1}) and water (0.6 W m^{-1} K^{-1}). White region denotes the range of relevant porosities.

alternates between flowing through the pore fill and the sediment, provide the upper and lower bounds, respectively, for thermal conductivity. The models of *Krupiczka* [1967], *Maxwell* [1954], and *Revil* [2000], collected by *Revil* [2000], yield similar results lying midway between the upper and lower bounds.

7.2. Specific Heat, c_p

[67] Specific heat measures the heat stored in, or extracted from, a material due to a temperature change. Unlike thermal conductivity, specific heat depends only on the mass fractions of sediment, hydrate, and water rather than on their pore-scale distribution and interfacial effects. Using the subscripts m, w, and h to refer to the host sediment mineral, pore water, and methane hydrate, respectively, the formation's bulk specific heat, $c_{p.b}$, is given for a gas-free system by

$$c_{p.b}\rho_b = c_{p.m}\rho_m(1-\phi) + c_{p.w}\rho_w(1-S_h)\phi + c_{p.h}\rho_h S_h\phi, \quad (2)$$

where ρ_b is given by the mass fractions of the sediment grains, water, and hydrate,

$$\rho_b = \rho_m(1-\phi) + \rho_w(1-S_h)\phi + \rho_h S_h\phi. \quad (3)$$

Here the porosity, ϕ, and hydrate saturation, S_h, must be considered in decimal notation rather than in units of percent.

[68] Because the specific heat of methane hydrate is less than half that of water, hydrate formation can significantly lower the specific heat of hydrate-bearing sediments [*Waite et al.*, 2007]. Hydrate-bearing layers with potentially economic hydrate saturations for production, such as the Mallik 5L-38 permafrost hydrate well with porosity, ϕ, of ~35% and methane hydrate saturation, S_h, of ~80% [*Collett et al.*, 2005], are particularly affected by the presence of hydrate [*Kurihara et al.*, 2005; *Moridis et al.*, 2005]. Depending on sediment porosity, even in sediments with moderate hydrate saturations of 20%–40%, the specific heat is reduced by ~10% relative to hydrate-free sediment [*Waite et al.*, 2007].

7.3. Thermal Diffusivity, κ

[69] Thermal diffusivity is a measure of the rate at which a body changes temperature when subjected to an external heat flux. In the absence of systematic studies of thermal diffusivity, we quantify the effect of hydrate on the properties of hydrate-bearing sediment by combining the thermal conductivity, λ; specific heat, c_p; and density, ρ, results discussed in sections 7.1 and 7.2 with the definition of thermal diffusivity, κ,

$$\kappa = \frac{\lambda}{\rho c_p}. \quad (4)$$

[70] The thermal diffusivity of methane hydrate is more than twice that of water; therefore, hydrate-bearing sedi-

TABLE 8. Common Thermal Conductivity Mixing Models[a]

Model	Equation for the Estimation of $\lambda_{effective}$
Parallel (upper bound) [*Huang and Fan*, 2005]	$\phi\,\lambda_f + (1-\phi)\lambda_s$
Series (lower bound) [*Huang and Fan*, 2005]	$\frac{\lambda_s\lambda_f}{\phi\,\lambda_s+(1-\phi)\,\lambda_f}$
Krupiczka [1967]	$\lambda_f\left(\frac{\lambda_s}{\lambda_f}\right)^{A+B\log_{10}\left(\frac{\lambda_s}{\lambda_f}\right)}$, $A = 0.280 - 0.757\log_{10}(\phi)$, $B = -0.057$
Maxwell [1954]	$\lambda_f\frac{2\phi\lambda_f+(3-2\phi)\lambda_s}{(3-\phi)\lambda_f+\phi\lambda_s}$
Random [*Huang and Fan*, 2005]	$\lambda_f^{\phi}\lambda_s^{(1-\phi)}$
Revil [2000]	$\frac{\lambda_f}{\xi}\left[\xi\,\Theta+\frac{1}{2}(1-\Theta)\left(1-\Theta+\sqrt{(1-\Theta)^2+4\xi\,\Theta}\right)\right]$, $\Theta=\frac{\lambda_s}{\lambda_f}$, $\xi=\phi^{\left(\frac{m}{1-m}\right)}$
Woodside and Messmer [1961]	$A\lambda_f + \frac{B\lambda_s\lambda_f}{\lambda_s(1-C)+C\lambda_f}$, $A=\phi-0.03$, $B=1-A$, $C=(1-\phi)/B$

[a]See Figure 6 for an illustration of their behavior in a quartz sediment and water system.

ments can change temperature more rapidly than hydrate-free sediments [*Waite et al.*, 2007]. In sediment with porosity $\phi = 35\%$, a hydrate saturation $S_h = 35\%$ increases heating rates by more than 10% relative to those in the absence of hydrate. This effect is magnified in high-porosity formations, such as the 74% porosity, near-surface sediments on the Congo continental slope [*Sultan et al.*, 2004b]. In this environment, hydrate saturations of only 19%–22% reduce heating times relative to hydrate-free sediment by more than 10%. Hydrate should therefore be accounted for in transient heat flow applications such as safety assessments for drilling into or through hydrate-bearing sediment [*Briaud and Chaouch*, 1997; *Hadley et al.*, 2008; *Ji et al.*, 2003; *Pooladi-Darvish*, 2004].

7.4. Enthalpy of Reaction, ΔH

[71] The organized hydrate structure has less internal energy than a freely moving, disordered combination of methane and water, so energy must be released for hydrate to form and reabsorbed for hydrate to dissociate [*Rydzy et al.*, 2007]. This energy change is defined as the enthalpy of reaction, ΔH.

[72] Calorimetry can provide measurements of ΔH, but only a limited number of studies are available. Enthalpies can also be estimated from phase equilibrium and thermodynamic data using the Clausius-Clapeyron equation to relate pressure, P; temperature, T; enthalpy, ΔH; and compressibility, Z:

$$\frac{d\ln P}{d\left(\frac{1}{T}\right)} = \frac{-\Delta H}{ZR}, \tag{5}$$

where R is the ideal gas constant. The validity of this method is contingent upon negligible changes in compressibility. There is good agreement between experimental results and indirectly derived enthalpies from the Clausius-Clapeyron method.

[73] The ice-water enthalpy of melting is $\sim$6 kJ mol^{-1} [*Handa*, 1986; *Kumano et al.*, 2007]. Per mole of guest molecule, the enthalpy of dissociation of structure I methane hydrate into methane gas and liquid water is ΔH = 52.7–56.9 kJ mol^{-1} at $T \sim 0$°C [*De Roo et al.*, 1983; *Deaton and Frost*, 1946; *Handa*, 1986; *Kang et al.*, 2001; *Kuuskraa et al.*, 1983; *Lee et al.*, 2005; *Lievois et al.*, 1990; *Rueff et al.*, 1988; *Sloan and Fleyfel*, 1992; *Voronov et al.*, 2008]. ΔH is insensitive to pressure and temperature for conditions typical in terrestrial applications, remaining in the range 54.44 ± 1.46 kJ mol^{-1} between 5.5 and 19.3 MPa and 7.5°C–18.5°C [*Gupta et al.*, 2008].

[74] Replacing just 1% of the hydrate methane with ethane, however, increases ΔH by $\sim$30% to 68.7 kJ mol^{-1} [*Rydzy et al.*, 2007], and a structure II propane hydrate has a ΔH of 129.2 kJ mol^{-1} [*Handa*, 1986]. This illustrates that ΔH depends on the guest molecule but is primarily controlled by the number of hydrogen-bonded water molecules. Typically, there are $\sim$6 water molecules per guest molecule in structure I hydrate [*Circone et al.*, 2005, 2006] but $\sim$17 per guest in structure II hydrate [*Davidson*, 1973].

[75] The heat of reaction can be significant when generating hydrate for storing large volumes of gases. When dissociating hydrate to produce methane from permafrost regions or beneath the ocean floor, the heat absorbed during hydrate dissociation can cool the surroundings, resulting in secondary hydrate or ice formation, both of which reduce the permeability of the producing formation [*Moridis et al.*, 2008]. Moreover, the enthalpy variation with guest occupant means the heat of reaction for dissociation may not be constant throughout a formation, nor over the lifetime of a production well, complicating production rate predictions.

8. PERMEABILITY AND FLUID MIGRATION

[76] Permeability controls fluid migration through sedimentary systems and plays an important role in heat and chemical transfer occurring via fluid migration. In hydrate-bearing sediments, permeability affects dissolved gas and free gas transport as well as the accumulation, distribution, and concentration of hydrate [*Bhatnagar et al.*, 2007; *Garg et al.*, 2008; *Liu and Flemings*, 2007; *Nimblett and Ruppel*, 2003]; the ability to produce gas from hydrate reservoirs [*Moridis*, 2003; *Moridis et al.*, 2004, 2007]; local perturbations of the hydrate stability field [*Wood et al.*, 2002]; and methane flux to the ocean [*Moridis and Reagan*, 2007a, 2007b; *Reagan and Moridis*, 2007]. In spite of the importance of flow through hydrate-bearing systems [*Gbaruko et al.*, 2007; *Haacke et al.*, 2007; *Hensen and Wallmann*, 2005; *Shankar et al.*, 2006], few reliable permeability measurements are available [*Minagawa et al.*, 2005, 2008; *Nadem et al.*, 1988].

[77] Macroscale analyses of single-phase and multiphase flow in sediments generally assume the sediments can be represented by an equivalent homogeneous porous medium; however, a proper understanding of conduction properties requires the pore-scale assessment of the multiple coexisting phases and of all relevant flow pathways.

8.1. Single-Phase Fluid Flow

[78] Single-phase flow rate, q (m^3 s^{-1}), through a porous medium under laminar conditions is described by Darcy's law,

$$q = \frac{-k\rho_f g}{\mu_f}\frac{d\left(\frac{P}{\rho_f g} + z\right)}{dl}A, \tag{6}$$

where A (m^2) is the cross-sectional area, z (m) is the elevation above a reference datum, P (Pa) is the pressure at elevation z, μ_f (Pa s) is the dynamic fluid viscosity, l (m) is the length over which the flow-driving change ($P/\rho g + z$) is measured, k (m^2) is the intrinsic permeability of the porous medium, ρ_f (kg m^{-3}) is the mass density of the fluid, and $g = 9.8$ m s^{-2} is the acceleration due to gravity.

[79] The intrinsic permeability is a measure of fluid flowability through a porous medium, and it is determined

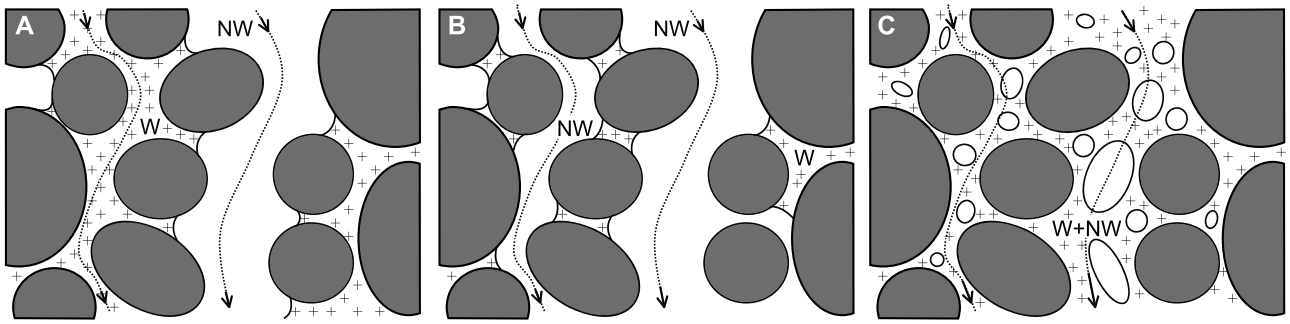

Figure 7. Illustrations showing end-member multiphase fluid saturations and complexity of multiphase flow. (a and b) Stable fluid interfaces and (c) unstable conditions. In Figure 7a, phases occupy different channels according to wettability properties: nonwetting phase (NW) occupies larger pores, and wetting phase (W) occupies smaller pores. In Figure 7b, wetting phase is discontinuous and isolated to small pore throats. The wetting phase irreducible saturation has been reached in Figure 7b, and only the nonwetting fluid flows. In Figure 7c, both phases flow together, one dispersed in the other.

by the interconnectivity and size of voids within the medium. The tortuosity, θ, defined as the ratio $(l/l_E)^2$ accounts for the effective flow path, l_E, being longer than the sample length, l. Typical values for θ range from 0.4 to 0.8 [*Bear*, 1972]. Physically, the dependence on void size, which can also be expressed as a specific surface area, S_s (m^2), represents the frictional drag between the flowing fluid and the sediment grain surfaces.

[80] The Kozeny-Carman model captures the permeability's strong dependence on sediment specific surface area, S_s; the role of tortuosity, θ; and the lesser effect of void ratio, e (form adapted from *Perloff and Baron* [1976]):

$$k = \left(\frac{\theta}{\rho_m^2 S_s^2}\right)\left(\frac{e^3}{1+e}\right), \tag{7}$$

where the grain mineral density, ρ_m, relates the gravimetric specific surface to the volumetric nature of permeability (see other models in Table 5). The intrinsic permeability of a sediment given in equation (7) can be converted to the hydraulic conductivity for a given fluid (Table 5) by taking into consideration the fluid dynamic viscosity, μ_f, and unit weight, $\rho_f g$, through a multiplicative factor, $\rho_f g/\mu_f$.

[81] The correlation beteween specific surface area and permeability is readily established with clays (Table 5 [*Carrier*, 2003]), but it can be useful to relate permeability to sediment size rather than specific surface area. To convert from specific surface area to grain size, consider that a particle's surface area is determined by its smallest dimension, which corresponds to the diameter of rotund sandy grains or the thickness of platy clay particles. When this observation is extended to the entire sediment mass, it follows that the specific surface of sediments is governed by the specific surface of the finest fraction. Hence, k correlates well with the size of the finer grains in sandy sediments, D_{10}, as in Hazen's equation (Table 5).

[82] Given the wide range in particle sizes, permeability varies over 10 orders of magnitude between clay and clean sand sediments [*Dullien*, 1992]. In general, expressions based on sediment index properties such as S_s and D_{10} provide order-of-magnitude permeability estimates only. In addition, other local geologic features such as grain orientation anisotropy, lithology, fractures, stratigraphic variability, or hydrate presence can all produce dramatic changes in the permeability field, and empirical relations should be used with care.

[83] Laboratory measurements show that permeability is scale-dependent [*Tidwell and Wilson*, 1997] as all natural media have some degree of spatial variability (Figures 4 and 5). Thus, permeability measured on the core scale will differ from permeability inferred from field-scale flow measurements. Complementary core-scale information gathered using X-ray CT imaging [*Jin et al.*, 2007], electrical measurements (section 9), and NMR [*Kleinberg et al.*, 2005; *Kleinberg et al.*, 2003] helps develop robust conceptual models that can then be upscaled based on seismic imagery to handle field-scale spatial variability in simulations of flow in hydrate-bearing sediments.

8.2. Multiphase Fluid Flow

[84] Steady state immiscible flow in multiphase systems, such as gas and water flow in hydrate systems, can be modeled as Darcian flow by incorporating relative permeabilities for water, k_{rw}, and gas, k_{rg},

$$q_w = -k_{rw}\frac{k\rho_w g}{\mu_w}\frac{d\left(\frac{P_w}{\rho_w g}+z\right)}{dl}A \tag{8}$$

$$q_g = -k_{rg}\frac{k\rho_g g}{\mu_g}\frac{d\left(\frac{P_g}{\rho_g g}+z\right)}{dl}A. \tag{9}$$

[85] The dimensionless relative permeabilities k_{rw} and k_{rg} vary from 0 to 1 and are functions of phase saturations, the

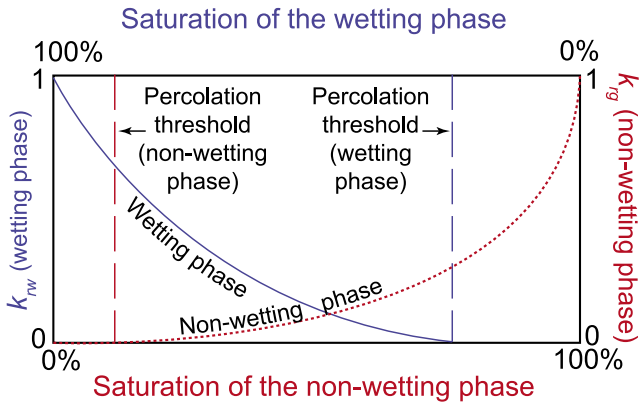

Figure 8. Relative permeability curves for a two-phase flow system. Interfacial tension causes the nonlinearity in the relative permeability curves for water, k_{rw}, and gas, k_{rg}, and imposes percolation thresholds marking the lower saturation limit required for conventional fluid flow. While the two phases interfere with each other's flow, $k_{rw} + k_{rg} < 1$. Shown are the typical curve shapes for water and gas. For water or gas saturations below their respective percolation limits, water can flow as a film or vapor phase, and gas can flow as a dissolved phase. These types of flow are limited and hence do not contribute to the relative permeabilities plotted in Figure 8.

spatial distribution of the phases, mineral wettability, and pore space geometry (Figure 7). Relative permeabilities k_{rw} and k_{rg} vary with water and gas saturations as shown in Figure 8 (see *Dong and Dullien* [2006] for numerical examples). Note that relative permeabilities typically add up to <1 because of fluid-to-fluid interactions. For example, water wets mineral surfaces in most sediments; this preferential wetting means that gas or oil will tend to occupy larger pore spaces and significantly reduce water flow.

[86] Water saturation, S_w, is determined by the pressure difference between fluid and gas, or capillary pressure, $\Delta P = P_g - P_w$, which depends on the pore size distribution in the sediment (see section 2.2). A common model used to capture this dependency follows the formulations of *van Genuchten* [1980], shown here in the form from *Parker et al.* [1987],

$$S_{\text{w\_eff}} = \left[1 + \alpha^n \left(\frac{\Delta P}{g\rho_w}\right)^n\right]^{-m} = \frac{S_w - S_{\text{w\_irr}}}{1 - S_{\text{w\_irr}}}, \qquad (10)$$

where $m = (n - 1)/n$. Note that the expression is in terms of the effective water saturation, $S_{\text{w\_eff}}$, which is the actual water saturation, S_w, corrected for the sediment irreducible water saturation, $S_{\text{w\_irr}}$. The fitting parameter α is related to the modal pore size, while n is a function of the spread of the pore size distribution. For example, α is 4.57 m^{-1} and n is 7.43 for a volcanic sand, α is 1.94 m^{-1} and n is 9.06 for Berea Sandstone, and α is 0.15 m^{-1} and n is 1.17 for Biet Netofa clay (values for additional materials are compiled by *Carsel and Parrish* [1988] and by *Ghezzehei et al.* [2007]).

[87] In terms of the effective water saturation, the relative permeabilities of water and gas are given by [*Parker et al.*, 1987]

$$k_{rw} = S_{\text{w\_eff}}^{1/2}\left[1 - \left(1 - S_{\text{w\_eff}}^{1/m}\right)^m\right]^2 \qquad (11)$$

$$k_{rg} = C(1 - S_{\text{w\_eff}})^{1/2}\left(1 - S_{\text{w\_eff}}^{1/m}\right)^{2m}, \qquad (12)$$

where C is a "gas slippage" correction that approaches 1 as the grain size increases. Other models include the Brooks and Corey model [*Honarpour et al.*, 1986; *Pruess and Moridis*, 1999] and the Stone power model [*Rutqvist and Moridis*, 2007].

8.3. Fluid Flow in Hydrate-Bearing Systems

[88] The presence of hydrate adds additional complications because hydrate can alter flow and affect permeability by reducing the pore size and changing the pore shape. Pore-filling hydrate reduces the permeability more significantly than mineral-coating hydrate [*Liu and Flemings*, 2007]; however, hydrate at grain contacts can readily block pore throats, causing a more pronounced reduction in permeability. Based on the limited data available for gas-free, hydrate-bearing systems [*Minagawa et al.*, 2008], pore-filling hydrate models provide the best estimates of permeability [*Kleinberg et al.*, 2003; *Lee*, 2008].

[89] Water-saturated systems evolve into multiphase gas and water systems if gas invades the hydrate stability field [*Flemings et al.*, 2003; *Liu and Flemings*, 2006, 2007] or if hydrate begins dissociating [*Tryon et al.*, 2002]. The van Genuchten model described in section 8.2 has been adapted to the simulation of dissociation in hydrate-bearing sediments [*Hong and Pooladi-Darvish*, 2005; *Moridis et al.*, 2005]. However, the evolution of water saturation and capillary pressure during dissociation differs from imbibition processes typically used to determine the water retention curve and relative permeability values for sediment.

[90] There are also additional particle-scale mechanisms that impact relative permeability. For example, where hydrate supports the frame of the medium, permeability may increase as hydrate is removed from the system but then decrease as the granular skeleton collapses. Hence, further research is still required to better quantify relative gas and water permeabilities in hydrate-bearing sediment and their evolution during dissociation.

9. ELECTROMAGNETIC PROPERTIES

[91] Three electromagnetic phenomena have direct applications to the study of hydrate-bearing sediments: steady state charge migration under an applied constant electric field (conduction), frequency-dependent polarization (permittivity), and magnetization (permeability). Inertial and viscous forces oppose charge displacement and rotations, meaning that permittivity and magnetic permeability are

frequency-dependent, and their response is partially out of phase with the electrical excitation. Permittivity and magnetic permeability are therefore expressed as complex numbers to capture both the magnitude of each parameter and its phase relative to the excitation. Symbolically, these three electromagnetic parameters are electrical conductivity, σ; complex permittivity (relative to "free space" ε_0), $\kappa^* = \kappa' - j\kappa''$; and complex permeability (relative to "free space" μ_0), $\mu^* = \mu' - j\mu''$.

[92] Components of hydrate-bearing sediments are generally nonferromagnetic, and the magnetic permeability is assumed to be $\mu^* \approx 1$. This section therefore focuses on the conductivity and permittivity of hydrate-bearing sediments. Both properties reflect characteristics of the sediment components, their volume fraction, and their spatial arrangement. Detailed reviews and estimation guidelines for these parameters are given by *Santamarina et al.* [2001, 2005]; a comprehensive database of permittivity and conductivity measurements for hydrate-bearing clay, silt, and sand at different effective stress and hydrate saturation levels is documented by *Lee* [2007] and J. Y. Lee et al. (Parametric study of the physical properties of hydrate-bearing sand, silt, and clay sediments. Part I: Electromagnetic properties, submitted to *Journal of Geophysical Research*, 2009).

9.1. Electrical Conductivity of Hydrate-Bearing Sediments

[93] Electrical conduction in sediments consists of the movement of hydrated ions in the pore fluid and in electrical double layers around mineral surfaces. The electrical conductivity of the pore water, σ_w, is proportional to the concentration, c, of mobile hydrated ions, $\sigma_w = \zeta c$. The molar conductivity, ζ, describes the ionic mobility, a characteristic parameter for each ion, which decreases as the ion's concentration approaches saturation. The following empirical approximation is valid for seawater [*Annan*, 1992]:

$$\sigma_w = 0.15(\mathrm{TDS}), \tag{13}$$

where σ_w is in mS m^{-1} and the total dissolved solids (TDS) are in mg L^{-1}. A nominal value for seawater conductivity is 3 S m^{-1}.

[94] Hydrated counterions are always present in the vicinity of minerals to neutralize their surface charge. These counterions also move when an electric field is imposed, contributing surface conduction, λ_{ddl}, to the bulk conduction. Mineral surface conduction becomes significant in sediments with a high specific surface area, S_s, such as clayey sediments; when the porosity is low, meaning that there is more mineral surface area per volume; and when the conductivity of the pore fluid is low, such as after hydrate dissociation and subsequent pore water freshening.

[95] The electrical conductivity of hydrate-bearing sediments is dominated by the electrical conductivity of the pore fluid, σ_f, scaled by the volume fraction of liquid in pores, $\phi(1 - S_h - S_g)$. However, surface conduction must also be considered in high surface area sediments. A first-order approximation to the conductivity of hydrate-bearing sediments is [*Klein and Santamarina*, 2003]

$$\sigma_b = \sigma_f \phi\left(1 - S_h - S_g\right) + \frac{2}{2+e}\,\lambda_{ddl}\rho_m S_s, \tag{14}$$

where e is the void ratio and the hydrate, gas, and water saturations are defined in terms of V_v, the pore volume in the mineral skeleton: $S_h = V_h/V_v$, $S_g = V_g/V_v$, and $S_w = V_w/V_v$ so that $1 = S_g + S_h + S_w$.

[96] Equation (14) does not account for the relative spatial arrangement of the mineral grains; fluid, hydrate, and gas phases; nor their interconnectedness [*Spangenberg*, 2001; *Spangenberg and Kulenkampff*, 2006]. Archie's semiempirical expression is often used to add degrees of freedom to the expression in order to describe these interactions but fails to capture surface conduction accounted for in equation (14) [*Archie*, 1942]. In terms of resistivities, $\rho = 1/\sigma$,

$$\left(1 - S_h - S_g\right) = \left(\alpha \frac{\rho_f}{\rho_b}\phi^{\beta}\right)^{\frac{1}{\chi}}, \tag{15}$$

where α, β, and χ are empirically determined parameters. This equation is extensively applied in hydrate studies, as summarized in Table 9 (see typical field data given by *Jin et al.* [2002]). Because Archie-type equations fail to properly capture the additive contribution of surface conduction, the reliability of Archie parameters (Table 9) in applications such as production monitoring studies requires careful reassessment [*Lee et al.*, 2008; *Santamarina and Ruppel*, 2008].

9.2. Permittivity of Hydrate-Bearing Sediments

[97] To avoid electrode polarization, conductivity is determined by imposing an AC field of frequency ω. As a result, the measured conductivity, σ_{AC}, contains Ohmic effects, σ_{DC}, as well as a contribution from the polarization losses, κ''; the measured value is $\sigma_{\mathrm{AC}} = \sigma_{\mathrm{DC}} + \kappa''\varepsilon_0\omega$. The contribution due to polarization losses is typically small when the operating frequencies are in the Hz to kHz range, so here we focus on κ', the real component of the complex permittivity.

[98] Nominal permittivity values for components of hydrate-bearing sediments in the microwave frequency range are as follows: unfrozen water, $\kappa_w' = 86$ (at 4°C); gas/air, $\kappa_g' \approx 1$; oil, $\kappa_{\mathrm{oil}}' = 3$–$5$; most minerals, $\kappa_m' = 4$–9; and methane hydrate, $\kappa_h' = 2.5$. The polarization of unfrozen water dominates the permittivity of hydrate-bearing sediments, though the permittivity of hydrate may be significantly higher at lower frequencies. A first approximation to the high-frequency permittivity of hydrate-bearing sediments, κ_b', is a volumetric linear combination,

$$\kappa_b' = (1 - \phi)\kappa_m' + \phi\left(\kappa_g' S_g + \kappa_h' S_h - \kappa_w' S_w\right). \tag{16}$$

[99] Geometric and spatial effects alter the permittivity of the mixture. Averaging by traveltime resembles the complex

TABLE 9. Applications of Archie's Law[a]

Site	Equation	α	β	χ	Reference
Blake Ridge (ODP Leg 164)	$S_h = 1 - (\rho_{sed}/\rho_b)^{\frac{1}{\chi}}$. The background resistivity of the fully water saturated sediment without hydrate is $\rho_{sed} = 0.8495 + (2.986 \times 10^{-4})z$ (m) for the Blake Ridge.	ϕ^β, α, and ρ_f cancel when ρ_{sed}/ρ_b is computed	ϕ^β, α, and ρ_f cancel when ρ_{sed}/ρ_b is computed	1.9386	*Lu and McMechan* [2002]
		1.05	−2.56	1.9386	*Collett and Ladd* [2000]
Hydrate Ridge (ODP Leg 204)	$\rho_f = 0.33\ \Omega$ m, $\phi = 0.65$ for GHSZ (CSEM, 5 and 15 Hz)	1	−2.8	1.9	*Weitemeyer et al.* [2006]
	$\rho_b = \alpha\rho_f\phi^\beta = 0.55\phi^\beta$	–	−1.3	1.9386	*Lee and Collett* [2006]
	>20 mbsf	0.967	−2.81	1.96	*Riedel et al.* [2006]
	shallow	1.35	−1.76	1.96	*Riedel et al.* [2006]
Mallik	$\rho_f = 0.56$ ($z = 738.23$ m), $\rho_f = 0.27$ ($z = 1141.02$ m)	0.62	−2.15	1.9386	*Lee and Collett* [2005], *Guerin and Goldberg* [2002], and *Reister* [2003]
Cascadia margin/ Makran region	$\rho_f = 1/(3 + T\ (^\circ\text{C})/10)$	1	−2.8	1.9	*Ghosh et al.* [2006]
Vancouver island	$\rho_f = (C_{sw}/C_f)\rho_{sw}$, where C_{sw} is salinity of the seawater reference and C_f is salinity of the in situ fluid	1.4	−1.76	1.76	*Hyndman et al.* [1999]
Milne Point, North Slope of Alaska	$\alpha\rho_f = 1\ \Omega$ m	–	−2.15	1.9386	*Lee* [2005]
	$\rho_f = 3\ \Omega$ m, $0.5 < \alpha < 2.5$, $-3 < \beta < -1.5$	1	−2	2	*Edwards* [1997]

[a]General form for no gas phase $S_g = 0$: $S_w = [\alpha(\rho_f/\rho_b)\phi^\beta]^{\frac{1}{\chi}}$ or $S_h = (1 - S_w) = 1 - [\alpha(\rho_f/\rho_b)\phi^\beta]^{\frac{1}{\chi}}$. $S_h = V_h/V_v$, $S_g = V_g/V_v$, $S_f = V_f/V_v$, and $1 = S_g + S_h + S_f$. GHSZ, gas hydrate stability zone; ODP, Ocean Drilling Program. The cautious use of these parameters is suggested by *Santamarina and Ruppel* [2008].

refraction index mixing model albeit assuming lossless media. In the case of hydrate-bearing sediments, this frequently adopted model becomes

$$\kappa'_b = \left[(1-\phi)\sqrt{\kappa'_m} + \phi\left(S_g\sqrt{\kappa'_g} + S_h\sqrt{\kappa'_h} + S_w\sqrt{\kappa'_w}\right)\right]^2. \quad (17)$$

Equation (17) and similar formulations have been applied to Gulf of Mexico sediments [*Francisca et al.*, 2005], Mallik permafrost hydrate field measurements [*Lee and Collett*, 2005; *Sun and Goldberg*, 2005], and laboratory measurements [*Lee et al.*, 2008]. Polynomial expressions are also used [*Kliner and Grozic*, 2006], and semiempirical equations developed for unsaturated soils can be adapted to hydrate-bearing sediments with free gas [*Topp et al.*, 1980; *Wensink*, 1993].

9.3. Field-Based Characterization of Hydrate-Bearing Sediments: Limitations

[100] Either resistivity or permittivity measurements can be used to distinguish between water and hydrate or other pore fillers such as gas or ice. Because ionic concentration has a second-order effect on permittivity but a primary effect on resistivity, permittivity is a more reliable parameter to estimate water saturation. For either measurement, hydrate saturation is extracted from the volumetric sum $1 = S_h + S_w + S_g + S_{ice}$. The common replacement $S_h = 1 - S_w$ presumes that $S_g = 0$, which is not true in water-limited systems or during gas production, and that $S_{ice} = 0$, which is not true in permafrost hydrate or during fast pressurization that results in secondary ice formation.

[101] At the field scale, resistivity-based measurements, such as the profiles measured by *Weitemeyer et al.* [2006], have been used to estimate in situ hydrate saturation. More commonly, though, electrical measurements are paired with well log data to provide a more reliable hydrate saturation estimate, which compliments information gathered from seismic data (section 10). Examples are provided by *Coren et al.* [2001], *Guerin and Goldberg* [2002], *Lee* [2002, 2005], *Lee and Collett* [2006], *Ghosh et al.* [2006], and *Ellis et al.* [2008], among others.

[102] The connection between electrical properties and hydrate saturation is generally based on Archie's equation (equation (15)). As noted in section 9.1 and Table 9, Archie parameters must be chosen with care. Several pore-scale characteristics, such as surface conduction and the nature of the sediment fabric in fine-grained sediments, are either disregarded or hidden in the Archie parameters [*Santamarina and Ruppel*, 2008; *Spangenberg*, 2001].

[103] Anisotropy and spatial heterogeneity, such as in sediments traversed by networks of hydrate lenses (section 4), add additional difficulty to data interpretation and the selection of proper models. Consider an example by *Lee and Collett* [2009], based on the NGHP-01 study of fine-grained sediments offshore India [*Collett et al.*, 2008]: Archie equation–based hydrate saturation estimates using parameters relevant for homogeneous sediment ranged from 50% to 80% at depths for which pressure cores taken in nearby wells indicate hydrate saturations are <26% [*Lee and Collett*, 2009].

10. SEISMIC WAVE VELOCITY, ATTENUATION, AND SMALL-STRAIN STIFFNESS

[104] Compressional P waves and shear S waves are extensively used for mapping hydrate occurrences and estimating the hydrate saturation within those occurrences. Acoustic remote sensing is possible because the presence of hydrate stiffens the host sediment, increasing the P and S wave velocities. This has been comprehensively demonstrated in hydrate-bearing clay, silt, and sand at different

TABLE 10. Elastic Constants of Selected Sediment Components[a]

Material	V_p (km s^{-1})	V_s (km s^{-1})	K (GPa)	G (GPa)	ρ (kg m^{-3})
Methane gas (10 MPa, 273 K)	0.412[b]	0	0.015[c]	0	90[d]
Water	1.5[e,f]	0	2250[e]	0	1000[e]
Ice Ih[g] (5 MPa, 273 K)	3.87	1.94	9.09	3.46	917
Methane hydrate[g] (5 MPa, 273 K)	3.77	1.96	8.41	3.54	925
Clay	3.41[c]	1.63[c]	20.9[h]	6.85[h]	2580[h]
Quartz	6.04[c]	4.12[c]	36.6[h]	45.0[h]	2650[i]

[a]Notation is as follows: V_p, compressional wave velocity; V_s, shear wave velocity; K, bulk modulus; G, shear modulus; and ρ, density.
[b]*Estela-Uriba et al.* [2006].
[c]Calculated from equation (18).
[d]*Sychev et al.* [1987].
[e]*Lee et al.* [1996].
[f]See *Mavko et al.* [1998, section 6.15] for variations with pressure, temperature, and salinity.
[g]*Helgerud et al.* [2009].
[h]*Helgerud et al.* [1999].
[i]*Dvorkin et al.* [2000].

effective stress and hydrate saturation levels by *Lee* [2007] and J. Y. Lee et al. (Parametric study of the physical properties of hydrate-bearing sand, silt, and clay sediments. Part II: Small-strain mechanical properties, submitted to *Journal of Geophysical Research*, 2009). This section relates wave velocity and stiffness properties to pore space hydrate saturation and discusses how seismic data can be used to characterize hydrate-bearing sediments.

10.1. Wave Velocities

[105] The propagation of P waves produces longitudinal strains with particle motion in the direction of wave propagation. In contrast, S waves cause shear strain with particle motion perpendicular to the direction of wave propagation. Their propagation speeds are controlled by the sediment's small-strain bulk modulus, K_b, and shear modulus, G, according to

$$V_p = \sqrt{\frac{K_b + \frac{4}{3}G}{\rho_b}}, \qquad V_s = \sqrt{\frac{G}{\rho_b}}, \tag{18}$$

where ρ_b is the bulk sediment density and V_p and V_s are the magnitudes of the compressional and shear wave velocities. Differences in their propagation modes mean that P and S waves are sensitive to different properties of the sediment: the bulk modulus, K_b, is determined by both the grains and pore fluid properties, but the shear modulus, G, is controlled by the shear stiffness of the granular skeleton.

[106] To relate V_p and V_s to hydrate saturations, moduli and density in equation (18) must be expressed as functions of mineral, sediment, pore fluid, and hydrate properties. The mass density of hydrate-bearing sediments, ρ_b, in equation (18) is given simply as a volume average of the individual densities, as a function of porosity, ϕ, and phase saturations, S,

$$\rho_b = \phi\left(\rho_w S_w + \rho_h S_h + \rho_g S_g + \rho_{\text{ice}} S_{\text{ice}}\right) + (1-\phi)\rho_m, \tag{19}$$

where the subscripts w, g, h, ice, and m signify the liquid, gas, hydrate, ice, and mineral phases, respectively.

[107] There are several ways to calculate the moduli. Empirical models have been based, for instance, on seismic traveltimes through layered sediments [*Wood et al.*, 1994] or on weighted combinations of traveltime estimates and stiffness predictions for fluid-saturated sediments [*Lee and Collett*, 1999] or follow the form of equations governing cemented soils [*Santamarina and Ruppel*, 2008]. Hydrate-bearing sediments have also been modeled as an effective medium [*Jakobsen et al.*, 2000] or as a combination of three distinct frameworks: a sediment framework, a hydrate framework, and pore fluid occupying the remaining volume [*Carcione and Gei*, 2004; *Carcione and Tinivella*, 2000; *Lee and Waite*, 2008]. To provide physical insight into the relationship between hydrate and the wave velocity in hydrate-bearing sediments, we summarize key equations in sections 10.1.1–10.1.3.

10.1.1. Bulk Stiffness

[108] The bulk stiffness or modulus, K_b, can be estimated from component properties using *Gassmann*'s [1951] equation,

$$K_b = K_{sk} + \frac{\left(1 - \frac{K_{sk}}{K_m}\right)^2}{\phi\left(\frac{S_w}{K_w} + \frac{S_g}{K_g} + \frac{S_h}{K_h} + \frac{S_{ice}}{K_{ice}}\right) + \frac{1-\phi}{K_m} - \frac{K_{sk}}{K_m^2}}, \tag{20}$$

where ϕ is the porosity and the subscripts b, w, g, h, ice, m, and sk stand for bulk hydrate-bearing sediment, water, gas, hydrate, ice, mineral, and sediment skeleton, respectively. Properties for the clay and quartz minerals are given in Table 10, along with the properties of methane hydrate, methane gas, water, and ice. The bulk stiffness of the skeleton, K_{sk}, is computed from the shear modulus, $G = G_{sk}$, using the standard theory of elasticity relation,

$$K_{sk} = \frac{2(1+\nu_{sk})}{3(1-2\nu_{sk})} G. \tag{21}$$

For this computation, one must use the Poisson ratio for the skeleton, ν_{sk}, which is typically $\sim 0.15 \pm 0.05$ in sediments

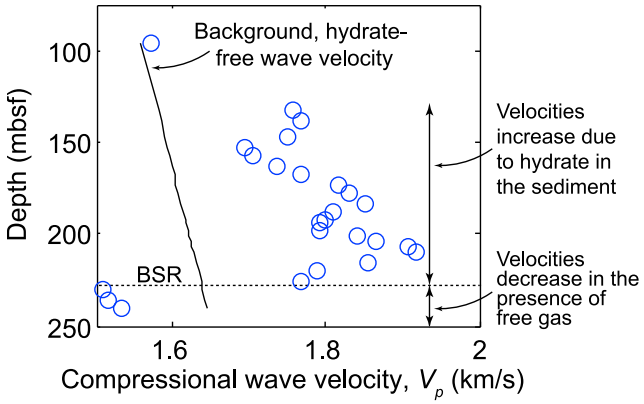

Figure 9. Effect of gas hydrate and free gas on measured in situ wave velocities for Ocean Drilling Program Site 889 in the Cascadian subduction zone offshore Vancouver, Canada (adapted from *Yuan et al.* [1996]). Relative to the regional "hydrate-free" velocity profile with depth (solid curve [from *Yuan et al.*, 1996]), VSP interval wave velocities [*MacKay et al.*, 1995] are elevated in the presence of hydrate. Below the bottom simulating reflector (BSR), where free gas is present rather than hydrate, the wave velocity falls below the water-saturated sediment wave velocity trend.

with hydrate saturations $S_h < 40\%$ and may increase to $\nu_{sk} \sim 0.3$ for sediments with $S_h > 60\%$.

[109] It follows from equation (20) that the presence of free gas ($K_g \ll K_w$, K_h, and K_m) has a pronounced effect in decreasing the bulk stiffness, K_b, and the longitudinal wave velocity, V_p (Figure 9). The decrease in bulk density is minor in comparison. Even at very low gas saturations, the presence of gas causes V_p to rapidly approach $\sim 1.5 V_s$.

10.1.2. Shear Stiffness Dependence on Hydrate Habit in Pore Space

[110] The presence of hydrate can alter the stiffness of both the pore fluid and sediment skeleton. The pore fluid stiffening impacts only the bulk modulus and is accounted for by the second term in equation (20). Skeletal stiffening increases the shear modulus, which, in turn, increases the skeletal bulk modulus as shown in equation (21). In hydrate-free sediment, shear stiffness is controlled by the mean effective stress, σ' (kPa),

$$G = \alpha \left(\frac{\sigma'}{1 \text{ kPa}} \right)^{\beta}, \tag{22}$$

where α is the shear stiffness when $\sigma' = 1$ kPa and β represents the sensitivity of G to effective stress. Parameters α and β depend on the sediment's granular packing and fabric properties, as well as the nature of the intergranular contacts [*Santamarina et al.*, 2001].

[111] In the presence of hydrate, the estimation of shear stiffness must also take into consideration pore space hydrate saturation, S_h, and where hydrate forms in the pore space.

10.1.2.1. Pore Filling

[112] The presence of hydrate does not affect the shear stiffness, which remains controlled by effective stress (equation (22)). Hydrate formers dissolved in water tend to promote pore-filling hydrate growth at low S_h that becomes load-bearing hydrate as S_h exceeds 25%–40% [*Berge et al.*, 1999; *Yun et al.*, 2005, 2007].

10.1.2.2. Load Bearing

[113] Load-bearing hydrate increases shear stiffness, but grain contact stiffness continues to reflect the state of effective stress (equation (22)). The relevance of effective stress decreases as hydrate saturation increases.

10.1.2.3. Cementation

[114] Hydrate formation at grain contacts readily takes over from effective stress as the primary control of the skeletal stiffness [*Dvorkin et al.*, 1999, 2000; *Fernandez and Santamarina*, 2001; *Guerin et al.*, 1999; *Xu et al.*, 2004].

10.1.3. Predicting Hydrate Saturations From Wave Velocities

[115] The dependence of skeletal stiffness $G = G_{sk}$ and K_{sk}, and hence wave velocity, on the pore space location of hydrate causes ambiguity when trying to infer hydrate saturations from measured wave velocities: the anomalously high interval wave velocity in Figure 9 could be due to a small amount of hydrate cementing sediment grains, a medium amount of hydrate supporting a portion of the sediment load, a large volume of hydrate floating in the pore space (see Figure 10), or some combination thereof.

[116] The combined interpretation of compressional and shear wave velocity data, together with directional resistivity measurements to characterize the anisotropy in fracture-dominated systems (see sections 4 and 9.3), can help reduce this ambiguity. Field measurements of shear wave velocity remain difficult, however, and even well log measurements of shear wave velocity can be untrustworthy [*Dai et al.*, 2008a; *Lee and Waite*, 2008].

[117] Seafloor compliance measurements, which provide a direct measure of the elastic deformation of the seafloor in response to passing waves on the ocean surface [*Willoughby et al.*, 2008], and controlled source electromagnetic surveys which measure electrical resistivity in sediment via detectors towed along the sediment surface [*Ellis et al.*, 2008; *Weitemeyer et al.*, 2006; *Yuan and Edwards*, 2000] can also provide independent elastic and electrical measures for the estimation of the in situ hydrate volumes.

[118] An independent estimate of in situ elastic properties at a given location can anchor, and thereby improve, the accuracy of seismic inversions in which elastic properties and hydrate saturations are estimated over broad regions [*Inks et al.*, 2008; *Jones et al.*, 2008]. The inversion, described in detail by *Xu et al.* [2004] and *Dai et al.* [2008b], seeks to build a model of the local geology such that synthetic seismic waveforms sent through the model space mimic the seismic waveforms measured in the field. The map of physical properties provided by the inversion is converted to a map of hydrate saturation by assuming a pore space hydrate configuration.

10.2. Attenuation

[119] Attenuation is a measure of energy loss as waves travel from a source to a sensor and is affected by hydrate

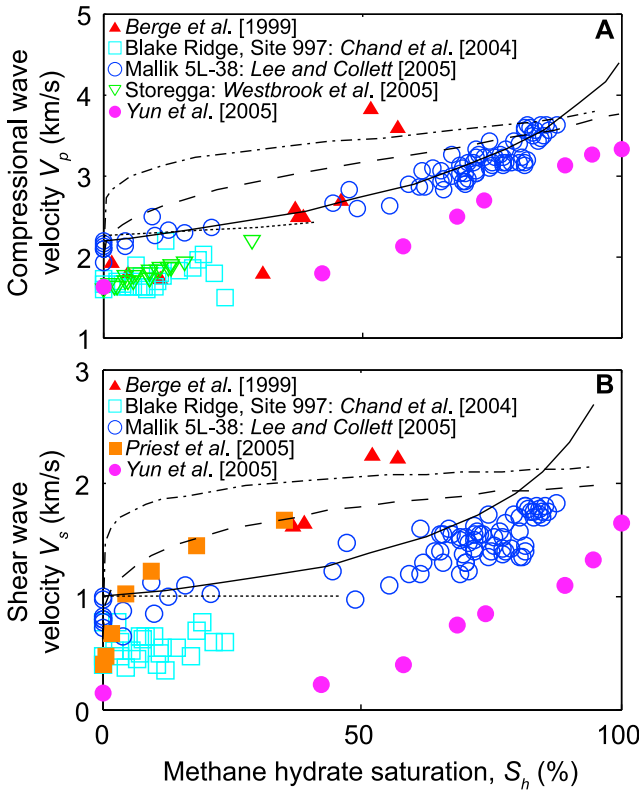

Figure 10. Comparison between field (open symbols), laboratory (solid symbols), and modeling results (solid and dashed curves) for (a) compressional and (b) shear wave velocities in hydrate-bearing sediments. Modeling results are from *Kleinberg and Dai* [2005]. Dot-dashed curves represent wave velocities for hydrate forming as cement at grain contacts. Particularly for low hydrate saturations, this distribution most significantly increases the wave velocity. Dashed curves predict wave velocities for hydrate that coats and cements sediment grains. Solid curves represent load-bearing hydrate, and dotted curves show the impact of pore-filling hydrate. Pore-filling distributions begin bridging sediment grains and behaving as load-bearing distributions for $S_h > \sim$25%–40%.

saturation [*Chand and Minshull*, 2004; *Dvorkin and Uden*, 2004; *Guerin and Goldberg*, 2005; *Guerin et al.*, 2005]. Unfortunately, measuring the "intrinsic attenuation" of hydrate-bearing sediment is hindered by the prevailing effects of geometric spreading and impedance mismatches in spatially heterogeneous media [*Huang et al.*, 2009]. For example, acoustic energy from borehole sources can reflect off the borehole wall due to the high stiffness of hydrate-bearing sediments and not propagate through the hydrate-bearing sediment at all [*Lee and Waite*, 2007]. Even if the intrinsic attenuation in sediment could be properly estimated in the field, its interpretation is made more difficult by the multiple coexisting energy loss mechanisms in sediments [*Wang and Santamarina*, 2007] which are further altered by the presence of hydrates in the pore space [*Lee*, 2006; *Matsushima*, 2006].

[120] Attenuation and wave velocity dispersion are causally related, as indicated by the Kramers-Kronig relations [e.g., *Toll*, 1956; *Wang and Santamarina*, 2007]. As discussed by *Lee* [2006], however, with the exception of the *Guerin and Goldberg* [2005] model, published attenuation models tend to treat attenuation and wave velocities independently, which can lead to predictions of unphysical behavior. These challenges have limited the reliability of attenuation as a tool for estimating in situ hydrate saturations.

11. STRENGTH AND DEFORMATION

[121] Sediment strength and the extent to which sediment deforms under a load are critical inputs for the analysis of potential failures around wells [*Masui et al.*, 2008; *Rutqvist and Moridis*, 2007] and for evaluating seafloor stability over larger length scales [*Nixon and Grozic*, 2007; *Sultan et al.*, 2004a].

11.1. Definition of Strength and Deformation Parameters

[122] Sediment strength is a combination of the cohesive resistance, c, and effective stress–dependent frictional resistance described by the friction angle, Φ, which includes resistance to sliding between particles, particle rearrangement, and particle crushing. The two contributions to shear strength are captured in the Coulomb failure criterion which relates the shear stress at failure, τ_f, to the normal effective stress, σ_n', acting on the failure plane,

$$\tau_f = c + \sigma_n' \tan \Phi. \tag{23}$$

This failure criterion plots as a straight line in $\tau - \sigma_n'$ space. The state of stress at a point in equilibrium within the test sample plots as a circle in $\tau - \sigma_n'$ space called the Mohr circle of stress. The sediment reaches failure when the Mohr circle becomes tangent to the Coulomb failure envelope (Figure 11).

11.2. Laboratory Measurements

[123] The strength parameters c and Φ can be measured in the laboratory using triaxial compression tests [*ASTM*

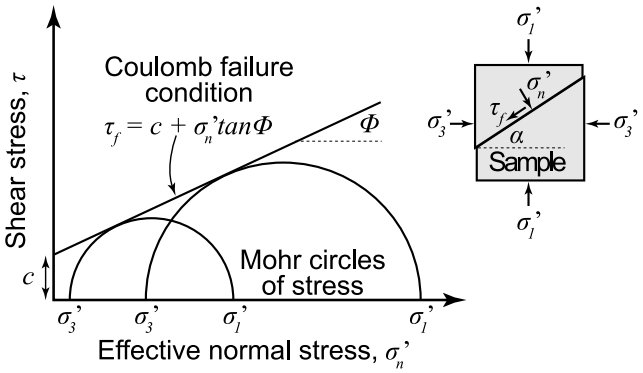

Figure 11. Mohr-Coulomb failure diagram. Within a sample subjected to the principal effective stresses σ_1' and σ_3', the state of stress falls on a Mohr circle in $\tau - \sigma_n'$ space. Shear failure occurs when the Mohr circle becomes tangent to the Coulomb failure line, meaning that the shear stress along the failure plane, τ_f, exceeds the combined resistance of cohesion, c, and friction, $\sigma_n'\tan\Phi$. The friction angle, Φ, and failure plane angle, α, are related by $\alpha = 45° + \Phi/2$.

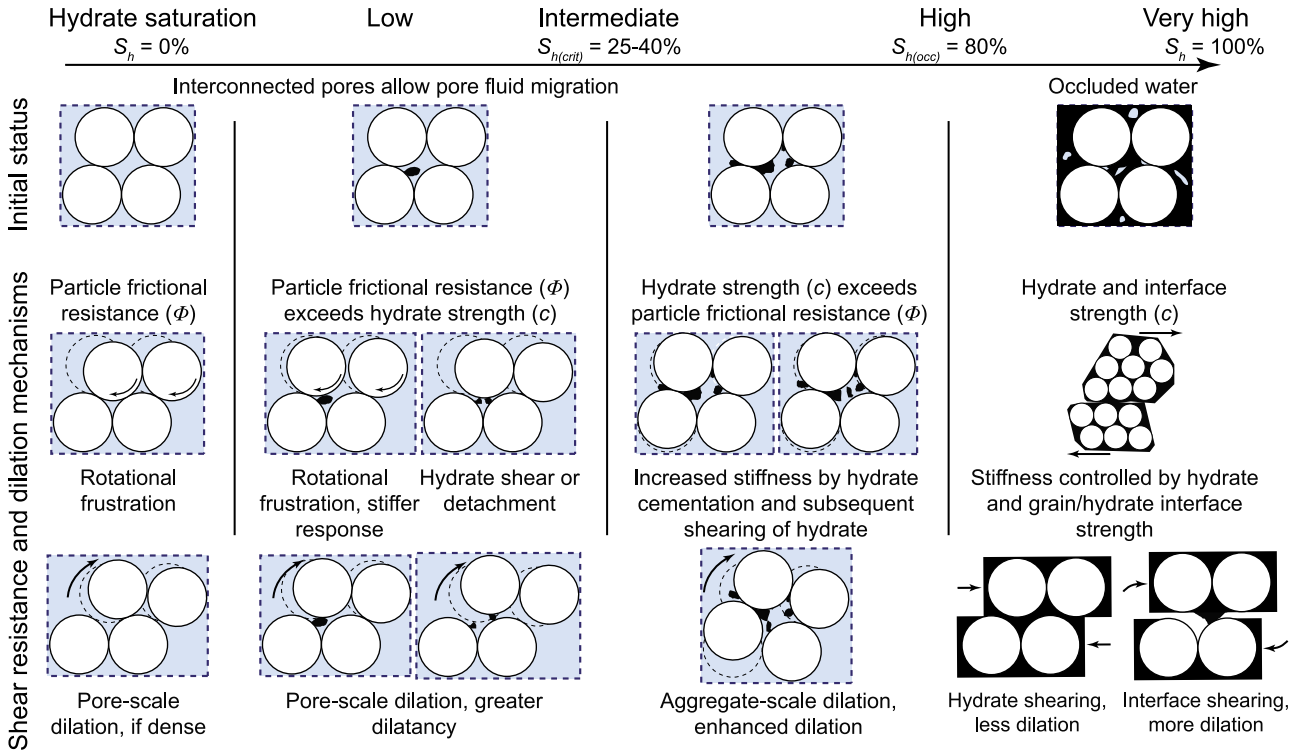

Figure 12. Mechanisms controlling the shear strength of hydrate-bearing sediments. Sediment grains are white circles, hydrate is black, and water is blue (modified from *Yun et al.* [2007]). Effective stress measurements are preferred when interpreting shear behavior, but at high hydrate saturations for which pressure in the occluded pores cannot be measured, interpretations must be based on total stress measurements.

Standard, 2004, 2006] in which a cylindrical specimen is subjected to an effective confining stress $\sigma_3' = \sigma_3 - P_p$ and then brought to failure by increasing the axial effective stress $\sigma_1' = \sigma_1 - P_p$ (Figure 11, inset). Triaxial test data obtained at different effective confining stress levels are combined to define the linear Coulomb failure envelope from which c and Φ are derived. Tests are generally run in either a drained mode, in which the pore pressure is maintained independently from the applied stress, or in an undrained mode, in which drainage of neither gas nor liquid pore fluid from the specimen is allowed and hence the pore pressure changes as the sample deforms. The specimen volume is assumed constant during undrained tests in water-saturated soft sediments, though this will not be the case in hydrate-bearing sediments if free gas forms during the test.

[124] Triaxial tests also provide prefailure information that can be used to determine Young's modulus, E; Poisson's ratio, ν; and dilatancy angle, ψ. Values of E and ν are often reported at 50% of the failure load, E_{50} and ν_{50}. The dilatancy angle measures the rate of volume increase with increasing shear strain. Dilative sediment subjected to undrained shear will experience a decrease in pore fluid pressure, thereby increasing the normal effective stress and sediment strength (equation (23)); the decrease in fluid pressure may cause gas dissolution and hydrate dissociation.

[125] When pores are interconnected, pore fluid pressure can be monitored or controlled independently of the confining stress in drained tests, and data are best interpreted within the framework of effective stresses, for which the pore pressure is subtracted from the applied stresses. The effective stress can be increased by either increasing the total stress under constant pore pressure or decreasing the pore pressure under constant total stress. Both should result in the same volume change for a given change in effective stress; however, decreasing the pore fluid pressure may lead to hydrate dissociation if reduced below the stability pressure at the test temperature. Once pores are occluded and therefore isolated from the external pore fluid reservoir, the local pore pressure evolves in response to the applied total stress and is not measurable using sensors outside the sample. Only the total stresses are known, restricting data analysis to a total stress framework.

11.3. General Trends

[126] The presence of methane hydrate increases stiffness, enhances prefailure dilation, and leads to higher strength. Figure 12 illustrates shear resistance and dilation mechanisms occurring at different levels of hydrate saturation in the pore space. Hydrate saturation is considered low for the purposes of shear strength when $S_h < \sim 30\%$ and high when $S_h > 40\%$. Conditions above S_h = 70%–80% are unusual and involve occluded pores inside the sediment. Specific results for coarse-grained sediment are given in sections 11.3.1 and 11.3.2, and fine-grained sediments are discussed in section 11.3.3. Further details are given by *Soga et al.* [2006].

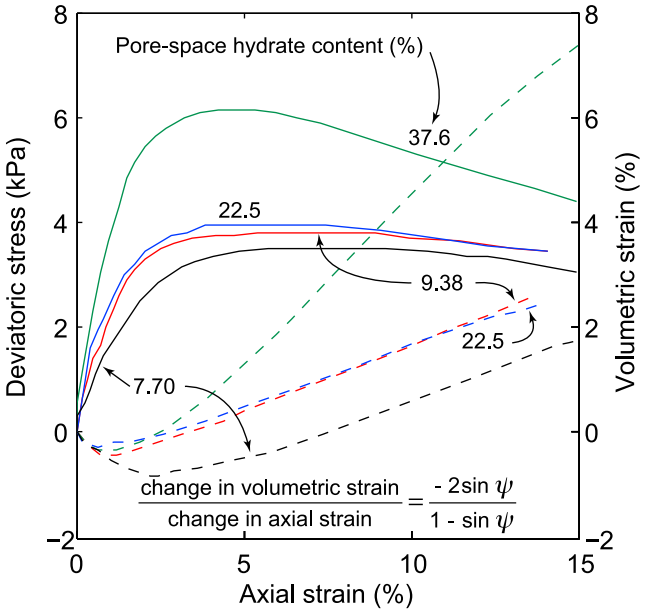

Figure 13. Dependence of stress (solid curves) and volumetric strain (dashed curves) on axial strain for four methane hydrate-bearing sands [*Masui et al.*, 2006]. The dilation angle, ψ, can be calculated from the slope of the volumetric strain as shown.

11.3.1. Coarse-Grained Soils: Drained Tests

[127] The measured stress-strain responses of natural hydrate-bearing sandy sediments retrieved from the Nankai Trough are shown in Figure 13 as a function of pore space hydrate saturation [*Masui et al.*, 2006]. In agreement with previous observations (Figure 12), the peak strength, E_{50}, and dilation generally increase with hydrate saturation [see also *Hyodo et al.*, 2007]. The Poisson's ratio, ν_{50}, varies between 0.10 and 0.19, with no apparent relationship to hydrate saturation.

[128] Effective stress strength parameters can depend strongly on the hydrate formation history (refer to section 3). There is a pronounced increase in strength and stiffness (Figure 14) as well as dilation angle (Figure 15b) when even a small amount of hydrate forms at interparticle contacts and cements particles together. In contrast, pore-filling hydrate begins to have a measurable effect on these parameters only when the hydrate saturation exceeds about $S_h \sim 30\%$. However, neither the friction angle nor the cohesion depend strongly on the mode of hydrate occurrence, and friction angle is nearly independent of hydrate saturation as well. It should be noted that the data were gathered from tests run at 1 MPa effective confining pressure; lower dilation is expected at higher confining pressures.

11.3.2. Coarse-Grained Soils: Undrained Tests

[129] Undrained triaxial test data show congruent trends to those gathered in drained tests. Gas hydrate–bearing sands from the Mackenzie Bay (Mallik 2L-38 between depths of 898 and 913 m, under 640 m of permafrost) exhibit a higher dilative tendency than the same sediments without hydrates (Figure 16) and are correspondingly stronger and stiffer. Similar conclusions are reached in undrained triaxial tests run on THF hydrate-bearing sands and silts at different stress levels and hydrate saturations [*Yun et al.*, 2007]; this study reached $S_h = 100\%$ and found that stiffness and undrained strength are determined by the hydrate phase in high hydrate saturation sediments rather than by the initial effective confining stress.

[130] In summary, available data show that (1) stiffness, cohesion, and dilation increase and friction angle remains constant as hydrate concentration increases; (2) at hydrate saturation $S_h < 30\%$, cementing hydrate has a more pronounced effect than pore-filling hydrate on mechanical properties; (3) formation history effects gradually diminish at high hydrate saturation; and (4) the initial effective stress loses relevance at very high hydrate concentrations, in which case the hydrate phase controls the strength and deformation characteristics.

11.3.3. Fine-Grained Soils

[131] Hydrate-bearing fine-grained soils have not been extensively studied due to a lesser interest from a resource potential perspective, coupled with difficulties in hydrate

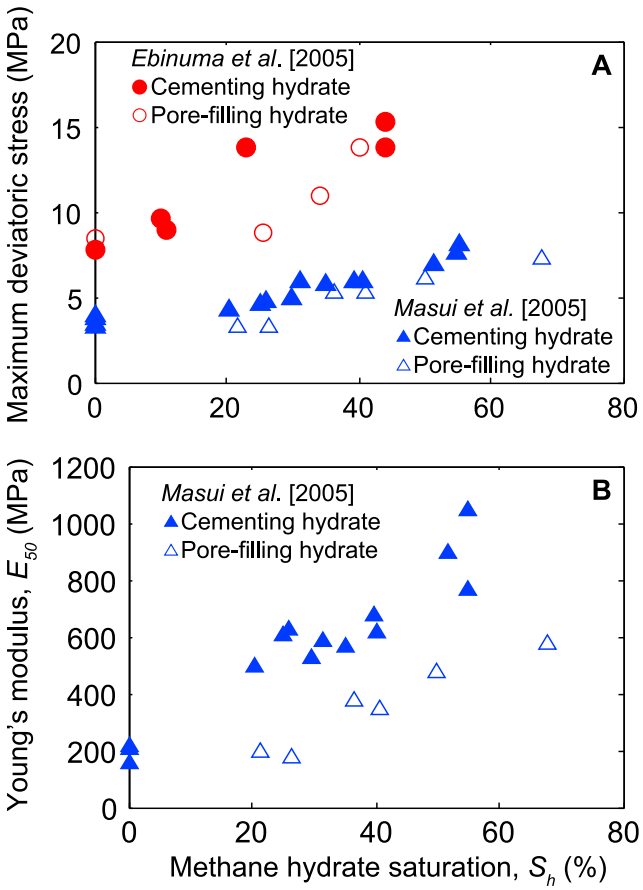

Figure 14. (a) Peak strength and (b) Young's modulus at 50% of the stress at failure, E_{50}, versus methane hydrate saturation. Cementing hydrate samples show significant impact of hydrate at low hydrate saturations, S_h. Pore-filling hydrate does not significantly impact peak strength or E_{50} until S_h exceeds 25%. The offset between the two studies is due to the 3 MPa confining pressure used by *Ebinuma et al.* [2005] compared to the 1 MPa confining pressure used by *Masui et al.* [2005].

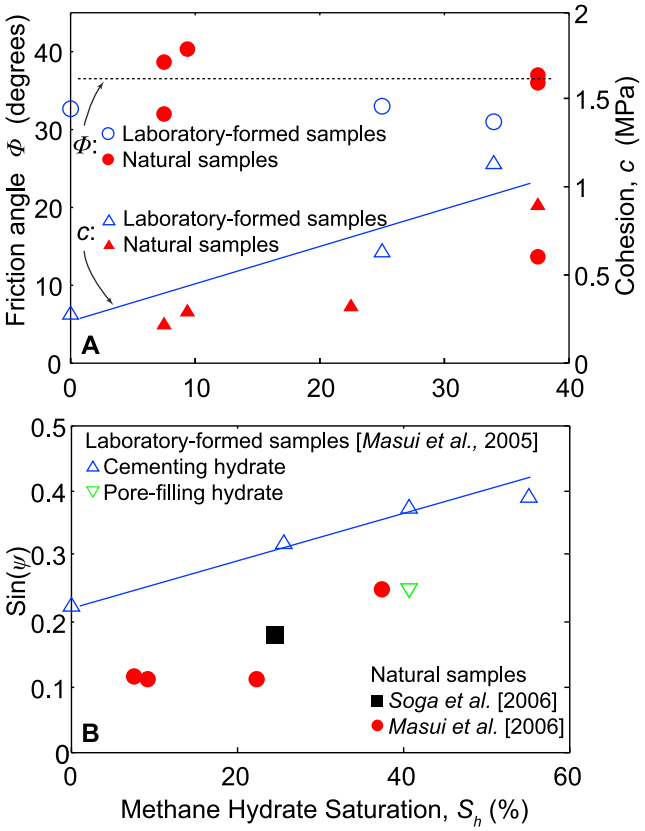

Figure 15. (a) Cohesion and friction angle and (b) dilation angle versus hydrate saturation in natural methane hydrate samples (solid symbols) [*Masui et al.*, 2006; *Soga et al.*, 2006] and laboratory-formed cemented methane hydrate samples (open symbols) [*Masui et al.*, 2005]. Though cohesion and dilation angle increase with increasing hydrate saturation (solid trend lines through the cementing hydrate data), friction angle is largely independent of hydrate saturation (dotted trend line).

formation and in mechanical testing. Therefore, limited data are available, and further work is needed to understand the mechanical behavior of hydrated bearing fine-grained sediments.

[132] Undrained, triaxial test data gathered for THF hydrate disseminated in Kaolinite clay and precipitated silt in which each silt grain is an agglomerate are summarized in Figure 17 [*Yun et al.*, 2007]. Specimens without hydrate exhibit a frictional, linear increase in undrained shear strength as the initial effective confining stress increases. In high hydrate saturation sediments, however, the undrained shear strength is insensitive to effective confining stress. The undrained modulus E_{50} follows a similar trend.

[133] Undrained shear strengths of natural fine-grained sediments with hydrate have been measured using a small cone-shaped penetrometer in pressure cores recovered in the Gulf of Mexico [*Yun et al.*, 2006]. These specimens were maintained at the in situ fluid pressure but with virtually no effective stress. The measured undrained strength therefore indicates only the in situ effects of hydrate and the granular porosity of these fine-grained sediments rather than the combined impact of hydrate, porosity, and effective stress. In all cases, undrained strength was higher in the hydrate-bearing sediments than in sediments without hydrates at the same burial depth [*Yun et al.*, 2006]. In situ cone resistance and friction during piezocone deployments offshore Nigeria also show an increased strength in the presence of hydrate [*Sultan et al.*, 2007]. These measurements are limited to shallow sediments (less than ~30 mbsf), however.

12. VOLUME CHANGE UPON DISSOCIATION

[134] Hydrate dissociation reduces the solid hydrate volume, produces gas and water, and decreases the water salinity. Depending on boundary conditions, these changes produce one or both of the following: (1) variations in the pore fluid pressure and effective stress and (2) changes in the volume occupied by the sediment.

[135] In natural settings, volume contraction typically follows hydrate dissociation once the initial pressure increase due to gas produced during dissociation dissipates. The magnitude of contraction depends on the soil type, the current in situ state of stress and the stress state when hydrate formed, the distribution of hydrate within the sediment, and the current mineral porosity defined in terms

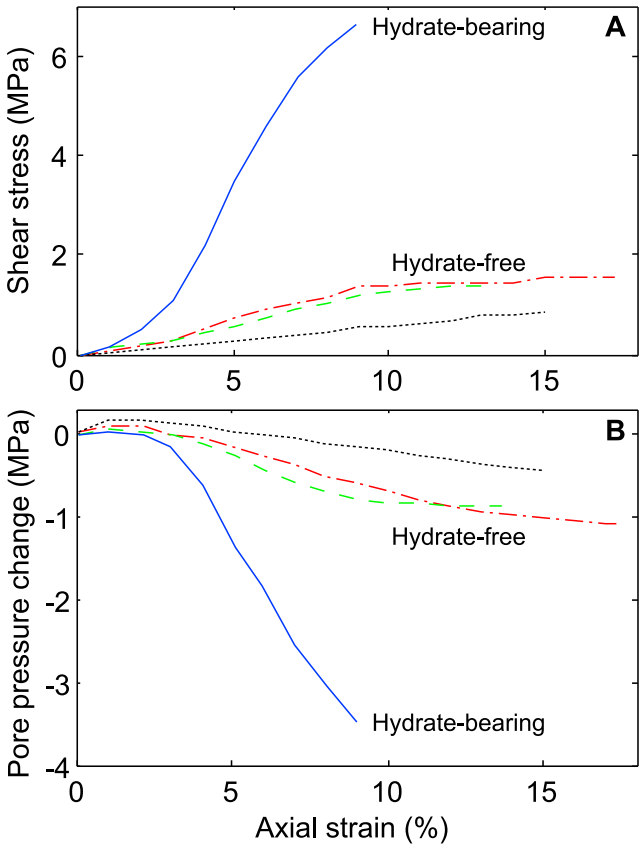

Figure 16. Dependence of (a) peak shear stress and (b) pore pressure change on pore content and axial strain in coarse sands recovered from the Mallik 2L-38 permafrost research well. Hydrate-free samples (broken curves) were sheared after the gas hydrate dissociated, and the hydrate-bearing sample (solid curve) was sheared with hydrate but no ice present [after *Winters et al.*, 2002].

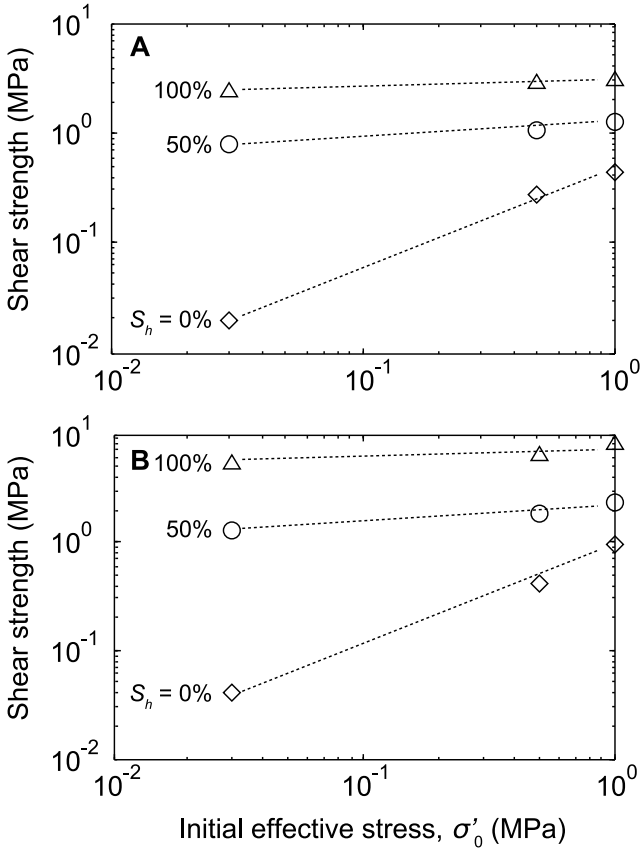

Figure 17. Undrained shear strength versus initial effective confining stress at different hydrate saturations for different soils: (a) Kaolinite and (b) precipitated silt [after *Yun et al.*, 2007]. With increasing tetrahydrofuran hydrate saturation, the dependence of shear strength on effective stress diminishes (dotted trend lines).

of $(V_T - V_m)/V_T$, where V_m is the volume of minerals and V_T is the total volume.

[136] Very limited data have been gathered for volume changes upon dissociation of hydrate-bearing sediments. However, there are data for similar processes that can provide useful insight to help constrain design parameters, such as the literature on cold regions engineering, which contains a wealth of data on material characterization and the effect of freeze-thaw cycles [*Gatto et al.*, 2001]. In particular, frozen ground characterization schemes can prove helpful in assessing hydrate-bearing sediments that are most susceptible to volume change.

[137] Several volume loss mechanisms are identified in the context of hydrate dissociation in sediments [*Lee et al.*, 2009]: (1) bulk hydrate dissociation, (2) sediment skeleton alteration, (3) consolidation, and (4) sand production. These mechanisms are briefly described in sections 12.1–12.4.

12.1. Contraction due to Bulk Hydrate Dissociation

[138] Segregated bulk hydrate exists in sediments in the form of lenses, veins, or nodules that are much larger than the pore size (e.g., Figure 4). The dissociation of bulk hydrate creates a void volume, V_v, equal to the hydrate volume, V_h. The upper bound estimate of the macroscale volumetric strain, ε_{vol}, is equal to the void volume, $V_v = V_h$, divided by the initial total volume of the sediment, V_T; therefore, $\varepsilon_{\text{vol}} \leq (V_h/V_T)$.

[139] Secondary mechanisms such as arching, in which the stress is transferred away from yielding sediment, or raveling, in which sediment collapses into void spaces, reduce the impact of void formation on volume change. In such cases, a reduction factor $0 \leq \beta \leq 1.0$ can be used to decrease the estimated upper bound volumetric strain,

$$\varepsilon_{\text{vol}} = \beta \frac{V_h}{V_T}. \tag{24}$$

The value of β is a function of the amount, size, and geometry of the bulk hydrate, along with the soil stiffness, strength, and state of stress. Though β could exceed 1.0 in very loose sediments when hydrate dissociation leads to volume collapse in the neighboring sediment, it is within the 0.2–0.4 range for most hydrate-bearing sediments.

12.2. Contraction due to Disseminated Hydrate Dissociation

[140] Disseminated hydrate within the intergranular pore space of the sediment can contribute to stiffening of the granular structure and can even carry part of the load (see sections 3, 10, and 11). Hydrate dissociation causes fabric changes such that the granular skeleton continues sustaining the applied effective stresses state. The consequence of this fabric alteration is either volume contraction or stress relaxation, depending on boundary conditions.

[141] The volumetric strain at constant boundary stresses is a function of the degree of hydrate saturation and distribution within the pore space, the soil compressibility, and the in situ state of stress. A comprehensive study conducted with various sediments, stress levels, and both 50% and 100% THF hydrate saturation is reported by *Lee* [2007] and *Lee et al.* [2007]; complementary data gathered with Gulf of Mexico sediments are given by *Lee et al.* [2008]. Results indicate the volumetric strain due to hydrate dissociation decreases as the effective stress increases, meaning less contraction should be expected in deeper sediments.

12.3. Contraction due to Increased Effective Stress: Depressurization

[142] Methane can be produced from hydrate-bearing sediments by reducing the pore fluid pressure by an amount ΔP that brings the system to the boundary of hydrate stability. There is a corresponding increase in effective stress state, and sediment compaction follows. In a one-dimensional system, the vertical strain, ε_z, is equal to the volumetric strain, ε_{vol}, and can be computed as

$$\varepsilon_z = \varepsilon_{\text{vol}} = \frac{C_c}{1 + e_0} \log\left(\frac{\sigma'_{z0} + \Delta P}{\sigma'_{z0}}\right), \tag{25}$$

where C_c is the sediment compressibility, e_0 is the initial void ratio, and σ_{z0}' is the initial vertical effective stress. The parameter C_c can be estimated from sediment properties (Table 5).

[143] Case histories for subsidence due to the depressurization of aquifers during water or hydrocarbon removal show that surface subsidence estimates must account for three processes: (1) the reservoir response, which is generally nonlinear, time-dependent, and spatially variable; (2) the behavior of the upper layers, including sediment stiffness, shear-induced volume changes, and time-dependent deformation processes; and (3) geometric-mechanical interaction effects, including reservoir thickness, thickness of the overlying sediment column, spatial extent of production, and production history [*Atkinson and Pedersen*, 1998; *Chan*, 2005; *Geertsma*, 1973; *Siriwardane*, 1992; *Sorey et al.*, 1993; *Sylte et al.*, 1999; *Xu et al.*, 2001; *Yerkes and Castle*, 1970].

12.4. Contraction due to Mineral Migration and Removal

[144] Volume loss associated with the transport of mineral particles out of the sediment and into the well can be an important volume contraction mechanism, particularly in sandy sediments. Sand production is facilitated by hydrate dissociation and mixed fluid flow conditions. The potential volume loss depends on flow rates, the geometry of the layer, and soil type.

12.5. Additional Consequences of Volume Contraction

[145] Compaction is not the only effect associated with hydrate dissociation. There is evidence that the horizontal effective stress also decreases during dissociation and that the sediment can reach internal shear failure conditions [*Shin and Santamarina*, 2009]. In geomechanical terms, the stress ratio at rest, k_o, decreases toward Rankine's active Earth pressure coefficient, k_a, defined as the minimum lateral effective stress for soils at their extensional failure condition. In strain-softening sediments, this situation may lead to the formation of shear planes within the sediment [*Shin et al.*, 2008].

13. FUTURE RESEARCH DIRECTIONS IN THE CHARACTERIZATION OF HYDRATE-BEARING SEDIMENTS

[146] Particle and pore-scale interactions between hydrate and its host sediment lead to a richly complex system of interdependent macroscale physical properties that govern the evolution of hydrate-bearing sediments. Understanding these interdependencies can provide a framework for understanding hydrate-bearing sediments as well as providing a robust basis for preliminary evaluations of gas production strategies and instability conditions, such as slope and borehole failures.

[147] The three most relevant properties for predicting the behavior of hydrate-bearing sediments are the pore space hydrate saturation, effective stress, and sediment grain size, particularly the content of fine-grained silts and clays. These parameters must be explicitly assessed and reported in all future studies.

[148] Above 25%–40% pore space hydrate saturation, hydrate behaves as a load-bearing member of the sediment, decreasing the permeability while increasing sediment stiffness and strength. As the hydrate saturation decreases, effective stress becomes the primary control on sediment stiffness and strength. The influence of hydrate on the host sediment properties can be subtle at low saturations, and fewer measurements have been made on these systems relative to the highly hydrate-saturated sands. The low-saturation case must nevertheless be examined because, for instance, the dissociation of small quantities of hydrate can still have pronounced effects on pore fluid pressure, effective stress, and stability conditions.

[149] The host sediment's silt and clay content, the fines, determines the mode of hydrate occurrence. In coarse-grained systems with a fines content below ~7%, hydrate generally occurs in the pore space between grains. When the fines content exceeds ~15%, hydrate is found disseminated in the sediment and forming veins and nodules that displace sediment grains. As a result, pronounced spatial variability is common in the fine-grained sediments that host the majority of the Earth's hydrate. Fines content also determines fluid permeability and plays a critical role in sediment evolution after hydrate dissociation. Future studies should further explore the effect of the amount of fines, their mineralogy, and specific surface area on the characteristics of hydrate-bearing sediments.

[150] The structure of hydrate-bearing sediments comprises the sediment fabric and the hydrate distribution at the pore scale. Both structural characteristics can be modified by changes in effective stress, fluid pressure, and/or temperature. Sampling and core extraction inherently modify the effective stress and physical state of sediments and may also cause hydrate dissociation. Therefore, emphasis must be placed on further developing comprehensive in situ sediment characterization through borehole logging tools that incorporate the simultaneous measurements of multiple properties from the minimally disturbed material surrounding the probe. For measurements that cannot be made in a borehole, the advent of routine pressure coring and the testing of such cores at their in situ pore pressure is invaluable. A key advance would be to maintain or quickly reinstate the in situ effective stresses.

[151] Laboratory studies using synthetic specimens attempt to emulate field conditions while avoiding core disturbance problems. The importance of emulating the noncementing methane hydrate observed in most marine field studies highlights the need to develop reproducible hydrate formation techniques, likely involving dissolved phase methane, that avoid the cementing nature of methane hydrate formed in the presence of free gas.

[152] Field and laboratory specimens tend to exhibit marked heterogeneity. Future experimental studies should routinely image specimens to visualize hydrate distribution

so that proper data inversion procedures can be implemented in the interpretation of measured properties.

NOTATION

The following subscripts, used throughout the paper, refer a parameter to a particular material or condition:

b bulk material, including all constituents.
f pore fluid.
g gas.
h hydrate.
m sediment grain mineral.
max maximum value.
min minimum value.
s solid sediment constituents.
T total value, including all constituents.
v void space or pore space.
w water.

Parameters given below are listed in SI units. When applicable, common usage units are given in the main text.

Section 2: solubility

a_i^j activity of species i in phase j (unitless).
f_i^j fugacity of species i in phase j (Pa).
f_i^0 fugacity of species i in a convenient reference state (Pa).
G Gibbs free energy (J).
H superscript referring to the hydrate phase.
L superscript referring to the liquid phase.
m molality (moles of solute per kilogram of solvent).
M molarity (moles of solute per liter of solution).
n_i^j number of moles of species i in phase j (mol).
P_i pressure in species i (Pa).
r interfacial radius of curvature (m).
R universal gas constant (8.314 J (mol K)$^{-1}$).
T temperature (K).
x_i^j concentration of species i in phase j (mole fraction).
β superscript referring to hypothetical empty hydrate phase with no guest molecules.
$\gamma_{i,w}$ interfacial tension between species i and water (N m^{-1}).
ΔP capillary pressure (Pa).
μ_i^j chemical potential of species i in phase j (J mol^{-1}).
μ_i^0 chemical potential of species i in a convenient reference state (J mol^{-1}).
ν_i^j activity coefficient of species i in phase j (unitless).

Section 3: formation history

S_h hydrate saturation in the pore space (% or unitless).

Section 4: spatial variability

V_p compressional wave velocity (m s^{-1}).
V_s shear wave velocity (m s^{-1}).

Section 5: sampling and handling effects

$G_{\max}$ small-strain shear stiffness (Pa).
PI plasticity index (% or unitless).

Section 6: index properties

C_c coefficient of compressibility (unitless).
C_{curv} coefficient of curvature (unitless).
C_H Hazen's empirical coefficient ($\sim 1 \times 10^4$ (m s)$^{-1}$) [*Carrier*, 2003].
C_{unif} coefficient of uniformity (unitless).
D_X grain diameter at which X% of the sample is finer (m).
e void ratio (unitless).
G_s specific gravity (unitless).
K hydraulic conductivity (m s^{-1}).
LI liquidity index (% or unitless).
LL liquid limit (% or unitless).
M mass (kg).
PI plasticity index (% or unitless).
PL plastic limit (% or unitless).
R particle roundness (unitless).
S_h hydrate saturation in the pore space (% or unitless).
S_s specific surface (m^2 kg^{-1}).
S_u undrained shear strength (Pa).
V volume (m^3).
w gravimetric water content, with respect to the specimen's mineral mass (unitless).
γ_w unit weight of water (N m^{-3}).
θ shape and tortuousity factor (unitless).
μ dynamic fluid viscosity (Pa s).
ρ mass density (kg m^{-3}).
σ_v' mean effective stress at failure (Pa).
ϕ porosity (% or unitless).
Φ_{cv} friction angle during constant volume shear (degrees or radians).

Section 7: thermal properties

c_p specific heat (J (kg K)$^{-1}$).
m cementation exponent (2 ± 0.5 for granular media, unitless) [*Revil*, 2000].
P pressure (Pa).
R universal gas constant (8.314 J (mol K)$^{-1}$).
S_h hydrate saturation in the pore space (% or unitless).
T temperature (K).
Z nonideal gas compressibility factor (unitless).
ΔH enthalpy of reaction (J mol^{-1}).
κ thermal diffusivity (m^2 s^{-1}).
λ thermal conductivity (W (m K)$^{-1}$).
ρ mass density (kg m^{-3}).
ϕ porosity (% or unitless).

Section 8: permeability and fluid flow

A cross-sectional area (m^2).
C gas slippage or Klinkenberg effect parameter (unitless).
D_X grain diameter at which X% of the sample is finer (m).
e void ratio (unitless).
g acceleration due to gravity (9.8 m s^{-2}).
k intrinsic permeability (m^2).
k_r relative permeability (unitless).
l length (m).
n van Genuchten curve-fitting parameter (unitless).
P pressure (Pa).

q flow rate ($m^3\ s^{-1}$).
S_s specific surface ($m^2\ kg^{-1}$).
S_w water saturation (unitless).
S_{w_eff} effective water saturation (unitless).
S_{w_irr} irreducible water saturation (unitless).
z depth or elevation (m).
α van Genuchten curve-fitting parameter (m^{-1}).
ΔP capillary pressure (Pa).
θ shape and tortuosity factor (unitless).
μ dynamic fluid viscosity (Pa s).
ρ mass density (kg m^{-3}).

Section 9: electromagnetic properties

c ionic concentration (mol m^{-3}).
C salinity (practical salinity unit).
e void ratio (unitless).
sed subscript indicating a property of hydrate-free sediment.
S_i pore space saturation of phase i (% or unitless).
S_s specific surface ($m^2\ kg^{-1}$).
sw subscript indicating a property of standard seawater.
T temperature (K).
TDS total dissolved solids (kg L^{-1}).
V volume (m^3).
z depth (m).
α empirical parameter in Archie's law (unitless).
β empirical parameter in Archie's law (unitless).
ε_0 permittivity of free space (8.85×10^{-12} F m^{-1}).
ζ ionic mobility ((S m^2) mol^{-1}).
κ^* complex electrical permittivity (relative to "free space," ε_0) (unitless).
κ' real component of the relative electrical permittivity (unitless).
κ'' imaginary component of the relative electrical permittivity (unitless).
λ_{ddl} surface conduction (S).
μ^* complex magnetic permeability (relative to "free space," μ_0) (unitless).
μ' real component of the relative magnetic permeability (unitless).
μ'' imaginary component of the relative magnetic permeability (unitless).
μ_0 magnetic permeability of free space (1.25×10^{-6} N A^{-2}).
ρ electrical resistivity (Ω m).
σ electrical conductivity (S m^{-1}).
σ_{AC} alternating current conductivity (S m^{-1}).
σ_{DC} direct current conductivity, zero frequency (S m^{-1}).
ϕ porosity (% or unitless).
χ empirical parameter in Archie's law (unitless).
ω frequency (Hz).

Section 10: seismic wave velocity, attenuation, and small-strain stiffness

G shear modulus (Pa).
K bulk modulus (Pa).
S_i pore space saturation of phase i (% or unitless).
sk subscript indicating a property of the sediment skeleton.
V_p compressional wave velocity (m s^{-1}).
V_s shear wave velocity (m s^{-1}).
α shear stiffness at 1 kPa effective stress (Pa).
β sensitivity of the shear stiffness to the effective stress (unitless).
ν Poisson's ratio (unitless).
ρ mass density (kg m^{-3}).
σ' mean effective stress (Pa).
ϕ porosity (% or unitless).

Section 11: strength and deformation

c cohesion (Pa).
E Young's modulus (Pa).
E_{50} secant Young's modulus at 50% failure stress (Pa).
P_P pore pressure (Pa).
S_h hydrate saturation in the pore space (% or unitless).
$S_{h(crit)}$ critical hydrate saturation, typically between 25% and 45%, indicating the transition from hydrate as a pore fill to hydrate as a structural component of the sediment (%).
$S_{h(occ)}$ hydrate saturation beyond which pores become occluded, typically ~80% (%).
α failure plane angle from horizontal (degrees or radians).
ν Poisson's ratio (unitless).
ν_{50} Poisson's ratio at 50% failure stress (unitless).
σ_1' maximum principal effective stress (Pa).
σ_3' minimum principal effective stress (Pa).
σ_n' normal effective stress acting on the failure plane (Pa).
τ shear stress (Pa).
τ_f shear stress at failure (Pa).
Φ friction angle (degrees or radians).
ψ dilatancy angle (degrees or radians).

Section 12: volume change upon dissociation

C_c coefficient of compressibility (unitless).
e_0 initial void ratio (unitless).
k_a Rankine's active Earth pressure coefficient (unitless).
k_o stress ratio "at rest," meaning under zero lateral strain (unitless).
V volume (m^3).
β reduction factor pertaining to the volumetric strain (unitless).
ΔP pressure change induced by depressurization (Pa).
ε_{vol} volumetric strain (unitless).
ε_z vertical strain (unitless).
σ_{z0}' initial vertical effective stress (Pa).

[153] **ACKNOWLEDGMENTS.** This work is the product of a Department of Energy (DOE)–sponsored Physical Property workshop held in Atlanta, Georgia, 16–19 March 2008. The workshop was supported by Department of Energy contract DE-AI21-92MC29214. U.S. Geological Survey contributions were supported by the Gas Hydrate Project of the U.S. Geological Survey's Coastal and Marine Geology Program. Lawrence Berkeley National Laboratory contributions were supported by the Assistant Secretary for Fossil Energy, Office of Oil and Natural Gas, through the National Energy Technology Laboratory of the U.S. DOE under contract DE-AC02-05CH11231. Georgia Institute of Technology contributions were supported by the Goizueta Foundation, DOE DE-FC26-06NT42963, and the DOE-JIP administered by Chevron award DE-FC26-610 01NT41330. Rice

University contributions were supported by the DOE under contract DE-FC26-06NT42960. The views expressed in this document are not necessarily those of the Department of Energy, and any use of trade names is for descriptive purposes only and does not imply endorsement by the U.S. Government. The authors thank Carolyn Ruppel and Stephen Kirby for their constructive reviews of this work.

[154] The Editor responsible for this manuscript was Ian Fairchild. He thanks technical reviewers Jocelyn Grozic and Martin Sharp and one additional anonymous reviewer.

REFERENCES

Andersland, O. B., and B. Ladanyi (2004), *Frozen Ground Engineering*, 384 pp., John Wiley, Hoboken, N. J.

Anderson, B. J., et al. (2008), Analysis of modular dynamic formation test results from the Mount Elbert-01 stratigraphic test well, Milne Point unit, North Slope Alaska, paper 5730 presented at the 6th International Conference on Gas Hydrates, Chevron, Vancouver, B. C., Canada, 6–10 July.

Anderson, R., M. Llamedo, B. Tohidi, and R. W. Burgass (2003), Experimental measurement of methane and carbon dioxide clathrate hydrate equilibria in mesoporous silica, *J. Phys. Chem. B*, *107*, 3507–3514, doi:10.1021/jp0263370.

Annan, A. P. (1992), *Ground Penetrating Radar: Workshop Notes*, Sensors and Software, Inc., Mississauga, Ont., Canada.

Archer, D. (2007), Methane hydrate stability and anthropogenic climate change, *Biogeosciences*, *4*, 521–544.

Archie, G. E. (1942), The electrical resistivity log as an aid in determining some reservoir characteristics, *Trans. Am. Inst. Min. Metall. Pet. Eng.*, *146*, 54–62.

Arman, A., and K. L. McManis (1977), *Effects of Conventional Soil Sampling Methods on the Engineering Properties of Cohesive Soils in Louisiana*, 294 pp., Div. of Eng. Res., La. State Univ., Baton Rouge.

ASTM Standard (2004), D 4767-04: Standard test method for consolidated undrained triaxial compression test for cohesive soils, ASTM Int., West Conshohocken, Pa.

ASTM Standard (2006), WK3821: New test method for consolidated drained triaxial compression test for soils, ASTM Int., West Conshohocken, Pa.

Atkinson, P. G., and J. R. Pedersen (1998), Using precision gravity data in geothermal reservoir engineering modeling studies, paper presented at the Thirteenth Workshop on Geothermal Reservoir Engineering, Stanford Univ., Stanford, Calif.

BASF Corporation (1998), Tetrahydrofuran (THF) storage and handling, report, 20 pp., Mount Olive, N. J. (Available at http://www2.basf.us/diols/pdfs/thf_brochure.pdf)

Bear, J. (1972), *Dynamics of Fluids in Porous Media*, 784 pp., Dover, Mineola, N. Y.

Berge, L. I., K. A. Jacobsen, and A. Solstad (1999), Measured acoustic wave velocities of R11(CCl_3F) hydrate samples with and without sand as a function of hydrate concentration, *J. Geophys. Res.*, *104*, 15,415–15,424, doi:10.1029/1999JB900098.

Bergeron, S., A. Macchi, and P. Servio (2007), Theoretical temperature dependency of gas hydrate former solubility under hydrate-liquid water equilibrium, *J. Chem. Thermodyn.*, *39*, 737–741, doi:10.1016/j.jct.2006.10.014.

Bhatnagar, G., W. G. Chapman, G. R. Dickens, B. Dugan, and G. J. Hirasaki (2007), Generalization of gas hydrate distribution and saturation in marine sediments by scaling of thermodynamic and transport processes, *Am. J. Sci.*, *307*, 861–900, doi:10.2475/06.2007.01.

Birchwood, R., R. Singh, and A. Mese (2008), Estimating the in situ mechanical properties of sediments containing gas hydrates, paper 5840 presented at the 6th International Conference on Gas Hydrates, Chevron, Vancouver, B. C., Canada, 6–10 July.

Bohrmann, G., J. Greinert, E. Suess, and M. Torres (1998), Authigenic carbonates from the Cascadia subduction zone and their relation to gas hydrate stability, *Geology*, *26*, 647–650, doi:10.1130/0091-7613(1998)026<0647:ACFTCS>2.3.CO;2.

Booth, J. S., M. M. Rowe, and K. M. Fischer (1996), Offshore gas hydrate sample database with an overview and preliminary analysis, *U.S. Geol. Surv. Open File Rep., 96-272*, 23 pp.

Booth, J. S., W. J. Winters, W. P. Dillon, M. B. Clennell, and M. M. Rowe (1998), Major occurrences and reservoir concepts of marine clathrate hydrates: Implications of field evidence, in *Gas Hydrates: Relevance to World Margin Stability and Climate Change*, edited by J. P. Henriet and J. Mienert, *Geol. Soc. Spec. Publ.*, *137*, 113–127.

Boswell, R., and T. Collett (2006), The gas hydrates resource pyramid, *Fire in the Ice: Methane Hydrate Newsletter*, fall, pp. 5–7, Off. of Fossil Energy, Natl. Energy Technol. Lab., U.S. Dep. of Energy, Washington, D. C.

Briaud, J. L., and A. Chaouch (1997), Hydrate melting in soil around hot conductor, *J. Geotech. Geoenviron. Eng.*, *123*, 645–653, doi:10.1061/(ASCE)1090-0241(1997)123:7(645).

Buffett, B., and O. Zatsepina (2000), Formation of gas hydrate from dissolved gas in natural porous media, *Mar. Geol.*, *164*, 69–77, doi:10.1016/S0025-3227(99)00127-9.

Carcione, J. M., and D. Gei (2004), Gas-hydrate concentration estimated from P- and S-wave velocities at the Mallik 2L-38 research well, Mackenzie Delta, Canada, *J. Appl. Geophys.*, *56*, 73–78, doi:10.1016/j.jappgeo.2004.04.001.

Carcione, J. M., and U. Tinivella (2000), Bottom-simulating reflectors: Seismic velocities and AVO effects, *Geophysics*, *65*, 54–67, doi:10.1190/1.1444725.

Carrier, W. D. (2003), Goodbye, Hazen; Hello, Kozeny-Carmen, *J. Geotech. Geoenviron. Eng.*, *129*, 1054–1056, doi:10.1061/(ASCE)1090-0241(2003)129:11(1054).

Carsel, R. F., and R. S. Parrish (1988), Developing joint probability distributions of soil water retension characteristics, *Water Resour. Res.*, *24*(5), 755–769.

Chan, A. W.-K. (2005), Production-induced reservoir compaction, permeability loss and land surface subsidence, doctoral thesis, 176 pp., Stanford Univ., Palo Alto, Calif.

Chand, S., and T. Minshull (2004), The effect of hydrate content on seismic attenuation: A case study for Mallik 2L-38 well data, Mackenzie delta, Canada, *Geophys. Res. Lett.*, *31*, L14609, doi:10.1029/2004GL020292.

Chand, S., T. A. Minshull, D. Gei, and J. M. Carcione (2004), Elastic velocity models for gas-hydrate-bearing sediments—A comparison, *Geophys. J. Int.*, *159*, 573–590, doi:10.1111/j.1365-246X.2004.02387.x.

Chapoy, A., C. Coquelet, and D. Richon (2003), Solubility measurement and modeling of water in the gas phase of the methane/water binary system at temperatures from 283.08 to 318.12 K and pressures up to 34.5 MPa, *Fluid Phase Equilibria*, *214*, 101–117, doi:10.1016/S0378-3812(03)00322-4. (Corrigendum, *Fluid Phase Equilibria*, *230*, 210–214, doi:10.1016/j.fluid.2004.07.005, 2005.)

Chen, Z., and K. G. Osadetz (2008), Regional study of methane hydrate occurrence and the geological controls, Beaufort-Mackenzie Basin, Canada, paper 5479 presented at the 6th International Conference on Gas Hydrates, Chevron, Vancouver, B. C., Canada, 6–10 July.

Chuvilin, E. M., T. Ebinuma, Y. Kamata, T. Uchida, S. Takeya, J. Nagao, and H. Narita (2003), Effects of temperature cycling on the phase transition of water in gas-saturated sediments, *Can. J. Phys.*, *81*, 343–350, doi:10.1139/p03-028.

Circone, S., L. A. Stern, and S. H. Kirby (2004), The role of water in gas hydrate dissociation, *J. Phys. Chem. B*, *108*, 5747–5755, doi:10.1021/jp0362584.

Circone, S., S. H. Kirby, and L. A. Stern (2005), Direct measurement of methane hydrate composition along the hydrate equilibrium boundary, *J. Phys. Chem. B*, *109*, 9468–9475, doi:10.1021/jp0504874.

Circone, S., S. H. Kirby, and L. A. Stern (2006), Thermodynamic calculations in the system CH_4-H_2O and methane hydrate phase equilibria, *J. Phys. Chem. B*, *110*, 8232–8239, doi:10.1021/jp055422f.

Clayton, C., E. Kingston, J. Priest, P. Schultheiss, and the NGHP Expedition 01 Scientific Party (2008), Testing of pressured cores containing gas hydrate from deep ocean sediments, paper 5811 presented at the 6th International Conference on Gas Hydrates, Chevron, Vancouver, B. C., Canada, 6–10 July.

Clennell, M. B., M. Hovland, J. S. Booth, P. Henry, and W. J. Winters (1999), Formation of natural gas hydrates in marine sediments: 1. Conceptual model of gas hydrate growth conditioned by host sediment properties, *J. Geophys. Res.*, *104*, 22,985–23,003, doi:10.1029/1999JB900175.

Collett, T. S. (2002), Energy resource potential of natural gas hydrates, *AAPG Bull.*, *86*, 1971–1992.

Collett, T. S., and J. Ladd (2000), Detection of gas hydrate with downhole logs and assessment of gas hydrate concentrations (saturations) and gas volumes on the Blake Ridge with electrical resistivity log data, *Proc. Ocean Drill. Program Sci. Results*, *164*, 179–191.

Collett, T. S., R. E. Lewis, and S. R. Dallimore (2005), Mallik 5L-38 gas hydrate production research well downhole well-log and core montages, in *Scientific Results From The Mallik 2002 Gas Hydrate Production Research Well Program, Mackenzie Delta, Northwest Territories, Canada* [CD-ROM], edited by S. R. Dallimore and T. S. Collett, *Bull. Geol. Surv. Can.*, *585*.

Collett, T., et al. (2008), Indian National Gas Hydrate Program Expedition 01 initial reports: Expedition 01 of the Indian National Gas Hydrate Program from Mumbai, India to Chennai, India; Sites NGHP-01-01 through NGHP-01-21, April 2006–August 2006, Dir. Gen. of Hydrocarbons, Minist. of Pet. and Nat. Gas, Noida, India.

ConocoPhillips–University of Bergen Hydrates Team (2008), Laboratory investigation of hydrate production through CO_2–CH_4 exchange, *Fire in the Ice: Methane Hydrate News Letter*, fall, pp. 1–4, Off. of Fossil Energy, Natl. Energy Technol. Lab., U.S. Dep. of Energy, Washington, D. C.

Cook, A., D. Goldberg, and R. L. Kleinberg (2008), Fracture-controlled gas hydrate systems in the northern Gulf of Mexico, *Mar. Pet. Geol.*, *25*, 932–941, doi:10.1016/j.marpetgeo.2008.01.013.

Coren, F., V. Volpi, and U. Tinivella (2001), Gas hydrate physical properties imaging by multi-attribute analysis—Blake Ridge BSR case history, *Mar. Geol.*, *178*, 197–210, doi:10.1016/S0025-3227(01)00156-6.

Cortes, D. D., A. I. Martin, T. S. Yun, F. M. Francisca, J. C. Santamarina, and C. Ruppel (2009), Thermal conductivity of hydrate-bearing sediments, *J. Geophys. Res.*, *114*, B11103, doi:10.1029/2008JB006235.

Dai, J., N. Banik, D. Gillespie, and N. Dutta (2008a), Exploration for gas hydrates in deepwater, northern Gulf of Mexico: Part II. Model validation by drilling, *Mar. Pet. Geol.*, *25*, 845–859, doi:10.1016/j.marpetgeo.2008.02.005.

Dai, J., F. Snyder, D. Gillespie, A. Koesoemadinata, and N. Dutta (2008b), Exploration for gas hydrates in the deepwater, northern Gulf of Mexico: Part I. A seismic approach based on geologic model, inversion, and rock physics principles, *Mar. Pet. Geol.*, *25*, 830–844, doi:10.1016/j.marpetgeo.2008.02.006.

Dallimore, S. R., and T. S. Collett (2005), Summary and implications of the Mallik 2002 gas hydrate production research well program, in *Scientific Results From the Mallik 2002 Gas Hydrate Production Research Well Program, Mackenzie Delta, Northwest Territories, Canada* [CD-ROM], edited by S. R. Dallimore and T. S. Collett, *Bull. Geol. Surv. Can.*, *585*.

Dallimore, S. R., T. S. Collett, and T. Uchida (1999), Overview of science program, JAPEX/JNOC/GSC Mallik 2L-38 gas hydrate research well, in *Scientific Results From JAPEX/JNOC/GSC Mallik 2L-38 Gas Hydrate Research Well, Mackenzie Delta, Northwest Territories, Canada*, edited by S. R. Dallimore et al., *Bull. Geol. Surv. Can.*, *544*, 11–17.

Davidson, D. W. (1973), Clathrate hydrates, in *Water: A Comprehensive Treatise*, vol. 2, *Water in Crystalline Hydrates: Aqueous Solutions of Simple Nonelectrolytes*, edited by F. Franks, pp. 115–234, Plenum, New York.

Davie, M. K., O. Y. Zatsepina, and B. A. Buffet (2004), Methane solubility in marine hydrate environments, *Mar. Geol.*, *203*, 177–184, doi:10.1016/S0025-3227(03)00331-1.

Deaton, W. M., and E. M. Frost (1946), Gas hydrates and their relation to the operation of natural-gas pipelines, *Monogr. 8*, 101 pp., Bur. of Mines, U.S. Dep. of the Interior, Washington, D. C.

deMartin, B. J. (2001), Laboratory measurements of the thermal conductivity and thermal diffusivity of methane hydrate at simulated in situ conditions, M.S. thesis, 135 pp., Ga. Inst. of Technol., Atlanta.

De Roo, J. L., C. J. Peters, R. N. Lichtenthaler, and G. A. M. Diepen (1983), Occurrence of methane hydrate in saturated and unsaturated solutions of sodium chloride and water in dependence of temperature and pressure, *AIChE J.*, *29*, 651–657, doi:10.1002/aic.690290420.

Dickens, G. R., J. R. O'Neil, D. K. Rea, and R. M. Owen (1995), Dissociation of oceanic methane hydrates as a cause of the carbon isotope excursion at the end of the Paleocene, *Paleoceanography*, *10*(6), 965–972, doi:10.1029/95PA02087.

Dickens, G. R., C. K. Paull, and P. Wallace (1997), Direct measurement of in situ methane quantities in a large gas-hydrate reservoir, *Nature*, *385*, 426–428, doi:10.1038/385426a0.

Dong, M., and F. A. L. Dullien (2006), Porous media flows, in *Multiphase Flow Handbook*, edited by C. T. Crowe, chap. 10, pp. 10-1–10-55, CRC Press, Boca Raton, Fla.

Duan, Z. H., and S. D. Mao (2006), A thermodynamic model for calculating methane solubility, density and gas phase composition of methane-bearing aqueous fluids from 273 to 523 K and from 1 to 2000 bar, *Geochim. Cosmochim. Acta*, *70*, 3369–3386, doi:10.1016/j.gca.2006.03.018.

Dullien, F. A. L. (1992), *Porous Media: Fluid Transport and Pore Structure*, 2nd ed., 574 pp., Academic, San Diego, Calif.

Dvorkin, J., and R. Uden (2004), Seismic wave attenuation in a methane hydrate reservoir, *Leading Edge*, *23*, 730–734, doi:10.1190/1.1786892.

Dvorkin, J., M. Prasad, A. Sakai, and D. Lavoie (1999), Elasticity of marine sediments: Rock physics modeling, *Geophys. Res. Lett.*, *26*, 1781–1784, doi:10.1029/1999GL900332.

Dvorkin, J., M. B. Helgerud, W. F. Waite, S. H. Kirby, and A. Nur (2000), Introduction to physical properties and elasticity models, in *Natural Gas Hydrate: In Oceanic and Permafrost Environments*, edited by M. D. Max, pp. 245–260, Kluwer Acad., Dordrecht, Netherlands.

Ebinuma, T., Y. Kamata, H. Minagawa, R. Ohmura, J. Nagao, and H. Narita (2005), Mechanical properties of sandy sediment containing methane hydrate, in *Fifth International Conference on Gas Hydrates*, pp. 958–961, Tapir Acad., Trondheim, Norway.

Edwards, R. N. (1997), On the resource evaluation of marine gas hydrate deposits using sea-floor transient electric dipole-dipole methods, *Geophysics*, *62*, 63–74, doi:10.1190/1.1444146.

Egorov, A. V., K. Crane, P. R. Vogt, and A. N. Rozhkov (1999), Gas hydrates that outcrop on the sea floor: Stability models, *Geo Mar. Lett.*, *19*, 68–75, doi:10.1007/s003670050094.

Ellis, M., R. L. Evans, D. Hutchinson, P. Hart, J. Gardner, and R. Hagen (2008), Electromagnetic surveying of seafloor mounds in the northern Gulf of Mexico, *Mar. Pet. Geol.*, *25*, 960–968, doi:10.1016/j.marpetgeo.2007.12.006.

Englezos, P., and P. R. Bishnoi (1988), Prediction of gas hydrate formation conditions in aqueous electrolyte solutions, *AIChE J.*, *34*(10), 1718–1721, doi:10.1002/aic.690341017.

Englezos, P., N. Kalogerakis, P. D. Dholabhai, and P. R. Bishnoi (1987), Kinetics of formation of methane and ethane gas hydrates, *Chem. Eng. Sci.*, *42*, 2647–2658, doi:10.1016/0009-2509(87)87015-X.

Estela-Uriba, J. F., J. P. M. Trusler, C. R. Chamorro, J. J. Segovia, M. C. Martin, and M. A. Villamanan (2006), Speeds of sound in $\{(1 - x)CH_4 + xN_2\}$ with x = (0.10001, 0.19999, and 0.5422) at temperatures between 170 K and 400 K and pressures up to 30 MPa, *J. Chem. Thermodyn.*, *38*, 929–937, doi:10.1016/j.jct.2005.10.006.

Expert Panel on Gas Hydrates (2008), Energy from gas hydrates: Assessing the opportunities and challenges for Canada, report, 222 pp., Counc. of Can. Acad., Ottawa, Ont., Canada.

Farouki, O. T. (1985), Ground thermal properties, in *Thermal Design Considerations in Frozen Ground Engineering*, edited by T. G. Krzewinski and R. G. Tart, pp. 186–202, Am. Soc. of Civ. Eng., New York.

Fernandez, A. L., and J. C. Santamarina (2001), Effect of cementation on the small-strain parameters of sands, *Can. Geotech. J.*, *38*, 191–199, doi:10.1139/cgj-38-1-191.

Flemings, P. B., X. Liu, and W. J. Winters (2003), Critical pressure and multiphase flow in Blake Ridge gas hydrate, *Geology*, *31*, 1057–1060, doi:10.1130/G19863.1.

Francisca, F., T. S. Yun, C. Ruppel, and J. C. Santamarina (2005), Geophysical and geotechnical properties of near-seafloor sediments in the northern Gulf of Mexico gas hydrate province, *Earth Planet. Sci. Lett.*, *237*, 924–939, doi:10.1016/j.epsl.2005.06.050.

Frye, M. (2008), Preliminary evaluation of in-place gas hydrate resources, *MMS Rep. 2008-004*, 136 pp., Min. Manage. Serv., U.S. Dep. of the Inter., Washington, D. C. (Available at http://www.mms.gov/revaldiv/GasHydrateAssessment.htm)

Garg, S. K., J. W. Pritchett, A. Katoh, K. Baba, and T. Fujii (2008), A mathematical model for the formation and dissociation of methane hydrates in the marine environment, *J. Geophys. Res.*, *113*, B01201, doi:10.1029/2006JB004768.

Gassmann, F. (1951), Uber die elastizitat poroser medien, *Vierteljahrsschr. Naturforsch. Ges. Zuerich*, *96*, 1–23.

Gatto, L. W., D. K. Halvorson, D. K. McCool, and A. J. Palazzo (2001), Effects of freeze-thaw cycling on soil erosion, in *Landscape Erosion and Evolution Modeling*, edited by R. S. Harmon and W. W. Doe, pp. 29–56, Kluwer Acad., New York.

Gbaruko, B. C., J. C. Igwe, P. N. Gbaruko, and R. C. Nwokeoma (2007), Gas hydrates and clathrates: Flow assurance, environmental and economic perspectives and the Nigerian liquified natural gas project, *J. Pet. Sci. Eng.*, *56*, 192–198, doi:10.1016/j.petrol.2005.12.011.

Geertsma, J. (1973), Land subsidence above compacting oil and gas reservoirs, *J. Pet. Technol.*, *25*, 734–744, doi:10.2118/3730-PA.

Ghezzehei, T. A., T. J. Kneafsey, and G. W. Su, (2007), Correspondence of the Gardner and van Genuchten-Mualem relative permeability function parameters, *Water Resour. Res.*, *43*, W10417, doi:10.1029/2006WR005339.

Ghosh, R., M. Ojha, K. Sain, and N. K. Thakur (2006), Physical parameters of hydrated sediments estimated from marine seismic reflection data, *Curr. Sci.*, *90*, 1421–1430.

Ginsburg, G. D., and V. A. Soloviev (1998), *Submarine Gas Hydrates*, 215 pp., VNII Okeangeologia, Saint Petersburg, Russia.

Ginsburg, G., V. Soloviev, T. Matveeva, and I. Andreeva (2000), Sediment grain-size control on gas hydrate presence, Sites 994, 995, and 997, *Proc. Ocean Drill. Program Sci. Results*, *164*, 237–245.

Goldsztein, G. H., and J. C. Santamarina (2004), Suspension extraction through an opening before clogging, *Appl. Phys. Lett.*, *85, 4535–4537, doi:10.1063/1.1818342.*

Grauls, D. (2001), Gas hydrates: Importance and applications in petroleum exploration, *Mar. Pet. Geol.*, *18*, 519–523, doi:10.1016/S0264-8172(00)00075-1.

Guerin, G., and D. Goldberg (2002), Sonic waveform attenuation in gas hydrate-bearing sediments from the Mallik 2L-38 research well, Mackenzie Delta, Canada, *J. Geophys. Res.*, *107*(B5), 2088, doi:10.1029/2001JB000556.

Guerin, G., and D. Goldberg (2005), Modeling of acoustic wave dissipation in gas hydrate-bearing sediments, *Geochem. Geophys. Geosyst.*, *6*, Q07010, doi:10.1029/2005GC000918.

Guerin, G., D. Goldberg, and A. Meltser (1999), Characterization of in situ elastic properties of gas hydrate-bearing sediments on the Blake Ridge, *J. Geophys. Res.*, *104*, 17,781–17,795, doi:10.1029/1999JB900127.

Guerin, G., D. Goldberg, and T. S. Collett (2005), Sonic attenuation in the JAPEX/JNOC/GSC et al. Mallik 5L-38 gas hydrate production research well, in *Scientific Results From the Mallik 2002 Gas Hydrate Production Research Well Program, Mackenzie Delta, Northwest Territories, Canada* [CD-ROM], edited by S. R. Dallimore and T. S. Collett, *Bull. Geol. Surv. Can.*, *585*.

Gupta, A., J. Lachance, E. D. Sloan, and C. A. Koh (2008), Measurements of methane hydrate heat of dissociation using high pressure differential scanning calorimetry, *Chem. Eng. Sci.*, *63*, 5848–5853, doi:10.1016/j.ces.2008.09.002.

Haacke, R. R., G. K. Westbrook, and R. D. Hyndman (2007), Gas hydrate, fluid flow and free gas: Formation of the bottom-simulating reflector, *Earth Planet. Sci. Lett.*, *261*, 407–420, doi:10.1016/j.epsl.2007.07.008.

Hadley, C., D. Peters, A. Vaughan, and D. Bean (2008), Gumusut-Kakap project: Geohazard characterisation and impact on field development plans, paper IPTC 12554 presented at the International Petroleum Technology Conference, Soc. of Pet. Eng., Kuala Lumpur, Malaysia, 3–5 Dec.

Haeckel, M., E. Suess, K. Wallmann, and D. Rickert (2004), Rising methane gas bubbles form massive hydrate layers at the seafloor, *Geochim. Cosmochim. Acta*, *68*, 4335–4345, doi:10.1016/j.gca.2004.01.018.

Handa, Y. P. (1986), Compositions, enthalpies of dissociation, and heat capacities in the range 85 to 270 K for clathrate hydrates of methane, ethane, and propane, and enthalpy of dissociation of isobutane hydrate, as determined by a heat-flow calorimeter, *J. Chem. Thermodyn.*, *18*, 915–921, doi:10.1016/0021-9614(86)90149-7.

Handa, Y. P. (1990), Effect of hydrostatic pressure and salinity on the stability of gas hydrates, *J. Phys. Chem.*, *94*, 2652–2657, doi:10.1021/j100369a077.

Handa, Y. P., R. E. Hawkins, and J. J. Murray (1984), Calibration and testing of a Tian-Calvet heat flow calorimeter. Enthalpies of fusion and heat capacities for ice and THF hydrate in the range 85 to 270 K, *J. Chem. Thermodyn.*, *16*, 623–632, doi:10.1016/0021-9614(84)90042-9.

Hashemi, S., A. Macchi, S. Bergeron, and P. Servio (2006), Prediction of methane and carbon dioxide solubility in water in the presence of hydrate, *Fluid Phase Equilibria*, *246*, 131–136, doi:10.1016/j.fluid.2006.05.010.

Helgerud, M. B., J. Dvorkin, A. Nur, A. Sakai, and T. Collett (1999), Elastic-wave velocity in marine sediments with gas hydrates: Effective medium modeling, *Geophys. Res. Lett.*, *26*, 2021–2024, doi:10.1029/1999GL900421.

Helgerud, M. B., W. F. Waite, S. H. Kirby, and A. Nur (2009), Elastic wave speeds and moduli in polycrystalline ice Ih, sI methane hydrate, and sII methane-ethane hydrate, *J. Geophys. Res.*, *114*, B02212, doi:10.1029/2008JB006132.

Henry, P., M. Thomas, and M. B. Clennell (1999), Formation of natural gas hydrate in marine sediments: 2. Thermodynamic calculations of stability conditions in porous sediments, *J. Geophys. Res.*, *104*, 23,005–23,022, doi:10.1029/1999JB900167.

Hensen, C., and K. Wallmann (2005), Methane formation at Costa Rica continental margin: Constraints for gas hydrate inventories and cross-decollement fluid flow, *Earth Planet. Sci. Lett.*, *236*, 41–60, doi:10.1016/j.epsl.2005.06.007.

Hight, D. W., R. Boese, A. P. Butcher, C. R. I. Clayton, and P. R. Smith (1992), Disturbance of Bothkennar clay prior to laboratory testing, *Geotechnique*, *42*, 199–217.

Holder, G. D., and V. A. Kamath (1984), Hydrates of (methane + *cis*-2-butene) and (methane + *trans*-2-butene), *J. Chem. Thermodyn.*, *16*, 399–400, doi:10.1016/0021-9614(84)90179-4.

Holder, G. D., V. A. Kamath, and S. P. Godbole (1984), The potential of natural gas hydrates as an energy resource, *Annu. Rev. Energy*, *9*, 427–445, doi:10.1146/annurev.eg.09.110184.002235.

Holland, M., P. Schultheiss, J. Roberts, and M. Druce (2008), Observed gas hydrate morphologies in marine sediments, paper 5691 presented at the 6th International Conference on Gas Hydrates, Chevron, Vancouver, B. C., Canada, 6–10 July.

Holtz, R. D., and W. D. Kovacs (1981), *An Introduction to Geotechnical Engineering*, 733 pp., Prentice-Hall, Englewood Cliffs, N. J.

Honarpour, M., L. Koederitz, and A. H. Harvey (1986), *Relative Permeability of Petroleum Reservoirs*, 208 pp., CRC Press, Boca Raton, Fla.

Hong, H., and M. Pooladi-Darvish (2005), Numerical study of constant-rate gas production from in situ gas hydrate by depressurization, in *Scientific Results From the Mallik 2002 Gas Hydrate Production Research Well Program, Mackenzie Delta, Northwest Territories, Canada* [CD-ROM], edited by S. R. Dallimore and T. S. Collett, *Bull. Geol. Surv. Can.*, *585*.

Huang, D., and S. Fan (2004), Thermal conductivity of methane hydrate formed from sodium dodecyl sulfate solution, *J. Chem. Eng. Data*, *49*, 1479–1482, doi:10.1021/je0498098.

Huang, D., and S. Fan (2005), Measuring and modeling thermal conductivity of gas hydrate-bearing sand, *J. Geophys. Res.*, *110*, B01311, doi:10.1029/2004JB003314.

Huang, J.-W., G. Bellefleur, and B. Milkereit (2009), Seismic modeling of multidimensional heterogeneity scales of Mallik gas hydrate reservoirs, Northwest Territories of Canada, *J. Geophys. Res.*, *114*, B07306, doi:10.1029/2008JB006172.

Hutchinson, D. R., et al. (2008), Site selection for DOE/JIP gas hydrate drilling in the northern Gulf of Mexico, paper presented at the 6th International Conference on Gas Hydrates, Chevron, Vancouver, B. C., Canada, 6–10 July.

Hvorslev, M. J. (1949), *Subsurface Exploration and Sampling of Soils for Civil Engineering Purposes*, 521 pp., Waterw. Exp. Stn., U.S. Army Corps of Eng., Vicksburg, Miss.

Hyndman, R. D., T. Yuan, and K. Moran (1999), The concentration of deep sea gas hydrates from downhole electrical resistivity logs and laboratory data, *Earth Planet. Sci. Lett.*, *172*, 167–177, doi:10.1016/S0012-821X(99)00192-2.

Hyodo, M., Y. Nakata, N. Yoshimoto, and T. Ebinuma (2005), Basic research on the mechanical behavior of methane hydrate-sediments mixture, *Soils Found.*, *45*, 75–85.

Hyodo, M., Y. Nakata, N. Yoshimoto, and R. Orense (2007), Shear behaviour of methane hydrate-bearing sand, paper presented at the 17th International Offshore and Polar Engineering Conference, Int. Soc. of Offshore and Polar Eng., Lisbon, Portugal, 1–6 July.

Inks, T., M. Lee, W. Agena, T. Collett, and R. Boswell (2008), Comparison of drilling results to pre-drill estimates of gas hydrate occurrence: ''Mount Elbert'' test site, Alaska North Slope, *Fire in the Ice: Methane Hydrate Newsletter*, winter, pp. 13–15, Off. of Fossil Energy, Natl. Energy Technol. Lab., U.S. Dep. of Energy, Washington, D. C.

Jakobsen, M., J. A. Hudson, T. A. Minshull, and S. C. Singh (2000), Elastic properties of hydrate-bearing sediment using effective medium theory, *J. Geophys. Res.*, *105*, 561–577, doi:10.1029/1999JB900190.

Ji, C., G. Ahmadi, and D. H. Smith (2003), Constant rate natural gas production from a well in a hydrate reservoir, *Energy Convers. Manage.*, *44*, 2403–2423, doi:10.1016/S0196-8904(03)00010-4.

Jin, S., J. Nagao, S. Takeya, Y. Jin, J. Hayashi, Y. Kamata, T. Ebinuma, and H. Narita (2006), Structural investigation of methane hydrate sediments by microfocus X-ray computed tomography technique under high-pressure conditions, *Jpn. J. Appl. Phys.*, *45*, L714–L716, doi:10.1143/JJAP.45.L714.

Jin, Y. K., M. W. Lee, and T. S. Collett (2002), Relationship of gas hydrate concentration to porosity and reflection amplitude in a research well, Mackenzie Delta, Canada, *Mar. Pet. Geol.*, *19*, 407–415, doi:10.1016/S0264-8172(02)00011-9.

Jin, Y., J. Hayashi, J. Nagao, K. Suzuki, H. Minagawa, T. Ebinuma, and H. Narita (2007), New method of assessing absolute permeability of natural methane hydrate sediments by microfocus X-ray computed tomography, *Jpn. J. Appl. Phys.*, *46*, 3159–3162, doi:10.1143/JJAP.46.3159.

JIP Leg II Science Team (2009), Gulf of Mexico gas hydrate drilling and logging expedition underway, *Fire in the Ice: Methane Hydrate Newsletter*, spring, pp. 1–6, Off. of Fossil Energy, Natl. Energy Technol. Lab., U.S. Dep. of Energy, Washington, D. C.

Jones, E., et al. (2008), Scientific objectives of the Gulf of Mexico gas hydrate JIP leg II drilling, paper OTC 19501 presented at the Offshore Technology Conference, Am. Assoc. of Pet. Geol., Houston, Tex., 5–8 May.

Judd, A., and M. Hovland (2007), *Seabed Fluid Flow: The Impact on Geology, Biology and the Marine Environment*, 475 pp., Cambridge Univ. Press, Cambridge, U. K.

Kamath, V. A., P. N. Mutalik, J. H. Sira, and S. L. Patil (1991), Experimental study of brine injection and depressurization methods for dissociation of gas hydrates, *SPE Form. Eval.*, *6*, 477–484, doi:10.2118/19810-PA.

Kang, S.-P., H. Lee, and B. J. Ryu (2001), Enthalpies of dissociation of clathrate hydrates of carbon dioxide, nitrogen, (carbon dioxide + nitrogen), and (carbon dioxide + nitrogen + tetrahydrofuran), *J. Chem. Thermodyn.*, *33*, 513–521, doi:10.1006/jcht.2000.0765.

Katsuki, D., R. Ohmura, T. Ebinuma, and H. Narita (2006), Formation, growth and ageing of clathrate hydrate crystals in a porous medium, *Philos. Mag.*, *86*, 1753–1761, doi:10.1080/14786430500509062.

Kayen, R. E., and H. J. Lee (1991), Pleistocene slope instability of gas hydrate-laden sediment on the Beaufort Sea Margin, *Mar. Geotechnol.*, *10*, 125–141, doi:10.1080/10641199109379886.

Kayen, R. E., and H. J. Lee (1993), Slope stability in regions of seafloor gas hydrate: Beaufort Sea continental slope, in *Submarine Landslides: Selected Studies in the US Exclusive Economic Zone*, edited by W. C. Schwab et al., *U.S. Geol. Surv. Bull.*, *2002*, 97–103.

Kim, Y. S., S. K. Ryu, S. O. Yang, and C. S. Lee (2003), Liquid water-hydrate equilibrium measurements and unified predictions of hydrate-containing phase equilibria for methane, ethane, propane, and their mixtures, *Ind. Eng. Chem. Res.*, *42*, 2409–2414, doi:10.1021/ie0209374.

Kimura, T., and K. Saitoh (1984), Effect of sampling disturbance on undrained strength of cohesive soils, *Geotech. Eng.*, *15*, 37–57.

Klapproth, A., K. S. Techmer, S. A. Klapp, M. M. Murshed, and W. F. Kuhs (2007), Microstructure of gas hydrates in porous media, in *Physics and Chemistry of Ice: Proceedings of the 11th International Conference on the Physics and Chemistry of Ice*, edited by W. F. Kuhs, pp. 321–328, R. Soc. of Chem., London.

Klein, K. A., and J. C. Santamarina (2003), Electrical conductivity in soils: Underlying phenomena, *J. Environ. Eng. Geophys.*, *8*, 263–273.

Kleinberg, R. L., and J. Dai (2005), Estimation of the mechanical properties of natural gas hydrate deposits from petrophysical measurements, paper OTC 17205 presented at the Offshore Technology Conference, Am. Assoc. of Pet. Geol., Houston, Tex.

Kleinberg, R. L., C. Flaum, D. D. Griffin, P. G. Brewer, G. E. Malby, E. T. Peltzer, and J. P. Yesinowski (2003), Deep sea NMR: Methane hydrate growth habit in porous media and its relationship to hydraulic permeability, deposit accumulation, and submarine slope stability, *J. Geophys. Res.*, *108*(B10), 2508, doi:10.1029/2003JB002389.

Kleinberg, R. L., C. Flaum, and T. S. Collett (2005), Magnetic resonance log of JAPEX/JNOC/GSC et al. Mallik 5L-38 gas hydrate production research well: Gas hydrate saturation, growth

habit and relative permeability, in *Scientific Results From the Mallik 2002 Gas Hydrate Production Research Well Program, Mackenzie Delta, Northwest Territories, Canada* [CD-ROM], edited by S. R. Dallimore and T. S. Collett, *Bull. Geol. Surv. Can.*, *585*.

Kliner, J. R., and J. L. H. Grozic (2006), Determination of synthetic hydrate content in sand specimens using dielectrics, *Can. Geotech. J.*, *43*, 551–562, doi:10.1139/T06-022.

Kneafsey, T. J., L. Tomutsa, L. Moridis, Y. Seol, B. Freifeld, C. E. Taylor, and A. Gupta (2005), Methane hydrate formation and dissociation in a partially saturated sand—Measurements and observations, in *Fifth International Conference on Gas Hydrates*, pp. 213–220, Tapir Acad., Trondheim, Norway.

Kneafsey, T. J., L. Tomutsa, G. J. Moridis, Y. Seol, B. M. Freifeld, C. E. Taylor, and A. Gupta (2007), Methane hydrate formation and dissociation in a partially saturated core-scale sand sample, *J. Petrol. Sci. Eng.*, *56*, 108–126, doi:10.1016/j.petrol.2006.02.002.

Kono, H. O., and B. Budhijanto (2002), Modeling of gas hydrate formation processes by controlling the interfacial boundary surfaces, paper presented at the 4th International Conference on Gas Hydrates, Jpn. Natl. Oil Corp., Yokohama, Japan, 19–23 May.

Krupiczka, R. (1967), Analysis of thermal conductivity in granular materials, *Int. Chem. Eng.*, *7*, 122–144.

Kumano, H., T. Asaoka, A. Saito, and S. Okawa (2007), Study on latent heat of fusion of ice in aqueous solutions, *Int. J. Refrigeration*, *30*, 267–273, doi:10.1016/j.ijrefrig.2006.07.008.

Kurihara, M., H. Ouchi, T. Inoue, T. Yonezawa, Y. Masuda, S. R. Dallimore, and T. S. Collett (2005), Analysis of the JAPEX/JNOC/GSC et al. Mallik 5l-38 gas hydrate thermal-production test through numerical simulation, in *Scientific Results From the Mallik 2002 Gas Hydrate Production Research Well Program, Mackenzie Delta, Northwest Territories, Canada* [CD-ROM], edited by S. R. Dallimore and T. S. Collett, *Bull. Geol. Surv. Can.*, *585*.

Kuuskraa, V. A., E. C. Hammerschaimb, G. D. Holder, and E. D. Sloan (1983), Handbook of gas hydrate properties and occurrence, *Rep. DOE/MC/19239-1546*, 234 pp., U.S. Govt. Print. Off., Washington, D. C.

Kvenvolden, K. A., and T. D. Lorenson (2001), The global occurrence of natural gas hydrates, in *Natural Gas Hydrates: Occurrence, Distribution, and Detection*, *Geophys. Monogr. Ser.*, vol. 124, edited by C. K. Paull and W. P. Dillon, pp. 3–18, AGU, Washington, D. C.

Kwon, T.-H., G.-C. Cho, and J. C. Santamarina (2008), Gas hydrate dissociation in sediments: Pressure-temperature evolution, *Geochem. Geophys. Geosyst.*, *9*, Q03019, doi:10.1029/2007GC001920.

Ladd, C. C., and T. W. Lambe (1963), The strength of undisturbed clay determined from undrained tests, *ASTM Spec. Tech. Publ.*, *361*, 342–371.

Lambe, T. W., and R. V. Whitman (1969), *Soil Mechanics*, 553 pp., John Wiley, New York.

Leaist, D. G., J. J. Murray, M. L. Post, and D. W. Davidson (1982), Enthalpies of decomposition and heat capacities of ethylene oxide and tetrahydrofuran hydrates, *J. Phys. Chem.*, *86*, 4175–4178, doi:10.1021/j100218a017.

Lee, J. H., Y. S. Baek, and W. M. Sung (2005), The kinetics on hydrate formation in pipelines, *Energy Sources*, *27*, 875–885.

Lee, J.-Y. (2007), Hydrate-bearing sediments: Formation and geophysical properties, Ph.D. thesis, 241 pp., Ga. Inst. of Technol., Atlanta.

Lee, J. Y., T. S. Yun, J. C. Santamarina, and C. Ruppel (2007), Observations related to tetrahydrofuran and methane hydrates for laboratory studies of hydrate-bearing sediments, *Geochem. Geophys. Geosyst.*, *8*, Q06003, doi:10.1029/2006GC001531.

Lee, J. Y., J. C. Santamarina, and C. Ruppel (2008), Mechanical and electromagnetic properties of northern Gulf of Mexico sediments with and without THF hydrates, *Mar. Pet. Geol.*, *25*, 884–895, doi:10.1016/j.marpetgeo.2008.01.019.

Lee, J. Y., J. C. Santamarina, and C. Ruppel (2009), Volume change associated with formation and dissociation of hydrate in sediment, *Geochem. Geophys. Geosyst.*, doi:10.1029/2009GC002667, in press.

Lee, M. W. (2002), Biot-Gassmann theory for velocities of gas hydrate-bearing sediments, *Geophysics*, *67*, 1711–1719, doi:10.1190/1.1527072.

Lee, M. W. (2005), Well log analysis to assist the interpretation of 3-D seismic data at Milne Point, North Slope of Alaska, *U.S. Geol. Surv. Sci. Invest. Rep.*, *2005-5048*, 18 pp.

Lee, M. W. (2006), Is amplitude loss of sonic waveforms due to intrinsic attenuation or source coupling to the medium?, *U.S. Geol. Surv. Sci. Invest. Rep.*, *2006-5120*, 13 pp.

Lee, M. W. (2008), Models for gas hydrate-bearing sediments inferred from hydraulic permeability and elastic velocities, *U.S. Geol. Surv. Sci. Invest. Rep.*, *2008-5219*, 20 pp.

Lee, M. W., and T. S. Collett (1999), Amount of gas hydrate estimated from compressional-and shear-wave velocities at the JPEX/JNOC/GSC Mallik 2L-38 gas hydrate research well, *Bull. Geol. Surv. Can.*, *544*, 313–322.

Lee, M. W., and T. S. Collett (2005), Assessments of gas hydrate concentrations estimated from sonic logs in the JAPEX/JNOC/GSC et al. Mallik 5L-38 gas hydrate research production well, in *Scientific Results From the Mallik 2002 Gas Hydrate Production Research Well Program, Mackenzie Delta, Northwest Territories, Canada* [CD-ROM], edited by S. R. Dallimore and T. S. Collett, *Bull. Geol. Surv. Can.*, *585*.

Lee, M. W., and T. S. Collett (2006), Gas hydrate and free gas saturations estimated from velocity logs on Hydrate Ridge, offshore Oregon, USA [online], *Proc. Ocean Drill. Progam Sci. Results*, *204*, 25 pp. (Available at http://www-odp.tamu.edu/publications/204_SR/103/103.htm)

Lee, M. W., and T. S. Collett (2009), Gas hydrate saturations estimated from fractured reservoir at Site NGHP-01-10, Krishna-Godavari Basin, India, *J. Geophys. Res.*, *114*, B07102, doi:10.1029/2008JB006237.

Lee, M. W., and W. F. Waite (2007), Amplitude loss of seismic waveform due to source coupling to the medium, *Geophys. Res. Lett.*, *34*, L05303, doi:10.1029/2006GL029015.

Lee, M. W., and W. F. Waite (2008), Estimating pore-space gas hydrate saturations from well log acoustic data, *Geochem. Geophys. Geosyst.*, *9*, Q07008, doi:10.1029/2008GC002081.

Lee, M. W., D. R. Hutchinson, T. S. Collett, and W. P. Dillon (1996), Seismic velocities for hydrate-bearing sediments using weighted equation, *J. Geophys. Res.*, *101*(B9), 20,347–20,358, doi:10.1029/96JB01886.

Lievois, J. S., R. Perkins, R. J. Martin, and R. Kobayashi (1990), Development of an automated, high pressure heat flux calorimeter and its application to measure the heat of dissociation and hydrate numbers of methane hydrate, *Fluid Phase Equilibria*, *59*, 73–97, doi:10.1016/0378-3812(90)85147-3.

Liu, X., and P. B. Flemings (2006), Passing gas through the hydrate stability zone at southern Hydrate Ridge, offshore Oregon, *Earth Planet. Sci. Lett.*, *241*, 211–226, doi:10.1016/j.epsl.2005.10.026.

Liu, X., and P. B. Flemings (2007), Dynamic multiphase flow model of hydrate formation in marine sediments, *J. Geophys. Res.*, *112*, B03101, doi:10.1029/2005JB004227.

Lu, S., and G. A. McMechan (2002), Estimating of gas hydrate and free gas saturation, concentration, and distribution from seismic data, *Geophysics*, *67*, 582–593, doi:10.1190/1.1468619.

Lu, S., T. Ren, Y. Gong, and R. Horton (2007), An improved model for predicting soil thermal conductivity from water content at room temperature, *Soil Sci. Soc. Am. J.*, *71*, 8–14.

Lu, W., I. M. Chou, and R. C. Burruss (2008), Determination of methane concentrations in water in equilibrium with sI methane hydrate in the absence of a vapor phase by in situ Raman spectroscopy, *Geochim. Cosmochim. Acta*, *72*, 412–422, doi:10.1016/j.gca.2007.11.006.

MacDonald, I. R., N. L. Guinasso, R. Sassen, J. M. Brooks, L. Lee, and K. T. Scott (1994), Gas hydrate that breaches the sea floor on

the continental slope of the Gulf of Mexico, *Geology*, *22*, 699–702, doi:10.1130/0091-7613(1994)022<0699:GHTBTS>2.3.CO;2.

MacKay, M. E., R. D. Jarrard, G. K. Westbrook, and R. D. Hyndman (1995), Technical notes and additions to origin of bottom-simulating reflectors: Geophysical evidence from the Cascadia accretionary prism, *Proc. Ocean Drill. Program Sci. Results*, *146*, 461–463.

Malinverno, A., M. Kastner, M. E. Torres, and U. G. Wortmann (2008), Gas hydrate occurrence from pore water chlorinity and downhole logs in a transect across the northern Cascadia margin (Integrated Ocean Drilling Program Expedition 311), *J. Geophys. Res.*, *113*, B08103, doi:10.1029/2008JB005702.

Masoudi, R., B. Tohidi, A. Danesh, and A. C. Todd (2004), A new approach in modelling phase equilibria and gas solubility in electrolyte solutions and its applications to gas hydrates, *Fluid Phase Equilibria*, *215*, 163–174, doi:10.1016/j.fluid.2003.08.009.

Masui, A., H. Haneda, Y. Ogata, and K. Aoki (2005), The effect of saturation degree of methane hydrate on the shear strength of synthetic methane hydrate sediments, in *Fifth International Conference on Gas Hydrates*, pp. 657–663, Tapir Acad., Trondheim, Norway.

Masui, A., H. Haneda, Y. Ogata, and K. Aoki (2006), Triaxial compression test on submarine sediment containing methane hydrate in deep sea off the coast of Japan (in Japanese), paper presented at the 41st Annual Conference, Jpn. Geotech. Soc., Kagoshima, Japan, 12–14 July.

Masui, A., K. Miyazaki, H. Haneda, Y. Ogata, and K. Aoki (2008), Mechanical characteristics of natural and artificial gas hydrate bearing sediments, paper 5697 presented at the 6th International Conference on Gas Hydrates, Chevron, Vancouver, B. C., Canada, 6–10 July.

Matsuo, M., and T. Shogaki (1988), Effects of plasticity and sample disturbance on statistical properties of undrained shear strength, *Soil Found.*, *28*, 14–24.

Matsushima, J. (2006), Seismic wave attenuation in methane hydrate-bearing sediments: Vertical seismic profiling data from the Nankai Trough exploratory well, offshore Tokai, central Japan, *J. Geophys. Res.*, *111*, B10101, doi:10.1029/2005JB004031.

Mavko, G., T. Mukerji, and J. Dvorkin (1998), *The Rock Physics Handbook: Tools for Seismic Analysis in Porous Media*, 329 pp., Cambridge Univ. Press, Cambridge, U. K.

Maxwell, J. C. (1954), *A Treatise on Electricity and Magnetism*, vol. 1, 506 pp., Dover, Mineola, N. Y.

Mayne, P. W., F. H. Kulhawy, and C. H. Trautmann (1992), Experimental study of undrained lateral and moment behavior of drilled shafts during static and cyclic loading, *Rep. TR-10221*, Electr. Power Inst., Palo Alto, Calif.

McIver, R. D. (1982), Role of naturally occurring gas hydrates in sediment transport, *AAPG Bull.*, *66*(6), 789–792.

Mienert, J., M. Vanneste, S. Bünz, K. Andreassen, H. Haflidason, and H. P. Sejrup (2005), Ocean warming and gas hydrate stability on the mid-Norwegian margin at the Storegga Slide, *Mar. Pet. Geol.*, *22*, 233–244, doi:10.1016/j.marpetgeo.2004.10.018.

Minagawa, H., R. Ohmura, Y. Kamata, T. Ebinuma, H. Narita, and Y. Masuda (2005), Water permeability measurements of gas hydrate-bearing sediments, in *Fifth International Conference on Gas Hydrates*, edited by T. Austvik, pp. 398–401, Tapir Acad., Trondheim, Norway.

Minagawa, H., Y. Nishikawa, I. Ikeda, K. Miyazaki, N. Takahara, Y. Sakamoto, T. Komai, and H. Narita (2008), Measurement of water permeability and pore-size distribution of methane-hydrate-bearing sediments, paper 5672 presented at the 6th International Conference on Gas Hydrates, Chevron, Vancouver, B. C., Canada, 6–10 July.

Mitchell, J. K., and K. Soga (2005), *Fundamentals of Soil Behavior*, 577 pp., John Wiley, New York.

Mohammadi, A. H., A. Chapoy, B. Tohidi, and D. Richon (2006), Gas solubility: A key to estimating the water content of natural gases, *Ind. Eng. Chem. Res.*, *45*, 4825–4829, doi:10.1021/ie051337i.

Moridis, G. J. (2003), Numerical studies of gas production from hydrates, *SPE J.*, *32*, 359–370.

Moridis, G. J., and T. Reagan (2007a), Gas production from oceanic Class 2 hydrate accumulations, paper OTC 18866 presented at the Offshore Technology Conference, Am. Assoc. of Pet. Geol., Houston, Tex., 30 April to 3 May.

Moridis, G. J., and T. Reagan (2007b), Strategies for gas production from oceanic Class 3 hydrate accumulations, paper OTC 18865 presented at the Offshore Technology Conference, Am. Assoc. of Pet. Geol., Houston, Tex., 30 April to 3 May.

Moridis, G. J., T. S. Collett, S. R. Dallimore, T. Satoh, S. Hancock, and B. Weatherill (2004), Numerical studies of gas production from several CH_4 hydrate zones at the Mallik site, Mackenzie Delta, Canada, *J. Petrol. Sci. Eng.*, *43*, 219–238, doi:10.1016/j.petrol.2004.02.015.

Moridis, G. J., T. S. Collett, S. R. Dallimore, T. Inoue, and T. Mroz (2005), Analysis and interpretation of the thermal test of gas hydrate dissociation in the JAPEX/JNOC/GSC et al. Mallik 5L-38 gas hydrate production research well, in *Scientific Results From the Mallik 2002 Gas Hydrate Production Research Well Program, Mackenzie Delta, Northwest Territories, Canada* [CD-ROM], edited by S. R. Dallimore and T. S. Collett, *Bull. Geol. Surv. Can.*, *585*.

Moridis, G. J., M. B. Kowalsky, and K. Pruess (2007), Depressurization-induced gas production from Class 1 hydrate deposits, *SPE Reservoir Eval. Eng.*, *10*, 458–481, doi:10.2118/97266-PA.

Moridis, G. J., T. S. Collett, R. Boswell, M. Kurihara, M. T. Reagan, C. Koh, and E. D. Sloan (2008), Toward production from gas hydrates: Current status, assessment of resources, and simulation-based evaluation of technology and potential, paper SPE 114163 presented at the SPE Unconventional Reservoirs Conference, Soc. of Pet. Eng., Keystone, Colo.

Mork, M., G. Schei, and R. Larsen (2000), NMR imaging study of hydrates in sediments, in *Gas Hydrates: Challenges for the Future*, edited by G. D. Holder and P. R. Bishnoi, *Ann. N. Y. Acad. Sci.*, *912*, 897–905.

Murray, D. R., R. L. Kleinberg, B. K. Sinha, M. Fukuhara, O. Osawa, T. Endo, and T. Namikawa (2006), Saturation, acoustic properties, growth habit, and state of stress of a gas hydrate reservoir from well logs, *Petrophysics*, *47*, 129–137.

Nadem, M., S. L. Patil, P. N. Mutalik, V. A. Kamath, and S. P. Godbole (1988), Measurement of gas permeability in hydrate saturated unconsolidated cores, paper presented at the 3rd Chemical Congress of North America and Annual Meeting, Am. Chem. Soc., Toronto, Ont., Canada, 6–10 June.

Nakagawa, R., A. Hachikubo, and H. Shoji (2008), Dissociation and specific heats of gas hydrates under submarine and sublacustrine environments, paper presented at the 6th International Conference on Gas Hydrates, Chevron, Vancouver, B. C., Canada.

Nimblett, J., and C. Ruppel (2003), Permeability evolution during the formation of gas hydrates in marine sediments, *J. Geophys. Res.*, *108*(B9), 2420, doi:10.1029/2001JB001650.

Nixon, M. F., and J. L. H. Grozic (2007), Submarine slope failure due to gas hydrate dissociation: A preliminary quantification, *Can. Geotech. J.*, *44*, 314–325, doi:10.1139/T06-121.

Parker, J. C., R. J. Lenhard, and T. Kuppusamy (1987), A parametric model for constitutive properties governing multiphase flow in porous media, *Water Resour. Res.*, *23*, 618–624, doi:10.1029/WR023i004p00618.

Paull, C. K., and R. Matsumoto (2000), Leg 164 overview, *Proc. Ocean Drill. Program Sci. Results*, *164*, 3–10.

Perloff, W. H., and W. Baron (1976), *Soil Mechanics*, 745 pp., John Wiley, New York.

Pooladi-Darvish, M. (2004), Gas production from hydrate reserves and its modeling, *J. Pet. Technol.*, *56*, 65–71, doi:10.2118/86827-MS.

Priest, J. A., A. Best, and C. R. Clayton (2005), A laboratory investigation into the seismic velocities of methane gas hydrate-

bearing sand, *J. Geophys. Res.*, *110*, B04102, doi:10.1029/2004JB003259.

Priest, J., E. Kingston, C. Clayton, P. Schultheiss, and M. Druce (2008), The structure of hydrate bearing fine grained marine sediments, paper 5810 presented at the 6th International Conference on Gas Hydrates, Chevron, Vancouver, B. C., Canada, 6–10 July.

Pruess, K., and G. Moridis (1999), TOUGH2 user's guide, version 2.0, Lawrence Berkeley Natl. Lab., Univ. of Calif., Berkeley.

Reagan, M. T., and G. J. Moridis (2007), Oceanic gas hydrate instability and dissociation under climate change scenarios, *Geophys. Res. Lett.*, *34*, L22709, doi:10.1029/2007GL031671.

Rehder, G., S. H. Kirby, W. B. Durham, L. A. Stern, E. T. Peltzer, J. Pinkston, and P. G. Brewer (2004), Dissolution rates of pure methane hydrate and carbon dioxide hydrate in undersaturated seawater at 1000-m depth, *Geochim. Cosmochim. Acta*, *68*, 285–292, doi:10.1016/j.gca.2003.07.001.

Reister, D. B. (2003), Using measured velocity to estimate gas hydrate concentration, *Geophysics*, *68*, 884–891, doi:10.1190/1.1581040.

Revil, A. (2000), Thermal conductivity of unconsolidated sediments with geophysical applications, *J. Geophys. Res.*, *105*, 16,749–16,768, doi:10.1029/2000JB900043.

Riedel, M., P. E. Long, and T. S. Collett (2006), Estimates of in situ gas hydrate concentration from resistivity monitoring of gas hydrate bearing sediments during temperature equilibration, *Mar. Geol.*, *227*, 215–225, doi:10.1016/j.margeo.2005.10.007.

Rinaldi, V. A., and J. C. Santamarina (2008), Cemented soils: Small strain stiffness, in *Deformational Characteristics of Geomaterials*, vol. 1, edited by S. E. Burns et al., pp. 267–273, IOS, Amsterdam.

Rosenbaum, E. J., N. J. English, J. K. Johnson, D. W. Shaw, and R. P. Warzinski (2007), Thermal conductivity of methane hydrate from experiment and molecular simulation, *J. Phys. Chem. B*, *111*, 13,194–13,205, doi:10.1021/jp074419o.

Rueff, R. M., and E. D. Sloan (1985), Effect of granular sediment on some thermal properties of tetrahydrofuran hydrate, *Ind. Eng. Chem. Process Des. Dev.*, *24*, 882–885, doi:10.1021/i200030a060.

Rueff, R. M., E. D. Sloan, and V. F. Yesavage (1988), Heat capacity and heat of dissociation of methane hydrates, *AIChE J.*, *34*, 1468–1476, doi:10.1002/aic.690340908.

Ruppel, C. (2000), Thermal state of the gas hydrate reservoir, in *Natural Gas Hydrate: In Oceanic and Permafrost Environments*, edited by M. D. Max, pp. 29–42, Kluwer Acad., Dordrecht, Netherlands.

Ruppel, C. (2007), Tapping methane hydrates for unconventional natural gas, *Elements*, *3*, 193–199, doi:10.2113/gselements.3.3.193.

Ruppel, C., and J. W. Pohlman (2008), Climate change and the global carbon cycle: Perspectives and opportunities, *Fire in the Ice: Methane Hydrate Newsletter*, winter, pp. 5–8, Off. of Fossil Energy, Natl. Energy Technol. Lab., U.S. Dep. of Energy, Washington, D. C.

Rutqvist, J., and G. J. Moridis (2007), Numerical studies of geomechanical stability of hydrate-bearing sediments, paper presented at the Offshore Technology Conference, Am. Assoc. of Pet. Geol., Houston, Tex., 30 April to 3 May.

Rutqvist, J., G. J. Moridis, T. Grover, and T. Collett (2008), Geomechanical response of known permafrost hydrate deposits to depressurization-induced production, paper 5726 presented at the 6th International Conference on Gas Hydrates, Chevron, Vancouver, B. C., Canada, 6–10 July.

Rydzy, M. B., J. M. Schicks, R. Naumann, and J. Erzinger (2007), Dissociation enthalpies of synthesized multicomponent gas hydrates with respect to the guest composition and cage occupancy, *J. Phys. Chem. B*, *111*, 9539–9545, doi:10.1021/jp0712755.

Sakamoto, Y., K. Miyazaki, N. Tenma, T. Komai, T. Yamaguchi, M. Shimokawara, and K. Ohga (2008), Simulation of a laboratory experiment for dissociation process of methane hydrate by depressurization, paper presented at the 6th International Conference on Gas Hydrates, Chevron, Vancouver, B. C., Canada, 6–10 July.

Santagata, M. C., and J. T. Germaine (2002), Sampling disturbance effects in normally consolidated clays, *J. Geotech. Geoenviron. Eng.*, *128*, 997–1006, doi:10.1061/(ASCE)1090-0241(2002)128:12(997).

Santamarina, J. C., and G. C. Cho (2004), Soil behaviour: The role of particle shape, paper presented at the Skempton Conference, Thomas Telford Serv. Ltd., London.

Santamarina, J. C., and C. Ruppel (2008), The impact of hydrate saturation on the mechanical, electrical, and thermal properties of hydrate-bearing sand, silts, and clay, paper 5817 presented at the 6th International Conference on Gas Hydrates, Chevron, Vancouver, B. C., Canada, 6–10 July.

Santamarina, J. C., K. A. Klein, and M. A. Fam (2001), *Soils and Waves: Particulate Materials Behavior, Characterization and Process Monitoring*, 488 pp., John Wiley, New York.

Santamarina, J. C., V. Rinaldi, D. Fratta, K. Klein, Y. H. Wang, G. C. Cho, and G. Cascante (2005), A survey of elastic and electromagnetic properties of near-surface soils, in *Near-Surface Geophysics*, edited by D. K. Butler, pp. 71–87, Soc. of Explor. Geophys., Tulsa, Okla.

Seo, Y., H. Lee, and B.-J. Ryu (2002), Hydration number and two-phase equilibria of CH_4 hydrate in the deep ocean sediments, *Geophys. Res. Lett.*, *29*(8), 1244, doi:10.1029/2001GL014226.

Servio, P., and P. Englezos (2002), Measurement of dissolved methane in water in equilibrium with its hydrate, *J. Chem. Eng. Data*, *47*, 87–90, doi:10.1021/je0102255.

Shankar, U., N. K. Thakur, and B. Ashalatha (2006), Fluid flow related features as an indicator of potential gas hydrate zone: Western continental margin of India, *Mar. Geophys. Res.*, *27*, 217–224, doi:10.1007/s11001-006-9001-6.

Shin, H., and J. C. Santamarina (2009), Mineral dissolution and the evolution of ko, *J. Geotech. Geoenviron. Eng.*, *135*, 1141–1147, doi:10.1061/(ASCE)GT.1943-5606.0000053.

Shin, H., J. C. Santamarina, and J. A. Cartwright (2008), Contraction-driven shear failure in compacting uncemented soils, *Geology*, *36*, 931–934, doi:10.1130/G24951A.1.

Siddique, A., S. M. Farooq, and C. R. I. Clayton (2000), Disturbances due to tube sampling in coastal soils, *J. Geotech. Geoenviron. Eng.*, *128*, 568–575.

Singh, D. N., and K. Devid (2000), Generalized relationships for estimating soil thermal resitivity, *Exp. Therm. Fluid Sci.*, *22*, 133–143, doi:10.1016/S0894-1777(00)00020-0.

Siriwardane, H. J. (1992), Ground movements associated with gas hydrate production, paper presented at the Natural Gas Research and Development Contractors Review Meeting, U.S. Dep. of Energy, Morgantown, W. V., 5–6 May.

Skempton, A. W. (1957), Discussion on the planning and design of the new Hong Kong airport, *Proc. Inst. Civ. Eng.*, *7*, 305–307.

Skempton, A. W., and V. A. Sowa (1963), The behavior of saturated clays during sampling and testing, *Geotechnique*, *13*, 269–290.

Sloan, E. D., Jr. (2004), Introductory overview: Hydrate knowledge development, *Am. Mineral.*, *89*, 1155–1161.

Sloan, E. D., and F. Fleyfel (1992), Hydrate dissociation enthalpy and guest size, *Fluid Phase Equilibria*, *76*, 123–140, doi:10.1016/0378-3812(92)85082-J.

Sloan, E. D., and C. A. Koh (2008), *Clathrate Hydrates of Natural Gases*, 3rd ed., 721 pp., CRC Press, Boca Raton, Fla.

Smallwood, I. (2002), *Solvent Recovery Handbook*, 2nd ed., 424 pp., Blackwell, Oxford, U. K.

Soga, K., S. L. Lee, M. Y. A. Ng, and A. Klar (2006), Characterisation and engineering properties of methane hydrate soils, in *Characterisation and Engineering Properties of Natural Soils*, edited by T. S. Tan et al., pp. 2591–2642, A. A. Balkema, Lisse, Netherlands.

Sorey, M. L., C. D. Farrar, and G. A. Marshall (1993), Hydrologic and topographic changes in Long Valley Caldera, California,

induced by geothermal development 1985–1992, paper presented at the 15th New Zealand Geothermal Workshop, Int. Geotherm. Assoc., Auckland, New Zealand, 10–12 Nov.

Spangenberg, E. (2001), Modeling of the influence of gas hydrate content on the electrical properties of porous sediments, *J. Geophys. Res.*, *106*, 6535–6548, doi:10.1029/2000JB900434.

Spangenberg, E., and J. Kulenkampff (2006), Influence of methane hydrate content on electrical sediment properties, *Geophys. Res. Lett.*, *33*, L24315, doi:10.1029/2006GL028188.

Spangenberg, E., J. Kulenkampff, R. Naumann, and J. Erzinger (2005), Pore space hydrate formation in a glass bead sample from methane dissolved in water, *Geophys. Res. Lett.*, *32*, L24301, doi:10.1029/2005GL024107.

Sridhar, M. R., and M. M. Yovanovich (1996), Elastoplastic contact conductance model for isotropic conforming rough surfaces and comparison with experiments, *J. Heat Transfer*, *118*, 3–9, doi:10.1115/1.2824065.

Stern, L. A., and S. H. Kirby (2008), Natural gas hydrates up close: A comparison of grain characteristics of samples from marine and permafrost environments as revealed by cryogenic SEM, paper 5330 presented at the 6th International Conference on Gas Hydrates, Chevron, Vancouver, B. C., Canada, 6–10 July.

Stern, L. A., S. H. Kirby, and W. B. Durham (1996), Peculiarities of methane clathrate hydrate formation and solid-state deformation, including possible superheating of water ice, *Science*, *273*, 1843–1848, doi:10.1126/science.273.5283.1843.

Stern, L. A., S. H. Kirby, and W. B. Durham (1998), Polycrystalline methane hydrate: Synthesis from superheated ice, and low-temperature mechanical properties, *Energy Fuels*, *12*, 201–211, doi:10.1021/ef970167m.

Subramanian, S., and E. D. Sloan (2002), Solubility effects on growth and dissolution of methane hydrate needles, paper presented at the 4th International Conference on Gas Hydrates, Jpn. Natl. Oil Corp., Yokohama, Japan, 19–23 May.

Sultan, N., P. Cochonat, J. P. Foucher, and J. Mienert (2004a), Effect of gas hydrates melting on seafloor slope instability, *Mar. Geol.*, *213*, 379–401, doi:10.1016/j.margeo.2004.10.015.

Sultan, N., J. P. Foucher, P. Cochonat, T. Tonnerre, J. F. Bourillet, H. Ondreas, E. Cauquil, and D. Grauls (2004b), Dynamics of gas hydrate: Case of the Congo continental slope, *Mar. Geol.*, *206*, 1–18, doi:10.1016/j.margeo.2004.03.005.

Sultan, N., M. Voisset, T. Marsset, A. M. Vernant, E. Cauquil, J. L. Colliat, and V. Curinier (2007), Detection of free gas and gas hydrate based on 3D seismic data and cone penetration testing: An example from the Nigerian Continental Slope, *Mar. Geol.*, *240*, 235–255, doi:10.1016/j.margeo.2007.02.012.

Sun, R., and Z. Duan (2007), An accurate model to predict the thermodynamic stability of methane hydrate and methane solubility in marine environments, *Chem. Geol.*, *244*, 248–262, doi:10.1016/j.chemgeo.2007.06.021.

Sun, Y. F., and D. Goldberg (2005), Dielectric method of high-resolution gas hydrate estimation, *Geophys. Res. Lett.*, *32*, L04313, doi:10.1029/2004GL021976.

Swartz, E. T., and R. O. Pohl (1989), Thermal boundary resistance, *Rev. Mod. Phys.*, *61*, 605–668, doi:10.1103/RevModPhys.61.605.

Sychev, V. V., A. A. Vasserman, V. A. Zagoruchenko, A. D. Kozlov, G. A. Spiridonov, and V. A. Tsymarny (1987), *Thermodynamic Properties of Methane*, 341 pp., Hemisphere, Washington, D. C.

Sylte, J. E., L. K. Thomas, D. W. Rhett, D. D. Bruning, and N. B. Nagel (1999), Water induced compaction in the Ekofisk Field, paper presented at the SPE Annual Technical Conference and Exhibition, Soc. of Pet. Eng., Houston, Tex., 3–6 Oct.

Tan, B., J. T. Germaine, and P. B. Flemings (2006), Data report: Consolidation and strength characteristics of sediments from ODP Site 1244, Hydrate Ridge, Cascadia continental margin [online], *Proc. Ocean Drill. Program Sci. Rep.*, *204*, 148 pp. (Available at http://www-odp.tamu.edu/publications/204_SR/102/102.htm)

Tarnawski, V. R., W. H. Leong, F. Gori, G. D. Buchan, and J. Sundberg (2002), Inter-particle contact heat transfer in soil systems at moderate temperatures, *Int. J. Energy Res.*, *26*, 1345–1358.

Terzaghi, K., R. B. Peck, and G. Mesri (1996), *Soil Mechanics in Engineering Practice*, 3rd ed., 549 pp., John Wiley, New York.

Tidwell, V. C., and J. L. Wilson (1997), Laboratory method for investigating permeability upscaling, *Water Resour. Res.*, *33*, 1607–1616, doi:10.1029/97WR00804.

Tishchenko, P., C. Hensen, K. Wallmann, and C. S. Wong (2005), Calculation of the stability and solubility of methane hydrate in seawater, *Chem. Geol.*, *219*, 37–52, doi:10.1016/j.chemgeo.2005.02.008.

Tohidi, B., R. Anderson, M. B. Clennell, R. W. Burgass, and A. B. Biderkab (2001), Visual observation of gas-hydrate formation and dissociation in synthetic porous media by means of glass micromodels, *Geology*, *29*, 867–870, doi:10.1130/0091-7613(2001)029<0867:VOOGHF>2.0.CO;2.

Toll, J. S. (1956), Causality and the dispersion relation: Logical foundations, *Phys. Rev.*, *104*, 1760–1770, doi:10.1103/PhysRev.104.1760.

Tombari, E., S. Presto, G. Salvetti, and G. P. Johari (2006), Heat capacity of tetrahydrofuran clathrate hydrate and of its components, and the clathrate formation from supercooled melt, *J. Chem. Phys.*, *124*, 154507, doi:10.1063/1.2188944.

Topp, G. C., J. L. Davis, W. G. Bailey, and W. D. Zebchuk (1980), The measurement of soil water content using a portable TDR hand probe, *Can. J. Soil Sci.*, *64*, 313–321.

Trebble, M. A., and P. R. Bishnoi (1987), Development of a new four-parameter cubic equation of state, *Fluid Phase Equilibria*, *35*, 1–18, doi:10.1016/0378-3812(87)80001-8.

Trehu, A. M., et al. (2004), Three-dimensional distribution of gas hydrate beneath southern Hydrate Ridge: Constraints from ODP Leg 204, *Earth Planet. Sci. Lett.*, *222*, 845–862, doi:10.1016/j.epsl.2004.03.035.

Trehu, A. M., C. Ruppel, M. D. Holland, G. R. Dickens, M. E. Torres, T. S. Collett, D. Goldberg, and P. Schultheiss (2006), Gas hydrates in marine sediments: Lessons from scientific ocean drilling, *Oceanography*, *19*, 124–142.

Tryon, M. D., K. M. Brown, and M. E. Torres (2002), Fluid and chemical flux in and out of sediments hosting methane hydrate deposits on Hydrate Ridge, OR, II: Hydrological processes, *Earth Planet. Sci. Lett.*, *201*, 541–557, doi:10.1016/S0012-821X(02)00732-X.

Turner, D. J., P. Kumar, and E. D. Sloan (2005), New technique for hydrate thermal diffusivity measurements, *Int. J. Thermophys.*, *26*, 1681–1691, doi:10.1007/s10765-005-8588-1.

Uchida, T., and T. Takashi (2004), Petrophysical properties of natural gas hydrate-bearing sands and their sedimentology in the Nankai Trough, *Resour. Geol.*, *54*, 79–87, doi:10.1111/j.1751-3928.2004.tb00189.x.

Uchida, T., T. Ebinuma, S. Takeya, J. Nagao, and H. Narita (2002), Effects of pore sizes on dissociation temperatures and pressures of methane, carbon dioxide, and propane hydrates in porous media, *J. Phys. Chem. B*, *106*, 820–826, doi:10.1021/jp012823w.

Ullerich, J. W., M. S. Selim, and E. D. Sloan (1987), Theory and measurement of hydrate dissociation, *AIChE J.*, *33*, 747–752, doi:10.1002/aic.690330507.

Valdes, J. R., and J. C. Santamarina (2007), Particle transport in a nonuniform flow field: Retardation and clogging, *Appl. Phys. Lett.*, *90*, 244101, doi:10.1063/1.2748850.

van Genuchten, M. T. (1980), A closed-form equation for predicting the hydraulic conductivity of unsaturated soils, *Soil Sci. Soc. Am. J.*, *44*, 892–898.

Vargaftik, N. B., L. P. Filippov, A. A. Tarzimanov, and E. E. Totskii (1993), *Handbook of Thermal Conductivity of Liquids and Gases*, CRC Press, Boca Raton, Fla.

Voronov, V. P., E. E. Gorodetskii, and S. Safonov (2008), Thermodynamic properties of methane hydrate in quartz powder, paper

5489 presented at the 6th International Conference on Gas Hydrates, Chevron, Vancouver, B. C., Canada, 6–10 July.

Waite, W. F., B. J. deMartin, S. H. Kirby, J. Pinkston, and C. D. Ruppel (2002), Thermal conductivity measurements in porous mixtures of methane hydrate and quartz sand, *Geophys. Res. Lett.*, *29*(24), 2229, doi:10.1029/2002GL015988.

Waite, W. F., W. J. Winters, and D. H. Mason (2004), Methane hydrate formation in partially water-saturated Ottawa sand, *Am. Mineral.*, *89*, 1202–1207.

Waite, W. F., L. Y. Gilbert, W. J. Winters, and D. H. Mason (2005), Thermal property measurements in tetrahydrofuran (THF) hydrate and hydrate-bearing sediment between −25 and +4°C, and their application to methane hydrate, in *Fifth International Conference on Gas Hydrates*, pp. 1724–1733, Tapir Acad., Trondheim, Norway.

Waite, W. F., L. A. Stern, S. H. Kirby, W. J. Winters, and D. H. Mason (2007), Simultaneous determination of thermal conductivity, thermal diffusivity and specific heat in sI methane hydrate, *Geophys. J. Int.*, *169*, 767–774, doi:10.1111/j.1365-246X.2007.03382.x.

Waite, W. F., J. P. Osegovic, W. J. Winters, M. D. Max, and D. H. Mason (2008), Seeding hydrate formation in water-saturated sand with dissolved-phase methane obtained from hydrate dissolution: A progress report, paper 5341 presented at the 6th International Conference on Gas Hydrates, Chevron, Vancouver, B. C., Canada, 6–10 July.

Walsh, M. R., S. H. Hancock, S. J. Wilson, S. L. Patil, G. J. Moridis, R. Boswell, T. S. Collett, C. A. Koh, and E. D. Sloan (2009), Preliminary report on the commercial viability of gas production from natural gas hydrates, *Energy Econ.*, *31*, 815–823, doi:10.1016/j.eneco.2009.03.006.

Wang, Y. H., and J. C. Santamarina (2007), Attenuation in sand: An exploratory study on the small-strain behavior and the influence of moisture condensation, *Granular Matter*, *9*, 365–376, doi:10.1007/s10035-007-0050-6.

Weast, R. C. (1987), *CRC Handbook of Chemistry and Physics*, 68 ed., CRC Press, Boca Raton, Fla.

Weitemeyer, K. A., S. C. Constable, K. W. Key, and J. P. Behrens (2006), First results from a marine controlled-source electromagnetic survey to detect gas hydrates offshore Oregon, *Geophys. Res. Lett.*, *33*, L03304, doi:10.1029/2005GL024896.

Wensink, W. A. (1993), Dielectric properties of wet soils in the frequency range 1–3000 MHz, *Geophys. Prospect.*, *41*, 671–696, doi:10.1111/j.1365-2478.1993.tb00878.x.

Westbrook, G. K., et al. (2005), Measurement of P- and S-wave velocities, and the estimation of hydrate concentration at sites in the continental margin of Svalbard and the Storegga region of Norway, paper 3004 presented at the Fifth International Conference on Gas Hydrates, pp. 726–735, Tapir Acad., Trondheim, Norway.

Wilder, J. W., et al. (2008), An international effort to compare gas hydrate reservoir simulators, paper 5727 presented at the 6th International Conference on Gas Hydrates, Chevron, Vancouver, B. C., Canada, 6–10 July.

Willoughby, E. C., K. Latychev, R. N. Edwards, K. Schwalenberg, and R. D. Hyndman (2008), Seafloor compliance imaging of marine gas hydrate deposits and cold vent structures, *J. Geophys. Res.*, *113*, B07107, doi:10.1029/2005JB004136.

Winters, W. J. (2000), Stress history and geotechnical properties of sediment from the Cape Fear Diapir, Blake Ridge Diapir, and Blake Ridge, *Proc. Ocean Drill. Program Sci. Results*, *164*, 421–429.

Winters, W. J., S. R. Dallimore, T. S. Collett, T. J. Katsube, K. A. Jenner, R. E. Cranston, J. F. Wright, F. M. Nixon, and T. Uchida (1999), Physical properties of sediments from the JAPEX/JNOC/GSC Mallik 2L-38 gas hydrate research well, in *Scientific Results From JAPEX/JNOC/GSC Mallik 2L-38 Gas Hydrate Research Well, Mackenzie Delta, Northwest Territories, Canada*, edited by S. R. Dallimore et al., *Bull. Geol. Surv. Can.*, *544*, 95–100.

Winters, W. J., W. F. Waite, D. H. Mason, W. P. Dillon, and I. A. Pecher (2002), Sediment properties associated with gas hydrate formation, paper presented at the Fourth International Conference on Gas Hydrates, Jpn. Natl. Oil Corp., Yokohama, Japan, 19–23 May.

Winters, W. J., I. Novosel, O. Boldina, W. F. Waite, S. A. Kelsey, and B. W. Hallett (2007), Physical properties of sediment obtained during the IMAGES VIII/PAGE 127 gas hydrate and paleoclimate cruise on the RV *Marion Dufresne* in the Gulf of Mexico, 2–18 July 2002, in *Initial Report of the IMAGES VIII/PAGE 127 Gas Hydrate and Paleoclimate Cruise on the RV Marion Dufresne in the Gulf of Mexico, 2–18 July 2002*, edited by W. J. Winters, T. D. Lorenson, and C. K. Paull, chap. 4, pp. 1–65, U.S. Geol. Surv., Boulder, Colo.

Winters, W. J., W. F. Waite, D. H. Mason, and P. Kumar (2008), Physical properties of repressurized samples recovered during the 2006 national gas hydrate program expedition offshore India, paper 5531 presented at the 6th International Conference on Gas Hydrates, Chevron, Vancouver, B. C., Canada, 6–10 July.

Wood, W. T., and C. Ruppel (2000), Seismic and thermal investigations of the Blake Ridge gas hydrate area: A synthesis, *Proc. Ocean Drill. Program Sci. Results*, *164*, 253–264.

Wood, W. T., P. L. Stoffa, and T. H. Shipley (1994), Quantitative detection of methane hydrate through high-resolution seismic velocity analysis, *J. Geophys. Res.*, *99*(B5), 9681–9695, doi:10.1029/94JB00238.

Wood, W. T., J. F. Gettrust, N. R. Chapman, G. D. Spence, and R. D. Hyndman (2002), Decreased stability of methane hydrates in marine sediments owing to phase-boundary roughness, *Nature*, *420*, 656–660, doi:10.1038/nature01263.

Woodside, W., and J. H. Messmer (1961), Thermal conductivity of porous media. I. Unconsolidated sands, *J. Appl. Phys.*, *32*, 1688–1699, doi:10.1063/1.1728419.

Wroth, C. P., and D. M. Wood (1978), The correlation of index properties with some basic engineering properties of soils, *Can. Geotech. J.*, *13*, 137–145.

Xu, H., J. Dvorkin, and A. Nur (2001), Linking oil production to surface subsidence from satellite radar interferometry, *Geophys. Res. Lett.*, *28*, 1307–1310, doi:10.1029/2000GL012483.

Xu, H., J. Dai, F. Snyder, and N. Dutta (2004), Seismic detection and quantification of gas hydrate using rock physics and inversion, in *Advances in the Study of Gas Hydrates*, edited by C. E. Taylor and J. Kwan, pp. 117–139, Kluwer Acad., New York.

Xu, W., and L. N. Germanovich (2006), Excess pore pressure resulting from methane hydrate dissociation in marine sediments: A theoretical approach, *J. Geophys. Res.*, *111*, B01104, doi:10.1029/2004JB003600.

Xu, W., and C. Ruppel (1999), Predicting the occurrence, distribution, and evolution of methane gas hydrate in porous marine sediments, *J. Geophys. Res.*, *104*, 5081–5095, doi:10.1029/1998JB900092.

Yerkes, R. F., and R. O. Castle (1970), Surface deformation associated with oil and gas field operations in the United States, paper presented at the 1st International Symposium on Land Subsidence, Int. Assoc. of Hydrol. Sci., Tokyo.

Yoon, J.-H., T. Kawamura, Y. Yamamoto, and T. Komai (2004), Transformation of methane hydrate to carbon dioxide hydrate: In situ raman spectroscopic observations, *J. Phys. Chem. A*, *108*, 5057–5059, doi:10.1021/jp0496831.

Young, A. G., G. W. Quiros, and C. J. Ehlers (1983), Effects of offshore sampling and testing on undrained soil shear strength, paper presented at the Offshore Technology Conference, Am. Assoc. of Pet. Geol., Houston, Tex.

Yuan, J., and R. N. Edwards (2000), The assessment of marine gas hydrates through electrical remote sounding: Hydrate without a BSR?, *Geophys. Res. Lett.*, *27*, 2397–2400, doi:10.1029/2000GL011585.

Yuan, T., R. D. Hyndman, G. D. Spence, and B. Desmons (1996), Seismic velocity increase and deep-sea gas hydrate concentration above a bottom-simulating reflector on the northern Cascadia

continental slope, *J. Geophys. Res.*, *101*, 13,655–13,671, doi:10.1029/96JB00102.

Yuan, T., G. D. Spence, R. D. Hyndman, T. A. Minshull, and S. C. Singh (1999), Seismic velocity studies of a gas hydrate bottom-simulating reflector on the northern Cascadia continental margin: Amplitude modeling and full waveform inversion, *J. Geophys. Res.*, *104*, 1179–1191, doi:10.1029/1998JB900020.

Yun, T. S., and J. C. Santamarina (2008), Fundamental study of thermal conduction in dry soils, *Granular Matter*, *10*, 197–207, doi:10.1007/s10035-007-0051-5.

Yun, T. S., F. M. Francisca, J. C. Santamarina, and C. Ruppel (2005), Compressional and shear wave velocities in uncemented sediment containing gas hydrate, *Geophys. Res. Lett.*, *32*, L10609, doi:10.1029/2005GL022607.

Yun, T. S., G. A. Narsilio, and J. C. Santamarina (2006), Physical characterization of core samples recovered from Gulf of Mexico, *Mar. Pet. Geol.*, *23*, 893–900, doi:10.1016/j.marpetgeo.2006.08.002.

Yun, T. S., J. C. Santamarina, and C. Ruppel (2007), Mechanical properties of sand, silt, and clay containing tetrahydrofuran hydrate, *J. Geophys. Res.*, *112*, B04106, doi:10.1029/2006JB004484.

Zatsepina, O. Y., and B. A. Buffett (1997), Phase equilibrium of gas hydrate: Implications for the formation of hydrate in the deep-sea floor, *Geophys. Res. Lett.*, *24*, 1567–1570, doi:10.1029/97GL01599.

Zatsepina, O. Y., and B. A. Buffett (1998), Thermodynamic conditions for the stability of gas hydrate in the seafloor, *J. Geophys. Res.*, *103*, 24,127–24,139, doi:10.1029/98JB02137.

Zatsepina, O. Y., and B. A. Buffett (2001), Experimental study of the stability of CO_2-hydrate in a porous medium, *Fluid Phase Equilibria*, *192*, 85–102, doi:10.1016/S0378-3812(01)00636-7.

Zhong, Y., and R. E. Rogers (2000), Surfactant effects on gas hydrate formation, *Chem. Eng. Sci.*, *55*, 4175–4187, doi:10.1016/S0009-2509(00)00072-5.

D. D. Cortes, D. N. Espinoza, J. Jang, J. W. Jung, J. C. Santamarina, and H. Shin, School of Civil and Environmental Engineering, Georgia Institute of Technology, 790 Atlantic Dr. NW, Atlanta, GA 30332-0355, USA.

B. Dugan, Department of Earth Science, Rice University, Houston, TX 77005, USA.

J. Germaine, Department of Civil and Environmental Engineering, Massachusetts Institute of Technology, 77 Massachusetts Ave., Cambridge, MA 02139, USA.

T. J. Kneafsey, Lawrence Berkeley National Laboratory, 1 Cyclotron Rd., MS 90R1116, Berkeley, CA 94720, USA.

K. Soga, Department of Engineering, University of Cambridge, Trumpington St., Cambridge CB2 1PZ, UK.

W. F. Waite and W. J. Winters, U.S. Geological Survey, 384 Woods Hole Rd., Woods Hole, MA 02543, USA. (wwaite@usgs.gov)

T.-S. Yun, School of Civil and Environmental Engineering, Yonsei University, 134 Sinchon-dong, Seodaemun-gu, Seoul 120-749, South Korea.